

HEPATITIS C VIRUS ENTRY RECEPTOR  
DYNAMICS

and

STUDIES OF PLATELET ACTIN DYNAMICS  
USING LIFEACT-GFP: A POTENTIAL ROLE FOR  
ACTIN NODULES IN FILOPODIA FORMATION

by

Amy Barnes

*This project is submitted in partial fulfilment of the requirements for the award of the  
Master of Research in Biomedical Research*

UNIVERSITY OF  
BIRMINGHAM

**University of Birmingham Research Archive**

**e-theses repository**

This unpublished thesis/dissertation is copyright of the author and/or third parties. The intellectual property rights of the author or third parties in respect of this work are as defined by The Copyright Designs and Patents Act 1988 or as modified by any successor legislation.

Any use made of information contained in this thesis/dissertation must be in accordance with that legislation and must be properly acknowledged. Further distribution or reproduction in any format is prohibited without the permission of the copyright holder.

# HEPATITIS C VIRUS ENTRY RECEPTOR DYNAMICS

by

Amy Barnes

*This project is submitted in partial fulfilment of the requirements for the award of the  
Master of Research in Biomedical Research*

College of Medical and Dental Sciences

University of Birmingham

Edgbaston

Birmingham

B292TT

August 2011

## ABSTRACT

Virus entry into target cells is mediated by the attachment of viral glycoproteins to cell surface receptors. Entry of the hepatitis C virus (HCV) into hepatocytes has been shown to require viral glycoprotein dimer E1E2 and the target cell receptor CD81, scavenger receptor-BI (SR-BI) and the tight junction proteins claudin-1 and occludin in an undefined mechanism. In this study, we aim to define the dynamic movements of these proteins in the membrane of the polarising hepatocarcinoma cell line HepG2. We further examine the extent to which these kinetics are perturbed following addition of the soluble viral glycoproteins sE2 and sE1E2, and the small molecule inhibitor of SR-BI ITX5061.

The results of this study show that the amount of mobile receptor and the speed at which it diffuses varies according to its location within the cell. CD81 and claudin-1 are expressed equally in the filopodia and plasma membrane, whereas SR-BI is expressed at lower levels in the filopodia compared to the plasma membrane. We show that addition of both sE2 and sE1E2 has varying effects on both the speed and mobility of CD81 and claudin-1 and that the majority of significant effects observed for claudin-1 are observed at areas of potential cell contact. Finally, we demonstrate that addition of ITX5061 affects the diffusion coefficient of CD81 and CLDN-1 and the amount of mobile SR-BI. Furthermore, the effects on SR-BI are limited to areas of cell contact or exploratory regions. In summary, we present data which we hope will further current knowledge of the activity of these receptors in relation to their role in HCV infection.

## TABLE OF CONTENTS

ABBREVIATIONS

LIST OF FIGURES

ACKNOWLEDGEMENTS

### 1. INTRODUCTION

1.1 Hepatitis C Virus tropism	1
1.2 HCV treatment	3
1.3 Mechanisms of HCV entry	4
1.4 HCV receptors	4
1.4.1 CD81	5
1.4.2 SR-BI	6
1.4.3 CLDN-1	7
1.4.4 Occludin	8
1.5 Models of HCV entry	9
1.5.1 The Coxsackie virus B (CVB) entry model	9
1.5.2 Basolateral entry model	10

1.6 Project objectives	12
<b>2. MATERIALS AND METHODS</b>	
2.1 Cell lines and reagents	12
2.2. Generation of fluorescently-tagged CD81, SR-BI, CDLN-1, occludin and glycoposphatidylinositol (GPI) proteins	12
2.3 Laser Scanning Confocal Microscopy	14
2.4 Fluorescence recovery after photobleaching (FRAP)	15
2.5 Regions of interest	18
2.6 Statistical analysis	19
<b>3. RESULTS</b>	
3.1 Receptor localisation	20
3.2 Variance between individual cells within a sample	21
3.3 Differences in receptor dynamics between the PM and filopodia	23
3.4 Differences in receptor dynamics between specific cellular locations	27
3.5 Addition of viral glycoproteins	31
3.6 Addition of ITX5061 and ITX7094	37

## **ABBREVIATIONS**

CVB - Coxsackie virus B

BC – Bile canaliculi

CAR- Coxsackievirus-adenovirus receptor

CLDN-1 – Claudin-1

DAA – Direct acting antivirals

ECL – Extracellular loop

FRAP – Fluorescence recovery after photobleaching

FRET – Fluorescence resonance energy transfer

GAGs – Glycosaminoglycans

GFP – Green fluorescent protein

GPI – Glycophosphatidylinositol

HCV – Hepatitis C virus

HCVcc – Hepatitis C virus infectious cell culture system

HCVpp – Hepatitis C virus pseudoparticle

HDL – High density lipoproteins

HVR – Hypervariable region

LDL – Low density lipoprotein

MDCK - Madin Darby canine kidney

PM – Plasma membrane

SR-BI – Scavenger receptor B1

TEM – Tetraspanin enriched microdomain

TIRF – Total internal reflectance fluorescence

TJ – Tight junction

## LIST OF FIGURES

Figure 1: The hepatitis C virus genome	2
Figure 2: Simple epithelial and hepatic polarity	3
Figure 3: The four essential HCV receptors	5
Figure 4: Hepatocyte filopodia extend through the sinusoidal membrane	11
Figure 5: Two possible modes of protein diffusion	16
Figure 6: Plot of diffusion intensity over time	17
Figure 7: Representative image of regions of interest and structures examined on a HepG2 cell expressing CD81-GFP	19
Figure 8: Representative images of receptor localisation	20
Figure 9: Variance in diffusion coefficient and diffusion coefficient between cells in a sample	22
Figure 10: Variance in diffusion coefficient and mobile fraction between PM and filopodia.	25
Table 1: Median, interquartile range (IQ range), mean, and standard deviation (S.D) of data presented in Figure 10.	26

Figure 11: Diffusion coefficient and mobile fraction of receptors at specific cellular structures.	29
Table 2: Median, interquartile range (IQ range), mean, and standard deviation (S.D) of data presented in Figure 11.	30
Figure 12: Diffusion coefficient and mobile fraction of CD81 and CLDN-1 following addition of viral glycoproteins.	33
Table 3a: Median, interquartile range (IQ range), mean, and standard deviation (S.D) of CD81 following addition of sE2 and sE1E2.	34
Table 3b: Median, interquartile range (IQ range), mean, and standard deviation (S.D) of CLDN-1 following addition of sE2 and sE1E2.	36
Figure 13: Diffusion coefficient and mobile fraction of CD81 and CLDN-1 following addition of ITX5061 and ITX7904	39
Table 4a: Median, interquartile range (IQ range), mean, and standard deviation (S.D) SR-BI following addition of ITX5061 and ITX7904.	40
Table 4b: Median, interquartile range (IQ range), mean, and standard deviation (S.D) of CD81 following addition of ITX5061 and ITX7904	41
Table 4c: Median, interquartile range (IQ range), mean, and standard deviation (S.D) of CLDN-1 following addition of ITX5061 and ITX7904	42
Table5: Comparison of diffusion kinetics presented in this study and those from previously published data	46

Figure 15: Trends observed from data presented in this report	51
<i>Supplementary Figure 1– Variance in diffusion coefficient and mobile fraction between PM and filopodia</i>	93
<i>Supplementary Table 1: Median, interquartile range (IQ range), mean, and standard deviation (S.D) of data presented in Figure 10</i>	94
<i>Supplementary Figure 2: Variance in diffusion coefficient and mobile fraction at specific cellular structures</i>	95
<i>Supplementary Table 2: Median, interquartile range (IQ range), mean, and standard deviation (S.D) of occludin and GPI at specific cellular locations</i>	96

## **ACKNOWLEDGEMENTS**

I would like thank Dr. Helen Harris and Prof. Jane McKeating for help and guidance, and members of the McKeating lab for useful discussions. This work was funded by the MRC.



## 1. INTRODUCTION

### *1.1 Hepatitis C Virus tropism*

The hepatitis C virus (HCV) is an enveloped positive sense single stranded RNA virus of the *Flaviviridae* family, and is a major worldwide cause of liver disease. HCV currently infects around 170 million people worldwide, with 60%-80% of new infections becoming persistent (Rehermann and Nascimbeni 2005; Dustin and Rice 2007). As a result, unresolved infection is a leading cause of repeated liver transplantation and creates a large healthcare burden. Currently, the common course of treatment is a period of pegylated interferon- $\alpha$  and ribavirin administration which has a relatively low success rate and unpleasant side effects.

The 9600bp genome of HCV varies across 6 genotypes and transcribes a polyprotein of around 3000 amino acids. This polyprotein is cleaved by cellular and viral proteases to form the structural proteins core, E1 and E2; and the non-structural proteins NS2-5 and p7 (Figure 1). HCV virus entry into a target cell involves the interaction of the glycoproteins E1 and E2 with four receptors on the target cell surface: scavenger receptor BI (SR-BI), CD81, claudin-1 (CLDN-1) and occludin (section 1.4).

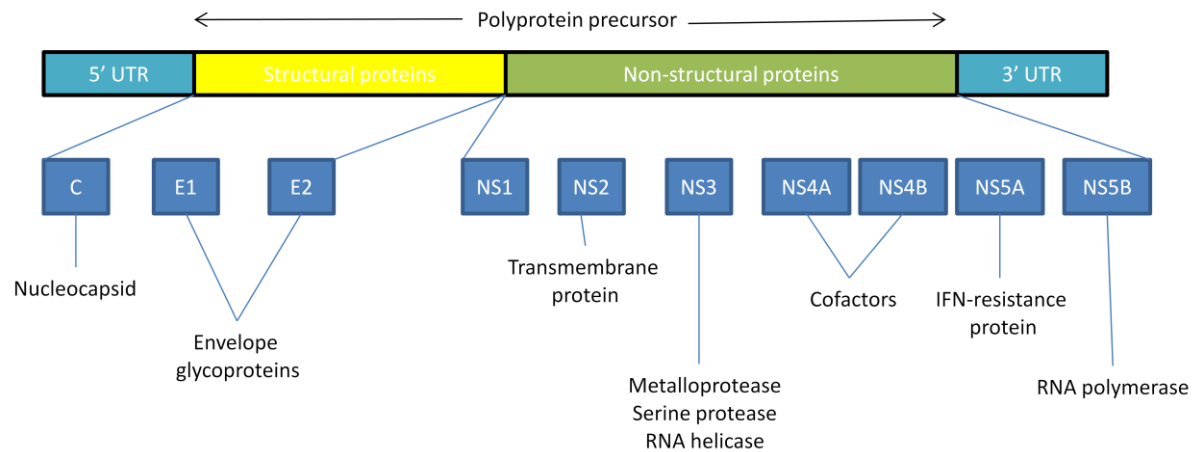


**Figure 1: The hepatitis C virus genome.** The HCV genome encodes both structural and non-structural proteins. Adapted from (Anzola and Burgos 2003).

The primary target of HCV is the hepatocytes of the liver, an epithelial cell type with complex polarity (Decaens *et al.* 2008) (Figure 2). Hepatocyte apical membranes form the continuous network of bile canaliculi (BC) with the basal pole contacting the sinusoids. Separating the two poles is the tight junction (TJ) which regulates paracellular diffusion (Farquhar and Palade 1963; Claude and Goodenough 1973).

The polarity of hepatocytes is critical for both liver function and HCV tropism. This study uses the HepG2 hepatocarcinoma line, which exhibits many markers of structural and functional polarity, including TJ-like structures (reviewed in Decaens *et al.* 2008). Recent studies on the role of cell polarity on HCV entry demonstrate that agents which reduce the hepatocellular polarity of CD81-HepG2 cells increase the efficiency of infection (Mee *et al.* 2008; Mee *et al.* 2009; Mee *et al.* 2010).

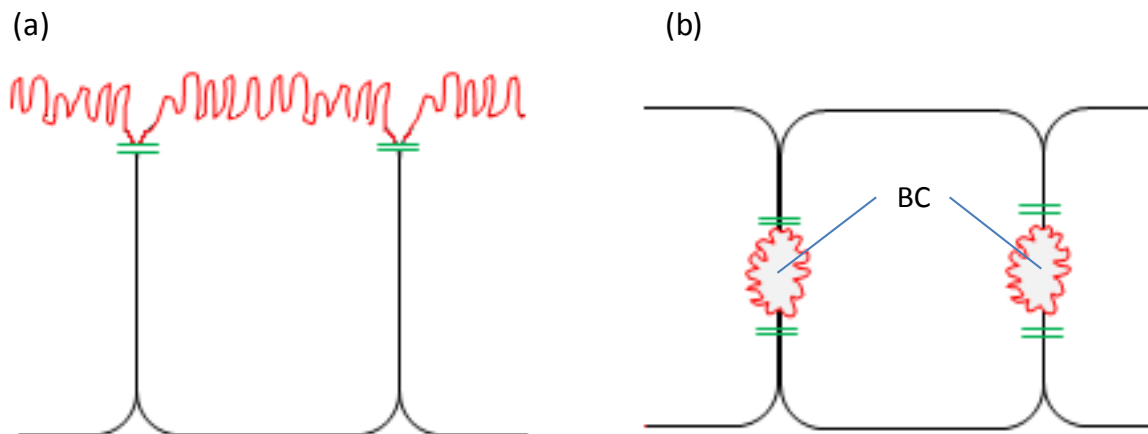


**Figure 2: Simple epithelial and hepatic polarity.** Apical membranes (red), basolateral membranes (black), tight junctions (green) . Simple epithelial polarity involves a single apical and basolateral membrane, separated by a tight junction (a). Hepatic polarity is more complex, with several basolateral and apical membranes separated by tight junctions. Apical membranes on adjacent cells form the continuous network of bile canaliculi (b). Adapted from (Decaens et al. 2008).

## 1.2 HCV treatment

All stages of the viral lifecycle may be considered as potential targets for anti-viral agents. New direct acting antivirals (DAAs) are protease and polymerase inhibitors, inhibiting the actions of the non-structural proteins NS3/4A and NS5B respectively. Promising results have been obtained from such drugs; the DAAs telaprevir and boceprevir are currently in phase II clinical trials (Asselah and Marcellin). In contrast, the majority of drugs targeting viral entry are still in preclinical trials but are an attractive target (Zeisel *et al.* 2009; Vermehren and Sarrazin, 2011). A small number of such drugs including Silibinin (Wagoner *et al.* 2010) and the small molecule inhibitor of SR-BI ITX5061 (Syder *et al.*, 2011) have been reported, and the latter is now in clinical trials.

### 1.3 Mechanisms of HCV entry

Viral glycoproteins confer attachment via high affinity particle interactions with cell surface receptors or molecules. Following this, viruses generally utilise endogenous receptor trafficking pathways to internalise. The HCV viral glycoproteins E1 and E2 are dependent on each other for proper folding of the non-covalent heterodimer E1E2 (Patel *et al.* 2000; Cocquerel *et al.* 2000; Brazzoli *et al.* 2005). Studies have shown residues in E1 to be involved in both fusion with the target cell membrane and virus entry (Lavillette *et al.* 2007; Li *et al.* 2009), whereas the hypervariable region (HVR) 1 of E2 is rapidly mutated during immune escape but retains a basic charge (Farci *et al.* 2000; Callens *et al.* 2005; von Hahn *et al.* 2007). This suggests a role for HVR1 a role in binding negatively charged glycosaminoglycans (GAGs) at the target cell surface (Callens *et al.* 2005).

### 1.4 Receptors

Following low affinity binding of the virus to heparin sulphate proteoglycans (Barth *et al.* 2006; Koutsoudakis *et al.* 2006), GAGs, lectins, and low density lipoprotein (LDL) receptors, four receptors have been shown to be essential for HCV entry: SR-BI, CD81, CLDN-1 and occludin (Figure 3).

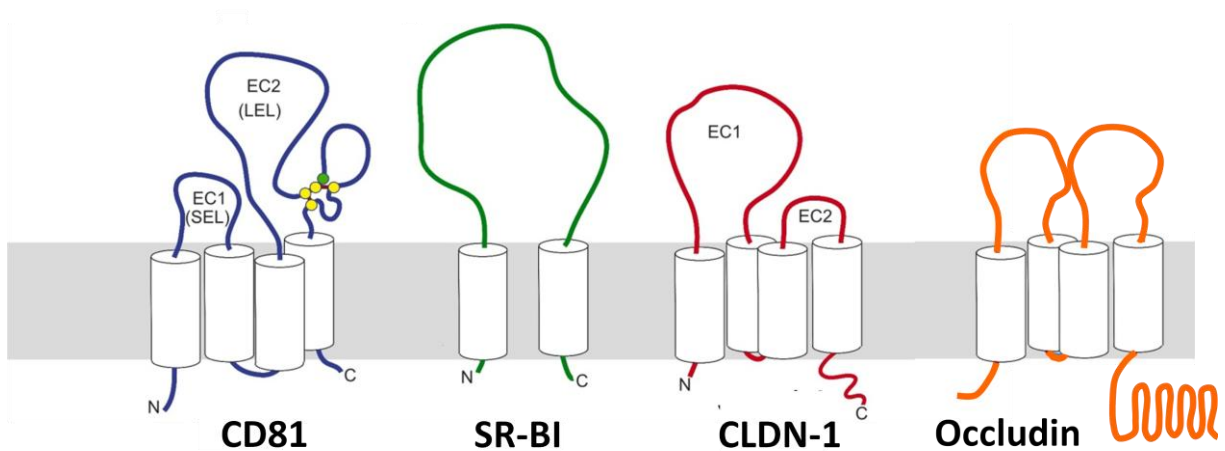


**Figure 3: The four essential HCV receptors.** The CD81 (a), SR-BI (b), CLDN-1 (c) and occludin (d). The tetraspanin CD81 and tight junction proteins CLDN-1 and occludin each contain four transmembrane domains, whereas SR-BI contains only two. The extracellular loops (EC) EC1 and EC2 of CD81 are termed small extracellular loops (SEL) and large extracellular loop (LEL) respectively (a). CLDN-1 also contains two EC loops (b). (Davis, *In press*).

#### 1.4.1 CD81

CD81 (Figure 3a) is expressed in most tissues and was first identified as an HCV receptor due to its interaction with E2 (Pileri *et al.* 1998). Its role was later confirmed by the discovery that its expression in the CD81-deficient HepG2 cell line confers infectivity (Zhang *et al.* 2004; Lavillette *et al.* 2005; Lindenbach *et al.* 2005).

CD81 is a tetraspanin and thus contains 4-6 cysteine residues which form critical disulphide bonds with the second large extra cellular loop, and these are essential in the CD81-HCV-E2 interaction (Petracca *et al.* 2000). Tetraspanins associate with other tetraspanin and non-

tetraspanin proteins at cholesterol enriched domains to form cell type-specific tetraspanin enriched microdomains (TEMs). These exert a wide array of biological functions, including signal transduction, cell migration, and membrane remodelling (reviewed in (Boucheix and Rubinstein 2001).

In non-polarised HepG2 cells, CD81 is present uniformly at the plasma membrane and does not relocate upon polarisation (Mee, Harris *et al.* 2009). This expression pattern is similar in healthy liver tissue, where it has been reported as mainly basolateral with some canalicular localisation (Reynolds *et al.* 2008; Mee *et al.* 2009).

#### 1.4.2 SR-BI

SR-BI (Figure 3b) is a scavenger protein and is expressed mainly on steroidogenic tissue, macrophages, and in the liver (Krieger *et al.* 2001). It is involved in the selective uptake of cholesterol from ligands such as high density lipoproteins (HDLs) and their particle endocytosis or selective transfer to the membrane (reviewed in *Fidge 1999*).

SR-BI was identified as an HCV receptor by virtue of its specific interaction with the HVR of E2 (Scarselli *et al.* 2002; Barth *et al.* 2005), likely facilitated by the HVR-1 domain (Scarselli *et al.* 2002; Bartosch *et al.* 2003a; Bartosch *et al.* 2003b; Callens *et al.* 2005; Voisset *et al.* 2005). Its importance has since been verified using gene silencing and addition of neutralising antibodies (Lavillette *et al.* 2005; von Hahn *et al.* 2006; Grove *et al.* 2007; Dreux and Cosset 2009). Furthermore, HDLs have been shown to promote HCV infection in an SR-BI dependent manner (Bartosch *et al.*, 2005; Meunier *et al.* 2005; Voisset *et al.*, 2005).

In non-polarised HepG2 cells SR-BI is expressed uniformly around the plasma membrane and does not relocate upon polarisation (Mee *et al.* 2009). Again, this reflects the localisation of the protein in healthy liver tissue, with presence of the protein at the basolateral membrane with minimal staining at canaliculi (Reynolds *et al.* 2008).

#### 1.4.3 CLDN-1

In 2007, a study of a permissive hepatocarcinoma cell line highlighted CLDN-1 (Figure 3c) as a potential HCV receptor (Evans *et al.* 2007), with CLDN- 6 and -9 able to compensate if CLDN-1 is absent. CLDN-1 is expressed at highest concentrations in the liver, but is also present in many other tissues (Furuse *et al.* 1998).

Claudins are able to form homo- and heterodimers with each other (Piontek *et al.* 2008), occludin and CD81, (Harris *et al.* 2010) and the formation of the CD81-CLDN-1 interaction is essential for HCV entry (Yang, Qiu *et al.* 2008; Cukierman *et al.* 2009; Harris *et al.* 2010; Krieger *et al.* 2010). These dimers can be formed between proteins on adjacent cells, and although no direct interaction between CLDN-1 and the HCV glycoproteins has so far been identified, it is thought that *cis*-interactions between claudins on adjoining cells are involved (Liu *et al.* 2009). Recent evidence also suggests that CLDN-1 may potentiate the interaction between CD81 and E2 (Krieger *et al.* 2010).

CLDN-1 has been shown to localise to the PM in non-polarised HepG2 cells and to redistribute to TJs on polarisation, with localisation retained but reduced at the basal

membrane (Mee *et al.* 2009). This pattern is similar to that seen in healthy liver tissue (Reynolds *et al.* 2008).

In healthy liver tissue, SR-BI colocalises with CLDN-1 at the basolateral surface, with minimal coexpression at the apical region (Reynolds *et al.* 2008). In polarised HepG2 cells, CLDN-1 colocalises with CD81 at the basolateral membrane, with minimal coexpression at the TJ (Harris *et al.* 2010). In healthy liver tissue, colocalisation between Cd81 and CLDN-1 is strongest at the apical canalicular region (Reynolds *et al.* 2008).

#### *1.4.4. Occludin*

Occludin is a tight junction protein, and internalises with CLDN-1 in caveolae and clathrin-dependent processes (Matsuda *et al.* 2004; Shen 2008; Stamatovic *et al.* 2009). cDNA screening identified the tight junction protein occludin (Figure 3d) as necessary to confer entry into non-permissive cell lines, and silencing of occludin to reduce infection of permissive Huh-7.5 hepatoma cells (Ploss *et al.* 2009). Occludin was independently identified as an HCV receptor by siRNA silencing of proteins known to associate with CLDN-1 (Liu *et al.* 2009).

In polarised HepG2 cells, occludin localises exclusively to the TJs surrounding the BC, replicating the pattern seen in healthy liver tissue (Reynolds *et al.*, 2008; Mee, *et al.*, 2010).

### 1.5 Models of HCV entry

Following initial binding of HCV to the target cell surface, the mechanism of entry is controversial, and two mechanisms have been proposed.

#### 1.5.1 Coxsackie virus B (CVB) entry model

A large number of viruses have been shown to utilise the TJ as a point of entry (Guttman and Finlay 2009), including CVB. Both CD81 (Brazzoli *et al.* 2008) and the CVB-receptor complex (Coyne *et al.*, 2007) have been observed to move away from the basolateral membrane to areas of cell-cell contact during infection. CVB enters a target cell via the following mechanism. The virus interacts with the decay accelerating factor (DAF) on the apical surface of the cell and this activates Abl kinase and Fyn kinase. Activation of Abl kinase induces Rac-dependent actin rearrangements which permit virus movement to the tight junction. Here, it interacts with the Coxsackievirus-adenovirus receptor (CAR) (Coyne and Bergelson 2006; Coyne *et al.*, 2007). As a result of which conformational changes in the virus capsid are induced which are essential for virus entry and RNA release. In contrast, activation of Fyn kinase, leads to phosphorylation of caveolin and transport of the virus into the cell inside caveolar vesicles (Coyne and Bergelson 2006).

However, there are a number of differences between CVB and HCV entry: firstly interaction with the TJ protein CAR is essential for CVB internalization, whereas there is limited evidence for direct association of HCV with the TJ proteins claudin-1 or occludin; secondly CVB enters via macropinocytosis whereas HCV internalizes by clathrin-dependent endocytosis (Blanchard *et al.*, 2006); and finally, CVB enters via the apical surface whereas it is

believed that HCV enters via the basolateral surface of their target cell types (Drummer *et al.*, 2011).

### *1.5.2 Basolateral entry model*

The basolateral entry model is based on the observation that the HCV pseudoparticle system (HCVpp) infects the polarised colorectal adenocarcinoma cell line Caco-2 in a polarisation-dependent but TJ-independent manner (Mee *et al.* 2008). The lack of dependence on the TJ for entry has been further supported by the observation that the CD81-CLDN-1 complex which shown to be essential in virus entry is entirely absent from the TJ (Harris *et al.* 2010). Furthermore, reduction in polarity mediated by addition of VEGF promotes HCV entry (Mee *et al.* 2010). Interestingly, it was shown that HCV infection actually modulated VEGF expression, suggesting that HCV infection causes a reduction in polarity (Mee *et al.* 2010).

In addition, it has been shown that hepatocyte filopodia extend through the sinusoidal membrane and into the sinusoids, where they contact T-cells (Warren *et al.* 2006) (Figure 4). Therefore, filopodia may make initial contacts with the virus here. To support this, DiD-HCV has been shown to associate with filopodia and travel along them towards the PM in Huh-7.5 cells (Coller *et al.* 2009). In the spread of HIV, long-lived interactions between filopodia-like structures on a target cell and an HIV-infected cell known as nanotubes have been shown to be important in virus transmission (Sowinski *et al.* 2008).

Therefore, the basolateral model of entry suggests that HCV enters the liver through the sinusoidal blood, encounters the basolateral-sinusoidal forms of the receptors first and enters the hepatocytes at this pole.

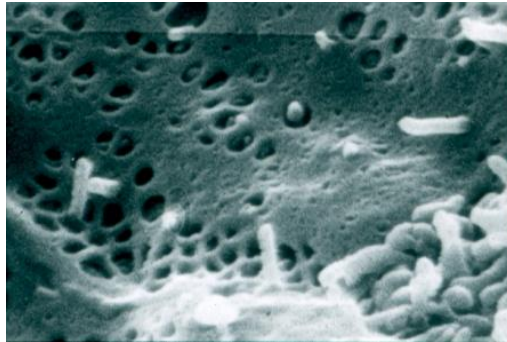


**Figure 4: Hepatocyte filopodia extend through the sinusoidal membrane.** From (Warren *et al.* 2006).

#### *1.6 Project objectives:*

We hypothesise that receptor diffusion will define HCV entry, and aim to cover the following points:

1. To characterise the mobility and diffusion of host cell molecules CD81, SR-BI, CLDN-1 and occludin in HepG2 cells and to ascertain whether cellular location alters receptor trafficking.
2. To ascertain whether HCV glycoproteins alter receptor mobility.
3. To define the effect of SR-BI antagonist ITX5601 on protein diffusion.

## 2 MATERIALS AND METHODS

### 2.1. Cell lines and reagents

HepG2 cells (ATCC) were propagated in Dulbecco's modified Eagle's medium (DMEM, 12491-023, Invitrogen) supplemented with 10% fetal bovine serum (10500-064, Invitrogen), 1% non-essential amino acids (11140-035, Invitrogen), 1%  $\gamma$ -glutamine (25030, Invitrogen) and 1% penicillin-streptomycin (15070063, Invitrogen) at 37°C.

Soluble (s) E2 and E1E2 (a kind gift from Chiron) were added to fluorescently tagged cells at a concentration of 0.7mM, which gave a 90% neutralisation of the HCV cell culture (HCVcc) system (data supplied by Chiron, not shown). The cells were then incubated for an hour at 37°C. Fluorescence recovery after photobleaching (FRAP) of proteins of interest was then carried out and analysed as described below (Section 2.4).

The small molecule inhibitor of SR-BI ITX5061 and the control compound ITX7094 (iTherX,) were added to fluorescently tagged cells at a concentration of 5 $\mu$ M (representing 90% neutralisation) and incubated for an hour at 37°C. FRAP on proteins of interest was then carried out and analysed as described below (Section 2.4).

### 2.2 Generation of fluorescently-tagged CD81, SR-BI, CDLN-1, occludin and glycosphatidylinositol (GPI) proteins

SR-BI, CD81, CLDN-1, occludin and GPI proteins were tagged with the monochlorionic *Aequorea coerulea* green fluorescent protein (AcGFP) tag or a *Discosoma sp.* Red monomer (DsRED) as previously described (Harris *et al.* 2008). These were transfected into HepG2 cells using Lipfectamine 200 (Invitrogen) according to manufacturer's instructions.

### 2.3 Laser Scanning Confocal Microscopy

HepG2 cells expressing AcGFP- tagged CD81, CLDN-1, OCLN-1, SR-BI, GPI, or DsRED-tagged CD81 were grown on 13-mm glass coverslips. The cells were imaged live in phenol red-free DMEM (11054001, Invitrogen) with 20 mM HEPES (15630049, Invitrogen) on a Zeiss Meta head laser scanning 780 confocal microscope with settings optimized for each fluorescent protein, and a 100 x1.4 NA oil immersion objective was used. The temperature was maintained at 37°C.

16 bit images were captured at 0.150s/frame, at 1024 pixels<sup>2</sup>. Using the Zeiss laser scanning confocal microscope software, regions of interest were selected were photobleached at 100% laser strength over 25 iterations to reduce the fluorescence of the fluorescently tagged proteins to around 50% of the original. Their recovery was monitored over time (see section 2.4) using the overlay, profiling and intensity frequency tools of the Zeiss laser scanning confocal microscope software. Fluorescence recovery was measured as average signal intensity, and the curves generated from background-subtracted and bleaching corrected images. Fluorescence signal was normalised to prebleach signals in the same region of interest.

Out of focus light was reduced by imaging a 0.5 $\mu$ m Z-section at the glass-cell interface using pseudo-total internal reflectance fluorescence (TIRF) microscopy.

#### *2.4 Fluorescence recovery after photobleaching (FRAP)*

The diffusion of proteins within a membrane is altered by a number of factors, including membrane composition, fluidity and associations with partner proteins and the cytoskeleton.

FRAP is widely used to find the speed of diffusion (diffusion coefficient), mobile fraction, and time to 50% recovery of original intensity ( $T_{1/2}$ ) of a protein within a membrane. In this technique, regions of membrane are bleached to 50% of the original fluorescence intensity and the recovery is monitored over time. Bleaching to this level prevents phototoxicity of the cell. In this study, the Zeiss Metahead laser scanning confocal microscope 780 was used to photobleach a Intensity recovery was then monitored over one minute using the Zeiss laser scanning confocal microscope software (Section 2.3).

It is necessary to take into account the possibility that the protein of interest may also be diffusing from within the cell in a process known as intracellular 'exchange' (Figure 5). If a protein is moving by lateral diffusion, then a small and large bleached area will each have a different  $T_{1/2}$ . However if the bleached patches are recovering by intracellular exchange then the two regions will have the same  $T_{1/2}$ .

By plotting the fluorescence of these bleached areas over time, it is possible to create a curve (Figure 6, Equation 1), and providing that the protein is only diffusing by one means it is possible to derive the  $T_{1/2}$  (equation 2) and mobile fraction of specific proteins

in selected areas (Figure 2). Furthermore, manipulation of the equation of the curve can give the diffusion coefficient of the protein (Equation 3).

If a protein is diffusing by both exchange and diffusion a more complex double exponential formulae will fit the curve more precisely.

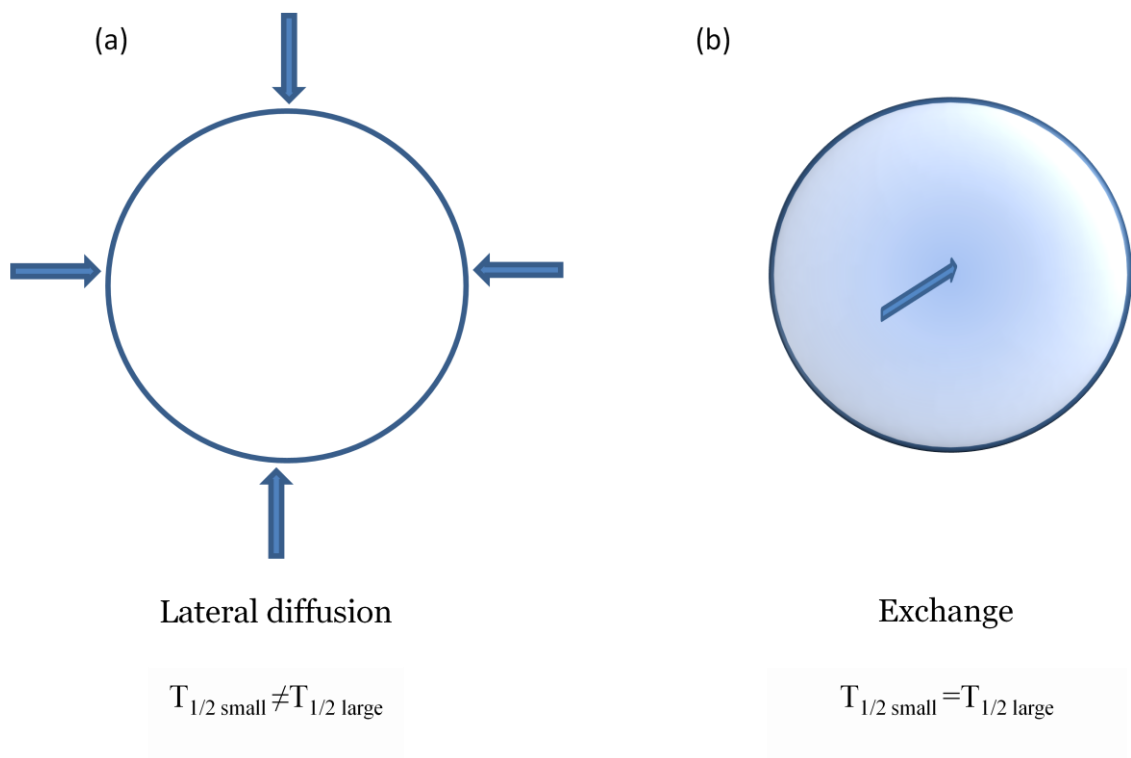


**Figure 5: Two possible modes of protein diffusion.** Lateral diffusion occurs from only within the plane of the membrane, where the  $T_{1/2}$  differs between small and large bleach spots (a). In exchange, the protein diffuses from intracellular compartments and the  $T_{1/2}$  is the same for small and large bleached regions.

In this study, the mode of diffusion was established by bleaching a range of sizes of regions of interest (ROI, Figure 7a) and observing that the  $T_{1/2}$  was not consistent i.e. the

time taken for half of fluorescence to recover was not consistent between bleached regions of different sizes in the time observed. Any regions of interest that did not fit these parameters were excluded. The only exception to this was occludin, which is trafficked to the tight junction from the cytoplasm. However, the fluorescence recovery of occludin fitted a single exponential curve and throughout the experiment the opportunity for diffusion by exchange was kept to a minimum by imaging a  $0.5\mu\text{m}$  Z-section at the glass-cell interface using pseudo-TIRF microscopy.

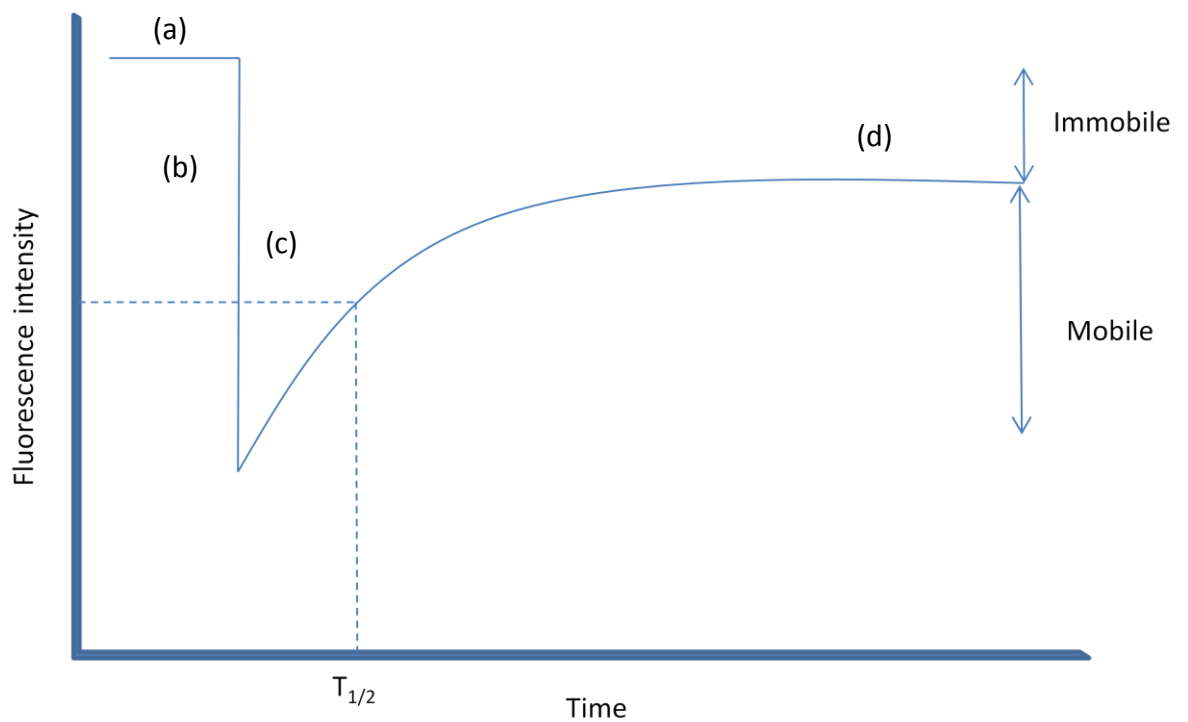


**Figure 6: Plot of diffusion intensity over time.** Initially, a prebleach value for the region of interest is recorded (a). Following bleaching (b), intensity recovers (c) before reaching a plateau of recovery (d). Plotting the recovery of fluorescence and establishing the equation of the resulting curve gives the mobile and immobile fractions,  $T_{1/2}$ , and diffusion coefficient.

$$Y = Y_{max}(1 - e^{-Kx}) \quad \text{Equation 1: Simple exponential}$$

$$T_{1/2} = \frac{0.69}{k} \quad \text{Equation 2}$$

$$\frac{0.224r^2}{t_{1/2}} \quad \text{Equation 3: Diffusion Coefficient}$$

## 2.5 Regions of interest

The structures examined in this report are detailed below (Figure. 7b). In all cases, filopodia are defined as small motile protrusions on the plasma membrane which are adhered to the glass surface and attached to the cell at one end only. As they are visible using confocal microscopy they are distinct from microvilli, but are smaller in length than nanotubes. The structures examined are as follows (Figure 7b): filopodia and plasma membrane (PM) in situations where there are no nearby cells ('free'), PM and filopodia in close proximity to another cell ('exploratory') and PM at cell junctions (cell contact). It should be noted that in order to qualify as 'exploratory' structures, there need not be contact between cells at other points.

Hepatocytes in the liver form intercellular contacts and extend filopodia through the sinusoidal membrane into the sinusoidal blood (Figure 4). These two regions are represented by 'contact' and 'exploratory' regions respectively in this study.

Regions of interest selected for bleaching were of various sizes, and more than 10 regions were bleached per cell (Figure 7a).

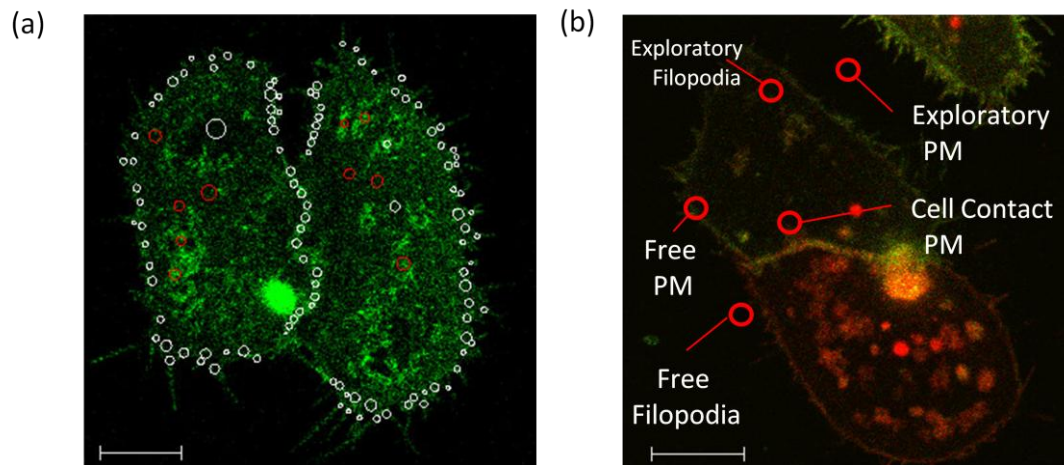


**Figure 7: Representative image of regions of interest and structures examined on a HepG2 cell expressing CD81-GFP.** Multiple bleach points were used for each structure. Image displayed is a HepG2 cell transfected to express AcGFP-CLDN-1 (a). Structures examined are as follows: ‘free’ filopodia and plasma membrane (PM), ‘exploratory’ PM and filopodia and ‘cell contact’ PM. Regions are displayed on HepG2 cells transfected with AcGFP-CLDN-1 and DsRED-CD81 (b). The cells were imaged on a Zeiss Meta head laser scanning 780 confocal microscope. Scale bars are 10  $\mu\text{m}$ .

## 2.6 Statistical analysis

Statistical analyses and data representation were carried out using GraphPad Prism software (GraphPad software), with significance calculated using one-way ANOVA with a Tukey’s post test. Where variances were unequal, the Student’s T test with a Mann-Whitney post test was use. The significances are represented as follows:  $p < 0.05$  (\*),  $p < 0.01$ (\*\*), and  $p < 0.001$  (\*\*\*). Unless otherwise stated, the values quoted are medians in order to take into account the non-Gaussian distribution of the data.

### 3. RESULTS

#### 2.1 Receptor localisation

HepG2 cells were transfected to express GFP-SR-BI, GFP-CD81, GFP-CLDN-1, GFP-occludin, and GFP-GPI. GFP-SR-BI was visible throughout the PM, although there were some areas of high PM staining (Figure 8a). However, there was very low expression in the filopodia, which were only just visible using confocal microscopy. In contrast, CD81 was visible uniformly around the PM with expression in the filopodia similar to that seen in the membrane. Again, there were areas of high PM staining (Figure 8b). In polarised cells, CLDN-1 had very high expression at the BC-like structure with lower basolateral PM staining (Figure 8c). Occludin had a distinctive expression pattern, with expression only visible at the tight junction around the BC-like structure (Figure 8d). The control protein GPI was visible uniformly throughout the membrane, with expression on all membranes (Figure 8e).

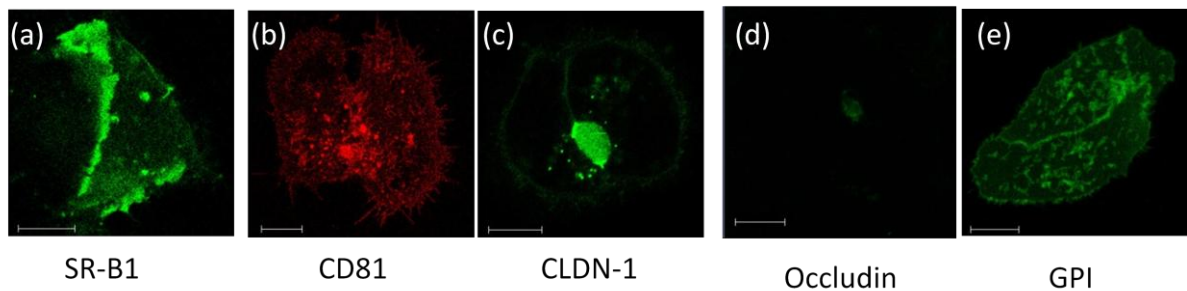


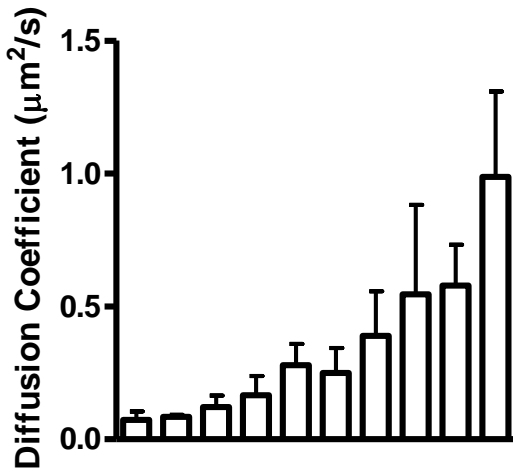
**Figure 8 : Representative images of receptor localisation.** Representative images of HepG2 cells transfected to express AcGFP-SRB-1(a), DsRed-CD81(b), AcGFP-CLDN-1(c), AcGFP-occludin (d), and AcGFP-GPI (e). The cells were imaged on a Zeiss Meta head laser scanning 780 confocal microscope. Scale bars are 10  $\mu$ m.

### *3.2 Variance between individual cells within a sample*

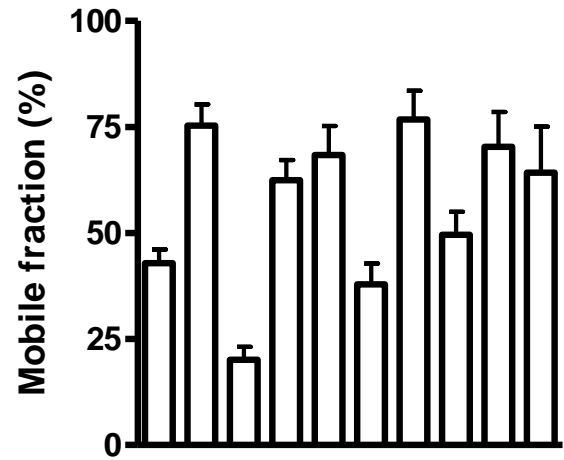
In order to examine the variance between cells within a sample, the diffusion coefficients and mobile fractions of CD81 were compared at both the plasma membrane and filopodia in 10 CD81-HepG2 cells (Figure 9). At both locations the diffusion coefficient appeared to vary widely between the samples, with a range of  $0.02 \mu\text{m}^2/\text{s}$  to  $1.5 \mu\text{m}^2/\text{s}$  in the filopodia and  $0.02 \mu\text{m}^2/\text{s}$  to  $1.7 \mu\text{m}^2/\text{s}$  in the PM (Figure 9 a, c). The mobile fraction also varied between cells within the sample (Figure 9 b, d) with mobile fractions ranging between 7.5% and 97% in the PM and 2.7% and 95.9% in the filopodia. These data show considerable variation in receptor kinetics between cells within a sample, and may represent multiple populations of protein as defined by different kinetics.

PM

(a)

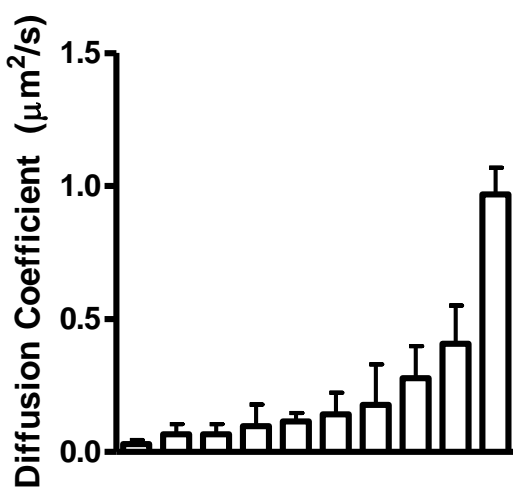


(b)



Filopodia

(c)



(d)

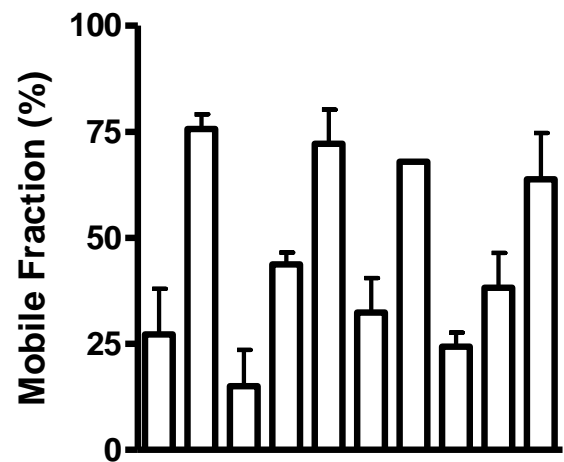


**Figure 9: Variance in diffusion coefficient and diffusion coefficient between cells in a sample.** Diffusion coefficient (a, c) and mobile fraction (c,d) at the PM ( a, b) and filopodia (c, d) between 10 HepG2 cells transfected to express GFP-CD81. Diffusion coefficient and mobile fraction were calculated using Zeiss software. Each bar represents the values for one cell, with more than 1 bleached spot per cell. Error bars represent SEM.

### *3.3 Differences in receptor dynamics between the PM and filopodia*

As it is possible that protein dynamics vary at different locations within in the cell, the diffusion coefficient and mobile fraction of the AcGFP-tagged proteins SRB1, CD81, CLDN-1 and occludin were measured in the plasma membrane and filopodia in HepG2 cells using FRAP. In addition, the lipid raft marker GPI was used as a non-HCV control (Figure 10).

Neither the diffusion coefficient nor mobile fraction of SR-BI varied significantly between the PM and filopodia. The median diffusion coefficients at the PM and filopodia were  $0.25 \mu\text{m}^2/\text{s}$  and  $0.22 \mu\text{m}^2/\text{s}$  respectively, and the mobile fractions 50.48% and 44.83% respectively. However, the diffusion coefficient appeared to display less variability than the mobile fraction between samples in both the PM and filopodia (Figure 10, Table 1).

The diffusion coefficient of CD81 at the filopodia was significantly higher than that in PM (Figure 10), with medians of  $0.23 \mu\text{m}^2/\text{s}$  and  $0.36 \mu\text{m}^2/\text{s}$  respectively, although the mobile fraction appeared lower at the latter with 55.6% of CD81 mobile at the PM compared to 41.14% at the filopodia (Table 1). Therefore, whilst the speed of diffusion of CD81 is greater in the filopodia, the mobility of the protein is reduced.

The mobile fraction of CLDN-1 showed a significantly larger variation in the filopodia than in the PM, whose values were more closely grouped at both regions than that of the mobile fraction. Again, the variance in diffusion coefficient was lower (Figure 10). Both diffusion coefficient and mobile fraction were significantly lower in the filopodia than the PM (Figure 10), with a median of 74.67% mobile at the PM and 53.27% at the filopodia, and median diffusion speeds of  $0.35 \mu\text{m}^2/\text{s}$  at the PM and  $0.24 \mu\text{m}^2/\text{s}$  at the filopodia (Table 1). This shows that both the speed and percentage of mobile CLDN-1 is reduced at the filopodia.

Data for GPI and occludin are presented in the appendix (Supplementary Figure 1, supplementary Table 1). Few data points were recorded for occludin as very few bleached areas recovered in the observation time. There was no significant difference in either diffusion coefficient or mobile fraction between the two structures at which occludin was visible – the plasma membrane and tight junction (Supplementary Figure 1). The data for the control protein GPI was very variable but displayed significant difference in both parameters (Supplementary Figure 1), with the mobile fraction appearing to be lower in the filopodia yet having a greater diffusion speed. The median mobile fraction of GPI at the PM was 64.94% with a median diffusion coefficient of  $0.06 \mu\text{m}^2/\text{s}$ , and the median mobile fraction at the filopodia was 50.47% with a median diffusion coefficient of  $0.02 \mu\text{m}^2/\text{s}$  (supplementary Table 1).

Therefore, receptor mobility and diffusion speed differ between intracellular sites, although the way in which these differ depends on the receptor. CLDN-1 and CD81 are particularly variable, whilst SR-BI is less so.

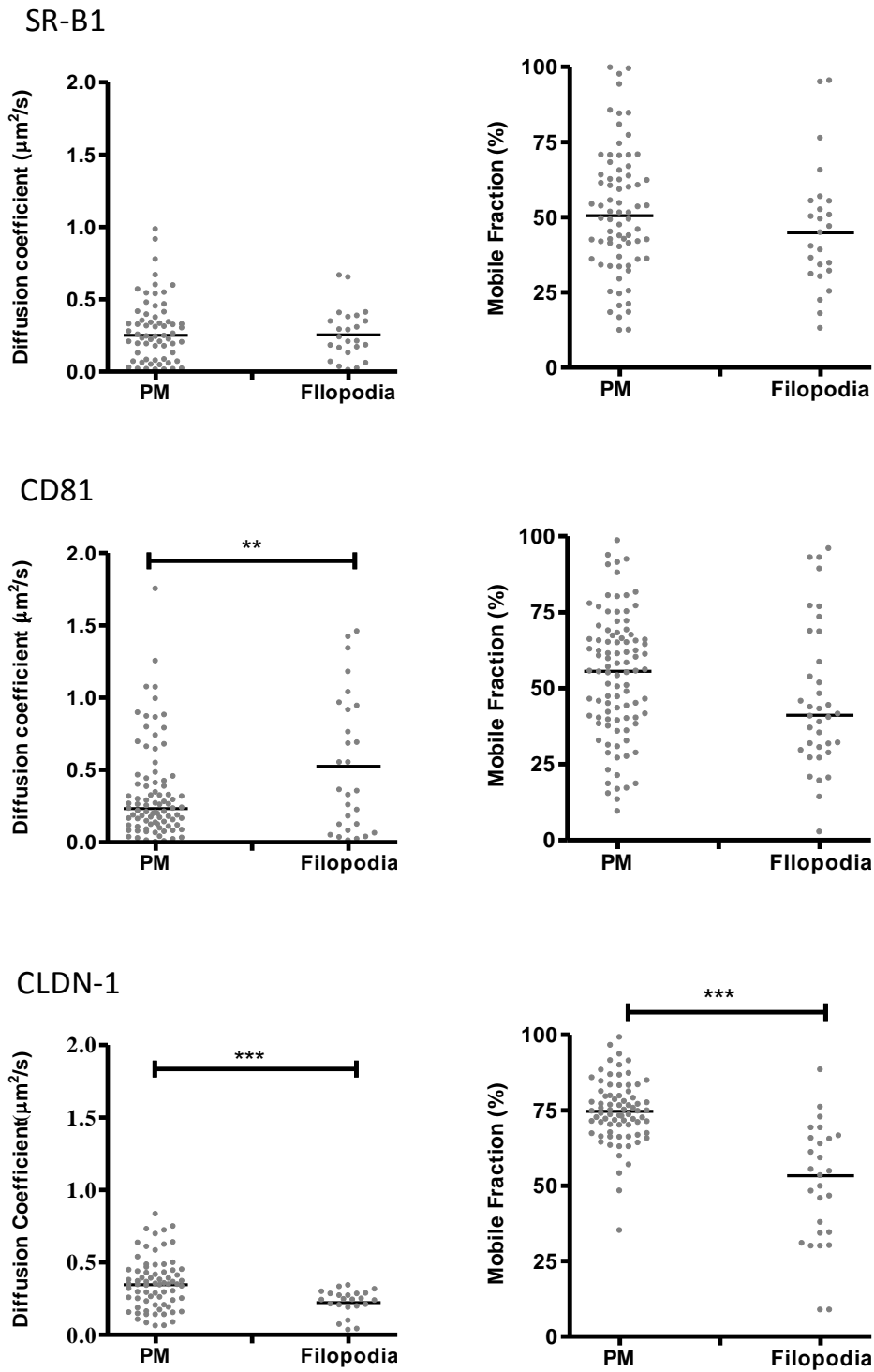


**Figure 10: Variance in diffusion coefficient and mobile fraction between PM and filopodia.** HepG2 cells were transfected to express GFP-SR-B1, GFP-CD81, DsRed-CD81, and GFP-CLDN-1 and bleached using a Zeiss Meta head laser scanning 780 confocal microscope. Diffusion coefficient and mobile fraction using data from Zeiss software. Each symbol represents one cell,  $n > 21$ , with more than 1 bleached region per cell.

Receptor/ parameter	Structure	Median (IQ range)	Mean	S.D
SR-B1 Diffusion coefficient ( $\mu\text{m}^2/\text{s}$ )	PM	<b>0.25</b> (0.28)	0.29	0.22
	Filopodia	<b>0.22</b> (0.22)	0.26	0.18
SR-B1 mobile fraction (%)	PM	<b>50.48</b> (28.7)	51.5	21
	Filopodia	<b>44.83</b> (23.76)	46	20.92
CD81 diffusion coefficient ( $\mu\text{m}^2/\text{s}$ )	PM	<b>0.23</b> (0.30)	0.34	0.32
	Filopodia	<b>0.36</b> (0.83)	0.53	0.47
CD81 mobile fraction (%)	PM	<b>55.6</b> (26.92)	53.77	20.29
	Filopodia	<b>41.12</b> (33.55)	46.48	23.95
CLDN-1 diffusion coefficient ( $\mu\text{m}^2/\text{s}$ )	PM	<b>0.35</b> (0.23)	0.35	0.18
	Filopodia	<b>0.24</b> (0.09)	0.22	0.09
CLDN-1 mobile fraction (%)	PM	<b>74.67</b> (11.67)	74.5	10.54
	Filopodia	<b>53.27</b> (31.52)	50.19	19.86

**Table 1: Median, interquartile range (IQ range), mean, and standard deviation (S.D) of data presented in Figure 10.** HepG2 cells were transfected to express GFP-SR-B1, GFP-CD81, DsRed-CD81, and GFP-CLDN-1 and bleached using a Zeiss Meta head laser scanning 780 confocal microscope. Statistics were calculated using data from Zeiss software.  $n > 21$ . Values calculated using GraphPad Prism Software.

### *3.4 Differences in receptor dynamics between specific cellular locations*

The large variances in receptor dynamics within the samples led us to examine the diffusion coefficient and mobility of the proteins in the PM and filopodia at areas of cell contact and exploratory regions as these may represent distinct 'pools' of receptors.

Again, there were no significant differences in the dynamics of SR-BI at more defined cellular locations. Also, the variability in results appeared to be greater in the mobile fraction, particularly at the exploratory PM edge (Figure 11, Table 2).

The variability in the diffusion coefficient of CD81 described in Figure 10 at the plasma membrane may be explained by the presence of two apparently separate pools of CD81—that at the exploratory membrane and that at the cell contact membrane. The latter was significantly higher than that at the exploratory membrane with a median diffusion coefficient of  $0.45 \mu\text{m}^2/\text{s}$  in comparison to  $0.19 \mu\text{m}^2/\text{s}$  at the exploratory PM (Table 2). This is matched by a non-significant increase in the mobile fraction of CD81 at the same region. However, mobile fraction data displayed large variability.

The data presented in Figure 10 show the variance of diffusion speed and mobile fraction of CLDN-1 between cells to be relatively low, suggesting that unlike CD81 there is only one pool of CLDN-1 as defined by receptor dynamics. Analysis of CLDN-1 mobility and diffusion speed at cell contact and exploratory filopodia and PM supported this hypothesis, and show that there are not multiple populations of CLDN-1 at the regions investigated.

As occludin was only visible at the TJs and at low levels in areas of cell contact its kinetics at more defined regions could not be examined (Supplementary Table 2). Again, the data for GPI is displayed in the appendix (Supplementary Figure 2, supplementary Table 2). Both the diffusion coefficient and mobile fraction of GPI were observed to be higher at the cell contact PM (median diffusion speed  $0.04 \mu\text{m}^2/\text{s}$  and mobile fraction 79.33%) than the filopodia (median diffusion speed  $0.003 \mu\text{m}^2/\text{s}$  and mobile fraction 50.4%) (Supplementary figure 2, Supplementary Table 2).

These data show that the speed of diffusion of CD81 is significantly higher in areas of cell contact, whereas other HCV receptors show no such significant diversity in dynamics between cellular sites.

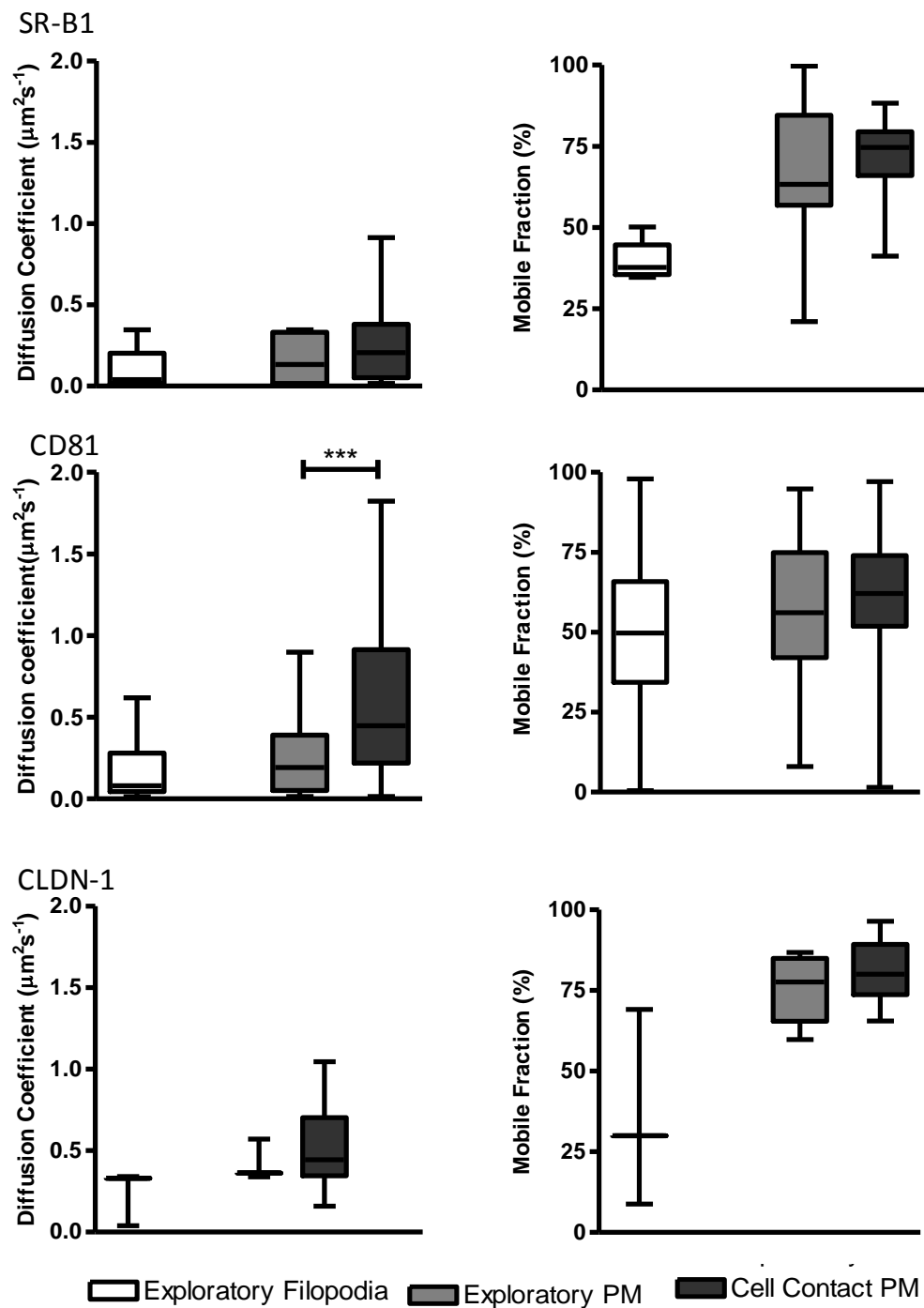


**Figure 11: Diffusion coefficient and mobile fraction of receptors at specific cellular structures.** Diffusion coefficient and mobile fraction measured in HepG2 cells transfected to express GFP-SR-BI, GFP-CD81, DsRed-CD81, and GFP-CLDN-1 at specific locations. Cells were bleached using a Zeiss Meta head laser scanning 780 confocal microscope and diffusion coefficient and mobile fraction were calculated using data from Zeiss software.  $n > 21$ , with more than 1 bleached region per cell. White bars represent exploratory filopodia, light grey exploratory PM, and dark grey cell contact PM.

	<b>Structure</b>	<b>Median (I.Q range)</b>	<b>Mean</b>	<b>S.D.</b>
SR-B1 Diffusion Coefficient ( $\mu\text{m}^2/\text{s}$ )	Exploratory PM	<b>0.13</b> (0.31)	0.16	0.15
	Exploratory filopodia	<b>0.04</b> (0.19)	0.11	0.16
	Cell contact PM	<b>0.21</b> (0.33)	0.26	0.26
SR-B1 Mobile Fraction (%)	Exploratory PM	<b>63.29</b> (27.67)	67.49	18.64
	Exploratory Filopodia	<b>37.73</b> (9.11)	40.07	6.97
	Cell Contact PM	<b>74.67</b> (13.52)	70.84	13.28
CD81 Diffusion Coefficient ( $\mu\text{m}^2/\text{s}$ )	Exploratory PM	<b>0.19</b> (0.34)	0.25	0.21
	Exploratory filopodia	<b>0.10</b> (0.34)	0.21	0.22
	Cell contact PM	<b>0.45</b> (0.69)	0.57	0.45
CD81 Mobile fraction (%)	Exploratory PM	<b>56.13</b> (32.84)	57.1	21.72
	Exploratory filopodia	<b>49.74</b> (31.55)	51.18	22.3
	Cell contact PM	<b>62.09</b> (22.17)	62.51	17.25
CLDN-1 Diffusion Coefficient ( $\mu\text{m}^2/\text{s}$ )	Exploratory PM	<b>0.36</b> (0)	0.42	0.13
	Exploratory filopodia	<b>0.33</b> (0)	0.24	0.17
	Cell Contact PM Edge	<b>0.44</b> (0.36)	0.51	0.22
CLDN-1 Mobile Fraction (%)	Exploratory PM	<b>77.64</b> (19.45)	75.69	10.66
	Exploratory filopodia	<b>29.96</b> (0)	35.96	30.64
	Cell contact PM	<b>73.86</b> (18.72)	74.5	13.63

**Table 2: Median, interquartile range (IQ range), mean, and standard deviation (S.D) of data presented in Figure 11.** HepG2 cells were transfected to express GFP-SR-BI, GFP-CD81, DsRed-CD81, and GFP-CLDN-1 and bleached using a Zeiss Meta head laser scanning 780 confocal microscope,  $n > 21$ . Diffusion coefficient and mobile fraction were calculated using data from Zeiss software. Values calculated using GraphPad Prism Software.

### *3.5 Addition of viral glycoproteins*

We were interested in whether addition of viral glycoproteins would alter the diffusion speed or mobility of HCV receptors. Therefore, we added the soluble viral glycoproteins sE2 (0.7mM) and sE1E2 (0.7mM) to cells expressing GFP-CLDN-1 or GFP/DsRed-CD81.

When looking at the effect of addition of sE2 and sE1E2 on filopodia and PM only, addition of sE2 caused a decrease in mobile fraction of both CD81 and CLDN-1, whereas addition of sE1E2 caused an increase in the diffusion coefficient of the filopodia (Figure 12).

However, when the regions of interest were expanded to include areas of exploratory regions and areas of cell contact, it became evident that the majority of the effects conferred by addition of the viral glycoproteins was on CLDN-1, particularly at areas of exploratory and cell contact rather than at 'free' regions (Table 3b).

Following addition of sE1E2, the mobile fraction of CLDN-1 was increased at the exploratory filopodia and exploratory PM from 48.08% to 72.72% and 48% to 62.37% respectively. In contrast, addition of sE1E2 decreased the diffusion coefficient of exploratory filopodia from  $0.91 \mu\text{m}^2/\text{s}$  to  $0.06 \mu\text{m}^2/\text{s}$  (Table 3b).

Addition of sE2 also caused a decrease in the mobile fraction of CLDN-1 at the exploratory PM and exploratory filopodia, with values decreasing from  $0.91 \mu\text{m}^2/\text{s}$  to  $0.09 \mu\text{m}^2/\text{s}$  and  $0.30$  to  $0.05 \mu\text{m}^2/\text{s}$  respectively. However, addition of sE2 did not exclusively cause decreases in diffusion coefficient, as addition of sE2 increased the diffusion coefficient of CLDN-1 from  $0.09 \mu\text{m}^2/\text{s}$  to  $0.54 \mu\text{m}^2/\text{s}$  at filopodia (Table 3b).

In contrast, the effects of addition of glycoproteins to cells expressing CD81 were not so varied, and were limited to the mobile fraction (Table 3a). Here, addition of sE1E2 caused a small but significant decrease in the mobile fraction at the filopodia from 61.74% to 60.20%. Addition of sE2 alone caused a decrease in mobile fraction of the protein from 68.23% to 56.84% (Table 3a).

During analysis it became evident that HepG2 cells expressing CD81 displayed small regions of high protein expression. As CD81 forms part of TEMs, we examined the diffusion parameters of CD81 at these regions, although they have not been identified as TEMs. When looking at these areas of high CD81 expression, addition of E2 significantly increased the mobile fraction at areas of high protein expression from 46.03% to 55.33% (Table 3a).

These data show that addition of the viral glycoproteins does cause a change in receptor movement, particularly CLDN-1 at exploratory regions.

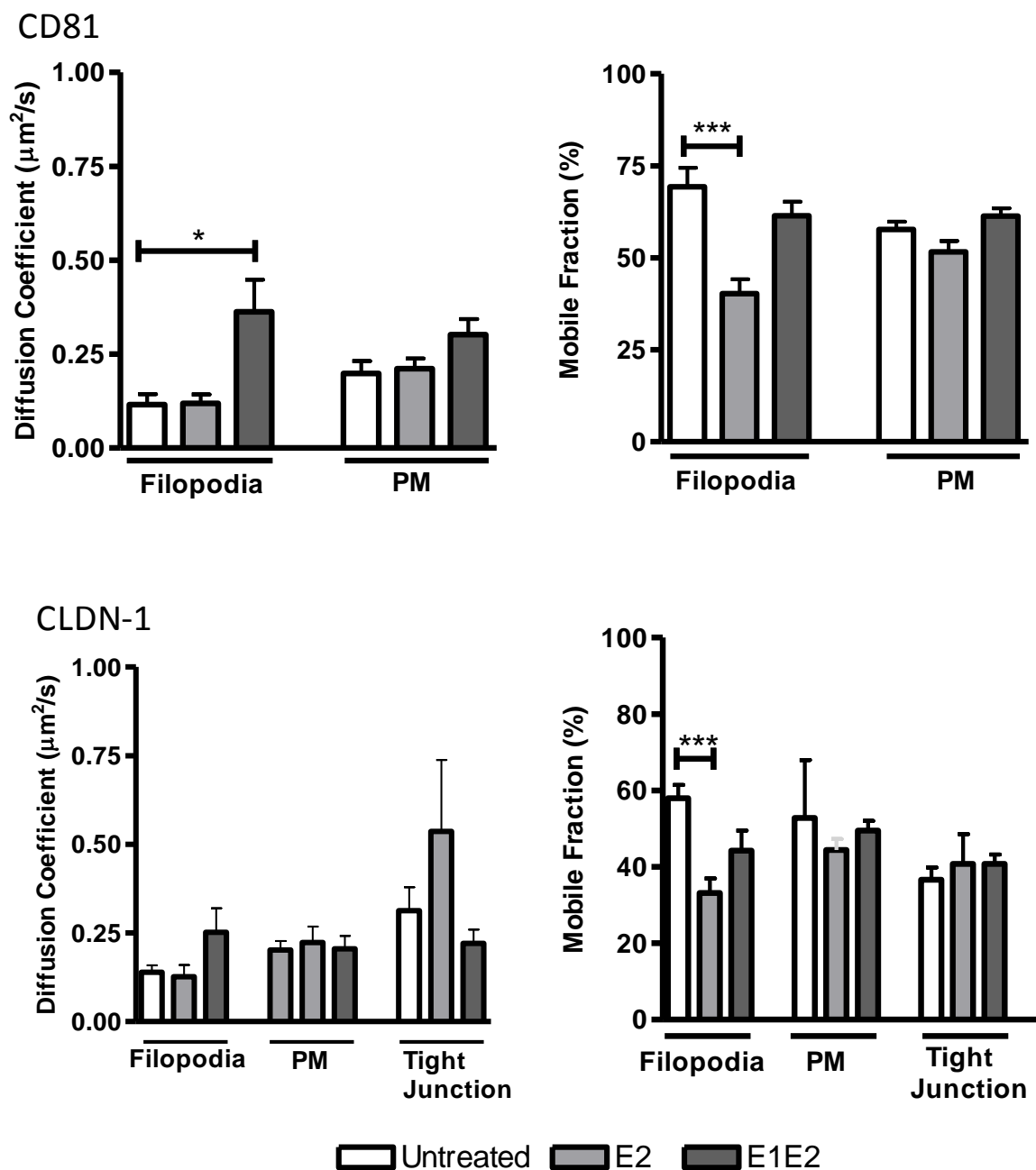


**Figure 12 : Diffusion coefficient and mobile fraction of CD81 and CLDN-1 following addition of viral glycoproteins.** Diffusion coefficient and mobile fraction measured in HepG2 cells transfected to express GFP-CD81, DsRed-CD81, and GFP-CLDN-1 at specific locations after the addition of the glycoproteins sE2 and sE1E2 at 0.7 mM. Cells were bleached using a Zeiss Meta head laser scanning 780 confocal microscope. Diffusion coefficient and mobile fraction were calculated using data from Zeiss software.  $n > 15$ , with more than one bleached region per cell. White bars correspond to untreated samples, light grey to addition of sE2 and dark grey to addition of sE1E2.

		Median (IQrange)	Mean	S.D	Significance
CD81 Diffusion Coefficient $\mu\text{m}^2/\text{s}$	<b>High PM</b>				
	Control	<b>0.16</b> (0.19)	0.21	0.23	
	sE2	<b>0.35</b> (0.21)	0.36	0.12	
	sE1E2	<b>0.20</b> (0.40)	0.28	0.23	
	<b>PM</b>				
	Control	<b>0.11</b> (0.11)	0.16	0.13	
	sE2	<b>0.10</b> (0.13)	0.15	0.17	
	sE1E2	<b>0.17</b> (0.12)	0.19	0.06	
	<b>Filopodia</b>				
	Control	<b>0.16</b> (0.37)	0.55	1.16	
	sE2	<b>0.07</b> (0.03)	0.09	0.05	
	sE1E2	<b>0.35</b> (0.27)	0.34	0.21	
	<b>Exploratory filopodia</b>				
	Control	<b>0.54</b> (0.00)	0.54	0.29	
	sE2	<b>0.05</b> (0.07)	0.06	0.04	
	sE1E2	<b>0.10</b> (0.00)	0.18	0.20	
	<b>Exploratory PM</b>				
	Control	<b>0.07</b> (0.86)	0.39	0.53	
sE2	<b>0.15</b> (0.29)	0.21	0.16		
sE1E2	<b>0.13</b> (0.11)	0.13	0.08		
<b>Cell contact PM</b>					
Control	<b>0.16</b> (0.19)	0.21	0.15		
sE2	<b>0.19</b> (0.28)	0.24	0.19		
sE1E2	<b>0.33</b> (0.49)	0.41	0.37		
CD81 Mobile Fraction (%)	<b>High PM</b>				
	Control	<b>46.03</b> (10.28)	45.81	10.96	
	sE2	<b>64.77</b> (20.87)	61.10	11.33	
	sE1E2	<b>55.22</b> (32.53)	55.73	19.11	*
	<b>PM</b>				
	Control	<b>56.11</b> (23.62)	50.92	11.93	
	sE2	<b>49.26</b> (20.09)	42.67	15.02	
	sE1E2	<b>65.14</b> (9.00)	64.16	10.17	
	<b>Filopodia</b>				
	Control	<b>61.74</b> (36.36)	71.86	19.80	
	sE2	<b>51.44</b> (12.33)	50.14	9.93	
	sE1E2	<b>60.20</b> (15.48)	58.20	11.57	**
	<b>Exploratory filopodia</b>				
	Control	<b>57.16</b> (0.00)	59.99	17.11	
	sE2	<b>18.27</b> (21.67)	23.40	12.31	
	sE1E2	<b>75.94</b> (0.00)	72.33	16.41	
	<b>Exploratory PM</b>				
	Control	<b>53.70</b> (33.26)	47.29	17.35	
sE2	<b>37.51</b> (10.03)	38.56	5.22		
sE1E2	<b>57.68</b> (9.58)	58.19	6.21		
<b>Cell contact PM</b>					
Control	<b>68.23</b> (11.44)	70.04	10.97		
sE2	<b>56.84</b> (37.85)	66.91	20.42	**	
sE1E2	<b>68.74</b> (22.89)	65.37	14.06		

**Table 3a: Median, interquartile range (IQ range), mean, and standard deviation (S.D) of CD81 following addition of sE2 and sE1E2. Diffusion coefficient and mobile fraction of CD81 at various cellular locations following addition of viral glycoproteins to HepG2 cells transfected to express AcGFP-CD81 and Ds-RED CD81.**

	Structure.compound	Median (IQ Range)	Mean	S.D.	Significance
CLDN-1 Diffusion Coefficient ( $\mu\text{m}^2/\text{s}$ )	<b>PM</b>				
	Control	<b>0.13</b> (0.24)	0.1596	0.1289	
	sE2	<b>0.10</b> (0.16)	0.1356	0.1144	
	sE1E2	<b>0.15</b> (0.16)	0.1678	0.1167	
	<b>Filopodia</b>				
	Control	<b>0.09</b> (0.09)	0.07363	0.04763	
	sE2	<b>0.54</b> (1.18)	0.6957	0.5723	**
	sE1E2	<b>0.23</b> (0.33)	0.2435	0.2086	
	<b>Exploratory filopodia</b>				
	Control	<b>0.30</b> (0)	0.5455	0.4993	
	sE2	<b>0.05</b> (0.20)	0.1036	0.09757	*
	sE1E2	<b>0.37</b> (0)	0.4071	0.1276	
	<b>Exploratory PM</b>				
	Control	<b>0.91</b> (1.28)	0.9595	0.751	
	sE2	<b>0.09</b> (0.11)	0.09265	0.07248	*
sE1E2	<b>0.06</b> (0.05)	0.07648	0.03999	*	
<b>Cell contact PM</b>					
Control	<b>0.13</b> (0.29)	0.1761	0.1448		
sE2	<b>0.06</b> (0.07)	0.05474	0.03282		
sE1E2	<b>0.07</b> (0.16)	0.09134	0.08051		
CLDN-1 Mobile Fraction (%)	<b>PM</b>				
	Control	<b>55.72</b> (25.65)	53.27	16.11	
	sE2	<b>45.41</b> (25.64)	45.55	14.39	
	sE1E2	<b>56.51</b> (17.67)	52.69	16.18	
	<b>Filopodia</b>				
	Control	<b>59.33</b> (14.92)	61.77	11.24	
	sE2	<b>42.41</b> (13.8)	43.24	9.168	
	sE1E2	<b>41.95</b> (20.63)	37.45	13.57	
	<b>Exploratory filopodia</b>				
	Control	<b>46.08</b> (0)	46.41	5.19	
	sE2	<b>11.06</b> (9.12)	15.91	11.01	
	sE1E2	<b>72.72</b> (0)	69.24	20.38	***
	<b>Exploratory PM</b>				
	Control	<b>48</b> (17.79)	50.29	9.255	
	sE2	<b>31.12</b> (17.06)	33.65	9.198	
sE1E2	<b>62.37</b> (11.21)	61.42	7.454	*	
<b>Cell contact PM</b>					
Control	<b>70.66</b> (8.53)	71.09	6.072		
sE2	<b>57.66</b> (40.82)	48.45	25.42		
sE1E2	<b>43.16</b> (20.76)	41.82	16.48		

**Table 3b: Median, interquartile range (IQ range), mean, and standard deviation (S.D) CLDN-1 following addition of sE2 and sE1E2. Diffusion coefficient and mobile fraction of CLDN-1 at various cellular locations following addition of viral glycoproteins in HepG2 cells transfected to express AcGFP-CLDN-1.**

### 3.6 Addition of ITX5061 and ITX7094

The small molecule inhibitor ITX5061 has been shown to reduce infection in an SR-BI dependent manner (Syder *et al.* 2011). This compound and the corresponding control compound ITX7094 were added to cells expressing GFP-SR-BI, GFP-CLDN-1, GFP and DsRed-CD81. The mobile fraction and diffusion coefficients of these proteins were examined after an hour of incubation with the compound.

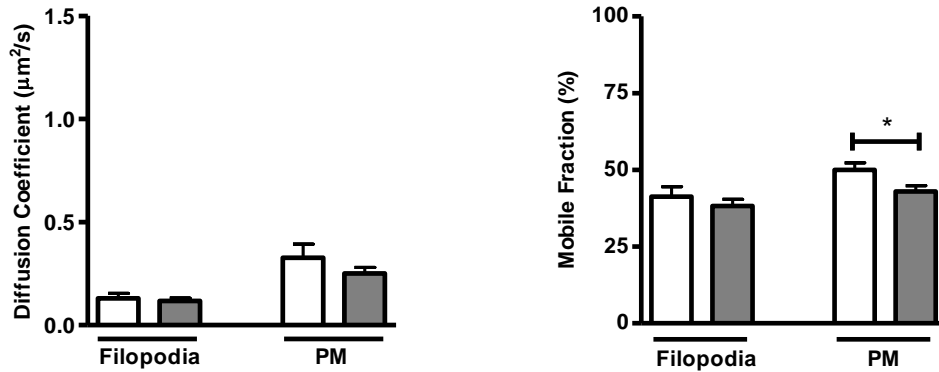
When looking at the PM and filopodia alone, addition of ITX5061 appeared only to affect the kinetics protein at the PM of SR-BI, CD81, and CLDN-1(Figure 13), with addition decreasing the mobile fraction of SR-BI at this region but increasing the diffusion coefficient of both CD81 and CLDN-1 at the PM (Figure 13). However when the regions were expanded to include exploratory and cell contact regions, many additional effects were observed.

Addition of ITX5061 caused a decrease in mobile fraction of SR-BI in three regions; at the exploratory PM from 45.68% to 34.13%; exploratory filopodia from 41.71% to 32.34%; and at the cell contact PM from 57.72 % to 33.18% (Table 4a). In contrast, the effects on CD81 and CLDN-1 were only on the diffusion coefficients of the protein, which in all cases resulted in an increase. Addition of ITX5061 increased the diffusion coefficients of both CD81 and CLDN-1 at the exploratory filopodia (Table 4b, c), but CD81 only at filopodia and areas of low expression and CLDN-1 only at the plasma membrane and exploratory PM Figure 4 (Table 4b, c).

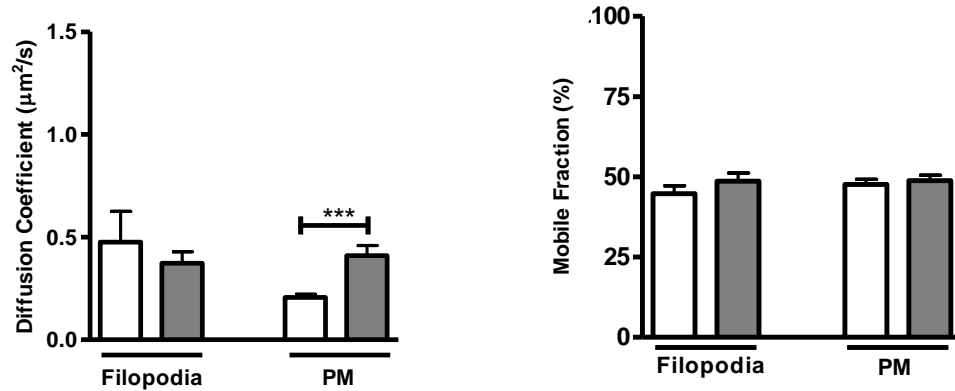
Addition of sE1E2 or sE2 alone had no effect on CD81 at areas of high CD81 expression, the putative TEMs (Table 4b).

Therefore, we show that the effects of addition of the small molecule SR-BI inhibitor ITX5061 are not restricted to SR-BI, but the effects on this protein is distinct the effects of the drug on CD81 and CLDN-1.

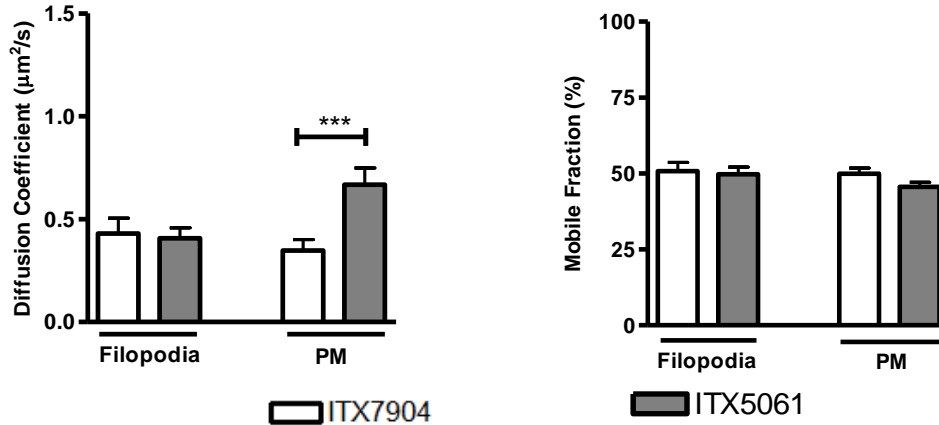
SR-B1



CD81



CLDN-1



□ ITX7904

■ ITX5061

**Figure 13: Diffusion coefficient and mobile fraction of CD81 and CLDN-1 following addition of ITX5061 and ITX7904.** Variance in diffusion coefficient and mobile fraction between HepG2 cells transfected to express GFP-SR-B1, GFP-CD81, DsRed-CD81, and GFP-CLDN-1 at specific locations after the addition of ITX5061 and ITX7904. Cells were bleached using a Zeiss Meta head laser scanning 780 confocal microscope n>15, with more than 1 bleached spot per cell. Diffusion coefficient and mobile fraction were calculated as previously described using data from Zeiss software. White bars represent addition of ITX7904, and light grey bars addition of ITX5061.

	Structure/compound	Median (IQ range)	Mean	S.D	Significance
SR-BI Diffusion Coefficient ( $\mu\text{m}^2/\text{s}$ )	PM				
	ITX7904	<b>0.17</b> (0.22)	0.22	0.16	
	ITX5061	<b>0.27</b> (0.21)	0.34	0.24	
	Filopodia				
	ITX7904	<b>0.21</b> (0.17)	0.27	0.22	
	ITX5061	<b>0.18</b> (0.17)	0.22	0.11	
	Exploratory filopodia				
	ITX7904	<b>0.04</b> (0.00)	0.04	0.00	
	ITX5061	<b>0.07</b> (0.13)	0.09	0.07	
	Exploratory PM				
	ITX7904	<b>0.44</b> (0.52)	0.45	0.25	
	ITX5061	<b>0.22</b> (0.40)	0.32	0.29	
Cell contact PM					
ITX7904	<b>0.25</b> (0.40)	0.27	0.20		
ITX5061	<b>0.24</b> (0.30)	0.27	0.30		
SR-BI Mobile Fraction (%)	PM				
	ITX7904	<b>48.86</b> (16.01)	44.01	11.98	
	ITX5061	<b>48.85</b> (18.19)	50.86	11.14	
	Filopodia				
	ITX7904	<b>43.59</b> (9.91)	47.98	11.04	
	ITX5061	<b>51.14</b> (10.86)	49.82	6.153	
	Exploratory filopodia				
	ITX7904	<b>41.71</b> (12.68)	44.14	21.59	
	ITX5061	<b>32.34</b> (11.19)	32.18	7.488	*
	Exploratory PM				
	ITX7904	<b>45.68</b> (17.39)	46.6	13.23	
	ITX5061	<b>34.13</b> (14.77)	33.92	12.27	*
Cell contact PM					
ITX7904	<b>57.72</b> (18.33)	63.23	17.09		
ITX5061	<b>33.18</b> (13.69)	36.25	10.75	***	

**Table 4a: Median, interquartile range (IQ range), mean, and standard deviation (S.D) of SR-BI following addition of ITX5061 and ITX7904. Diffusion coefficient and mobile fraction of SR-BI at various cellular locations following addition of ITX5061 and ITX 7904 HepG2 cells transfected to express GFP-SR-BI.**

		Median (IQ range)	Mean	S.D.	Significance
Cd81 Diffusion Coefficient ( $\mu\text{m}^2/\text{s}$ )	<b>High PM</b>				
	ITX7904	<b>0.24</b> (0.19)	0.286	0.1436	
	ITX5061	<b>0.41</b> (0.17)	0.401	0.1015	
	<b>PM</b>				
	ITX7904	<b>0.13</b> (0.19)	0.168	0.1291	
	ITX5061	<b>0.21</b> (0.24)	0.293	0.3743	*
	<b>Filopodia</b>				
	ITX7904	<b>0.15</b> (0.12)	0.188	0.1748	
	ITX5061	<b>0.30</b> (0.30)	0.286	0.1826	
	<b>Exploratory filopodia</b>				
	ITX7904	<b>0.10</b> (0.19)	0.253	0.3974	
	ITX5061	<b>0.41</b> (0.64)	0.557	0.4761	*
	<b>Exploratory PM</b>				
	ITX7904	<b>0.20</b> (0.27)	0.333	0.3202	
ITX5061	<b>0.37</b> (0.77)	0.567	0.5426	*	
<b>Cell contact PM</b>					
ITX7904	<b>0.35</b> (0.17)	0.365	0.1516		
ITX5061	<b>0.42</b> (0.40)	0.547	0.4818		
CD81 Mobile Fraction (%)	<b>High PM</b>				
	ITX7904	<b>60.40</b> (4.54)	59.54	3.616	
	ITX7904	<b>55.95</b> (14.51)	55.22	8.77	
	<b>PM</b>				
	ITX7904	<b>55.36</b> (13.78)	52.93	9.308	
	ITX5061	<b>54.94</b> (18.52)	58.13	12.15	
	<b>Filopodia</b>				
	ITX7904	<b>50.91</b> (16.14)	49.72	11.94	
	ITX5061	<b>55.35</b> (10.88)	56.44	11.95	
	<b>Exploratory PM</b>				
	ITX7904	<b>43.54</b> (15.9)	43.25	13.23	
	ITX5061	<b>47.2</b> (17.62)	46.71	12.69	
	<b>Exploratory Filopodia</b>				
	ITX7904	<b>38.14</b> (20.38)	43.51	21.48	
ITX5061	<b>33.92</b> (23.87)	37.93	14.97		
<b>Cell contact PM</b>					
ITX7904	<b>36.23</b> (15.11)	36.54	12.75		
ITX5061	<b>39.84</b> (10.22)	41.48	11.47		

**Table 4b: Median, interquartile range (IQ range), mean, and standard deviation (S.D) of CD81 following addition of ITX5061 and ITX7904. Diffusion coefficient and mobile fraction of CD81 at various cellular locations following addition of ITX5061 and ITX7904 HepG2 cells transfected to express GFP-CD81.**

		Median (IQ range)	Mean	S.D	Significance
CLDN-1 Diffusion Coefficient ( $\mu\text{m}^2/\text{s}$ )	<b>PM</b>				
	ITX7904	<b>0.19</b> (0.13)	0.2369	0.1449	
	ITX5061	<b>0.34</b> (0.28)	0.3541	0.2194	*
	<b>Filopodia</b>				
	ITX7904	<b>0.33</b> (0.39)	0.385	0.2705	
	ITX5061	<b>0.34</b> (0.39)	0.4641	0.3049	
	<b>Exploratory filopodia</b>				
	ITX7904	<b>0.15</b> (0.20)	0.1703	0.1433	
	ITX5061	<b>0.45</b> (0.24)	0.521	0.1837	*
	<b>Exploratory PM</b>				
	ITX7904	<b>0.04</b> (0.16)	0.1111	0.1436	
	ITX5061	<b>0.39</b> (0.31)	0.4227	0.2203	**
<b>Cell Contact PM</b>					
ITX7904	<b>0.28</b> (0.20)	0.2782	0.1501		
ITX5061	<b>0.39</b> (0.82)	0.5355	0.5069		
CLDN-1 Mobile Fraction (%)	<b>PM</b>				
	ITX7904	<b>57.96</b> (13.83)	56.24	10.89	
	ITX5061	<b>50.72</b> (17.28)	49.21	10.3	
	<b>Filopodia</b>				
	ITX7904	<b>53.42</b> (18.63)	53.52	12.59	
	ITX5061	<b>53.75</b> (20.23)	55.5	11.85	
	<b>Exploratory filopodia</b>				
	ITX7904	<b>44.95</b> (0)	43.15	3.95	
	ITX5061	<b>47.59</b> (24.24)	45.8	14.62	
	<b>Exploratory PM</b>				
	ITX7904	<b>55.76</b> (29.42)	53.68	15.28	
	ITX5061	<b>58.96</b> (34)	56.08	17.85	
<b>Cell Contact PM</b>					
ITX7904	<b>38.21</b> (12.06)	39.57	12.06		
ITX5061	<b>42.29</b> (9.85)	42.04	5.746		

**Table 4c: Median, interquartile range (IQ range), mean, and standard deviation (S.D) CLDN-1 following addition of ITX5061 and ITX7904. Diffusion coefficient and mobile fraction of CLDN-1 at various cellular locations following addition of ITX5061 and ITX7904 HepG2 cells transfected to express GFP-CLDN-1.**

## 4 DISCUSSION

This study aimed to define the kinetics of the essential HCV receptors SR-BI, CD81, CLDN-1 and occludin in HepG2 cells. Furthermore, we aimed to discern the effects of addition of the viral glycoproteins sE2 and sE1E2 and the small molecule inhibitor ITX5061.

### 4.1 Protein localisation

The results of this report show all SR-BI, CD81, CLDN-1 and occludin to be localised in HepG2 cells as previously reported (Mee *et al.* 2009). Both SR-BI and CD81 were visible throughout the cell membrane, whereas CLDN-1 was shown to be localised at high levels at the TJ/ BC-like region and at lower levels in the basolateral membrane. Additionally, occludin was localised exclusively to TJs.

SR-BI showed poor expression in filopodia in HepG2 cells in comparison to that the plasma membrane (Figure 8). In non-polarised Huh-7.5 cells DiD-HCV particles have been reported to initially bind to filopodia and travel along them to the plasma membrane, as has been reported for other viruses and cell types (Duus *et al.*, 2004; Smith and Helenius, 2004; Lehmann *et al.*, 2005, Schelhaas *et al.*, 2008; Collier *et al.*, 2009). It is possible that SR-BI is necessary at an early stage in the infection process for delipidating the virus particle and allowing cell surface receptors access to the viral glycoprotein complex E1E2. Therefore, the low level of SR-BI observed suggests one of three possibilities: binding of glycoproteins to HepG2 cells does not require transport along filopodia (1); in *in vitro* assays using HepG2 cells, glycoproteins bind to another receptor first in the filopodia, before binding to SR-BI (2); in HepG2 cells, transport of HCV glycoproteins along filopodia does not occur (3). Continuation of this study could quantitatively assess the effect of glycoprotein addition on

SR-BI protein levels at the filopodia in HepG2 cells, and look for binding of fluorescently tagged virus particles to filopodia.

In addition, SRB1 has been shown to be particularly important in cell-cell transmission, whereas CD81 and CLDN-1 have similar much the same levels of importance in both cell-cell and cell free transmission (Brimacombe *et al.* 2011). As filopodia would not be present at areas of cell contact, SR-BI may be preferentially localised to other sites. Again, further work could examine SRB-1 levels at specific sites and quantitatively observe the changes in these levels on addition of HCV glycoproteins or fluorescent virus.

The actin cytoskeleton is central to the formation of filopodia, which are formed downstream of Cdc42 and Rif (Ridley *et al.*, 2011). Little is known about the membrane of filopodia with regards to its composition and receptor expression, but it is possible that such a structure may express a different receptor profile to the rest of the cell.

The results presented here show that although there is no significant change in SR-BI dynamics between the PM and filopodia, there is a small decrease at the filopodia which could be further examined.

The diffusion coefficient of CD81 was shown to be higher in the filopodia than at the PM, whereas CLDN-1 was the opposite. However, two had a relatively similar diffusion speed in the PM, and therefore the receptor complexes formed by CD81 and CLDN-1 may be separated in the filopodia.

To examine the possibility of the CD81-CLDN-1 complex being separated, fluorescence resonance energy transfer (FRET) could be used to investigate the relationship between the

two at PM and filopodia. Investigation of the role of actin dynamics would be interesting, and perturbation of actin polymerisation could be achieved by the addition of cytochalasin D or similar compound.

#### 4.2 Protein diffusion kinetics

The diffusion coefficient and mobile fraction of CD81 and SR-BI have not previously been reported, although that of the close relative of CD81, CD9, has (Espenel *et al.* 2008). Using the prostatic carcinoma cell line PC3, the diffusion coefficient of CD9 was shown to be  $0.23 \pm 0.15 \mu\text{m}^2/\text{s}$ . This data corresponds with that seen in this study for CD81 diffusion at the PM (Table 5). This study also examined the diffusion coefficient of CD46, which is not present in TEMs or rafts, and therefore it may be used as a comparison for SR-BI. The diffusion coefficient of CD46 was  $0.13 \mu\text{m}^2/\text{s} \pm 0.08 \mu\text{m}^2/\text{s}$ . This is lower than that seen in this study for SR-BI, likely due to significant differences in association with other components of the cell membrane along with cell type differences.

Observation of occludin showed the protein to be very static within the tight junction (Table 5), in direct contrast to recent paper (Shen *et al.*, 2008) using MDCK cells. MDCK cells overexpressing EMK1 may be used as a model for looking at hepatic phenotype (Cohen *et al.* 2004). However, the cells used in that study did not overexpress EMK1, and therefore may form a functionally different TJ structure.

Again, the figures quoted for CLDN-1 show a more restricted diffusion pattern for the protein than observed in this study, and this may be due to cell-type specific differences. However, despite showing a higher diffusion coefficient in HepG2 cells ( $0.26 \mu\text{m}^2/\text{s}$ ) in

comparison to MDCK cells ( $0.01 \mu\text{m}^2/\text{s}$ ); the mobile fractions at the tight junction were similar between the two cell types. 33.14% of CLDN-1 was mobile at the tight junction in HepG2 cells, and 40% in MDCK cells (Shen 2008).

GPI appeared to diffuse at a lower speed than previously described, with a median of  $0.06 \mu\text{m}^2/\text{s}$  in comparison to  $1.2 \pm 0.2 \mu\text{m}^2/\text{s}$ , (Barreiro *et al.* 2008). However, the quoted speeds were calculated in HUVECs, and therefore these differences may be due to differences between cell types. In contrast the mobile fraction was much higher in HepG2 cells, 64.94% in comparison to <10% in HUVECs.

Receptor	Diffusion coefficient ( $\mu\text{m}^2/\text{s}$ )	Reported diffusion coefficient ( $\mu\text{m}^2/\text{s}$ )	Mobile fraction (%)	Reported mobile fraction (%)	Cell type	Reference
<b>SRB1</b>	Filopodia: 0.29 PM: 0.26		Filopodia: 46 PM: 51.50			
<b>CD81</b>	Filopodia: 0.53 PM: 0.23	-	Filopodia: 46.48 PM: 53.77	-	-	-
<b>CLDN-1</b>	Filopodia: 0.22 PM: 0.35 Tight junction: 0.26	Tight Junction: 0.01	Filopodia: 50.19 PM: 74.50 Tight junction: 33.14%	Tight Junction: 40 PM: 0	MDCK	Shen <i>et al.</i> , 2008
<b>Occludin</b>	Tight Junction: 0.38 PM: 0.58	Tight Junction: 0.01 PM: 0.1	Tight junction: 7.75 PM: 11.17	Tight Junction: 80 PM: 20	MDCK	Shen <i>et al.</i> , 2008

**Table 5: Comparison of diffusion kinetics presented in this study and those from previously published data**

### *4.3 Addition of viral glycoproteins*

The soluble viral glycoproteins sE2 and sE1E2 were added to assess their affect on receptor dynamics. If considering only the broad groupings seen in figure 12, the two treatments had similar effects on both CD81 and CLDN-1; addition of sE2 caused a significant decrease in mobile fraction at the filopodia, and addition of sE1E2 caused an increase in diffusion coefficient at both. However, for this latter point only the data for CD81 showed a significant change.

When the regions of interest were expanded to include exploratory and cell contact regions, it became obvious that the majority of the effects mediated by addition of the glycoproteins occurred with CLDN-1. The mobile fraction of CLDN-1 was increased and the diffusion coefficient decreased by addition of sE1E2 at both exploratory regions; and addition of addition of sE2 also caused a decrease in the protein at the exploratory PM and an increase at filopodia. In contrast, there were few effects observed on addition of the glycoproteins to cells expressing CD81. In these cells, addition of sE2 and sE1E2 caused a decrease in mobile fraction at the cell contact PM and filopodia respectively, and addition of sE1E2 increase the mobile fraction of CD81 at areas of high protein expression.

Therefore, the majority of the effects of glycoprotein addition were in the areas of cell contact or exploratory regions of the cells, particularly at the filopodia. CLDN-1 and CD81 were both visible in the filopodia (Figure 4), and engagement of CD81 has been shown to activate the Rho GTPase, Cdc42, which coordinates actin cytoskeletal rearrangements in a

manner which is complimentary to infection (Brazzoli *et al.*, 2008). Engagement of CD81 has been shown to result in the movement of CD81 to areas of cell contact (Brazzoli *et al.* 2008) and therefore, the decrease in mobile fraction of CD81 at the cell contact plasma membrane may relate to this movement. Additionally, the changes in diffusion coefficient and mobile fraction of CDLN-1 at areas other than cell contact following addition of the viral glycoproteins may be caused by the relocation of CD81 causing a breakdown of CD81-CDLN-1 receptor complexes as the protein moves. However, Harris *et al.*, (Harris *et al.*, 2008) showed that in Huh-7.5 cells addition of sE1E2 did not increase or decrease the colocalisation of the proteins, but it did decrease the distance between the two. However, these interactions may differ in a more polarised cell line.

Additionally, filopodia form downstream of Cdc42 (Ridley *et al.*, 2011); and therefore engagement of CD81 leading to cytoskeletal rearrangements may lead to an increase in the number of filopodia per cell. This may cause a change in receptors dynamics at the cell surface, as we have shown previously that receptor dynamics at the PM are different to those at the filopodia for these two proteins.

#### ***Addition of ITX5061 and ITX7094***

Whether ITX5061 acts as a functional or structural inhibitor is unknown. As it reduces HCV binding to hepatoma cells, the drug certainly appears to impair structural interactions (Syder *et al.* 2011). Furthermore, evidence suggests that the structural interaction between sE2 and SRB1 is important (Scarselli *et al.*, 2002; Syder *et al.*, 2011).

However, there is a large amount of evidence supporting the importance of lipoproteins in HCV infection, with HDL addition enhancing infectivity and cholesterol depletion reducing it (Syder *et al.*, 2011). ITX5061 promotes plasma HDL levels in human and animal models, apparently by preventing their catabolism without increasing LDL or very low density lipoproteins (vLDL) (Masson *et al.* 2009). Furthermore, *in vitro* data show addition of ITX5061 to reduce SR-BI-mediated HDL lipid transfer (Masson *et al.*, 2009) and ITX5061 will only inhibit forms of SR-BI which can bind HDL or LDL (Gu *et al.* 2000).

Therefore, it has been suggested that ITX5061 may mimic oxidised lipid species, as oxLDL has been shown to inhibit HCV infection in an SR-B dependent manner (Bartosch *et al.*, 2005; Voisset *et al.*, 2005; von Hahn *et al.*, 2006).

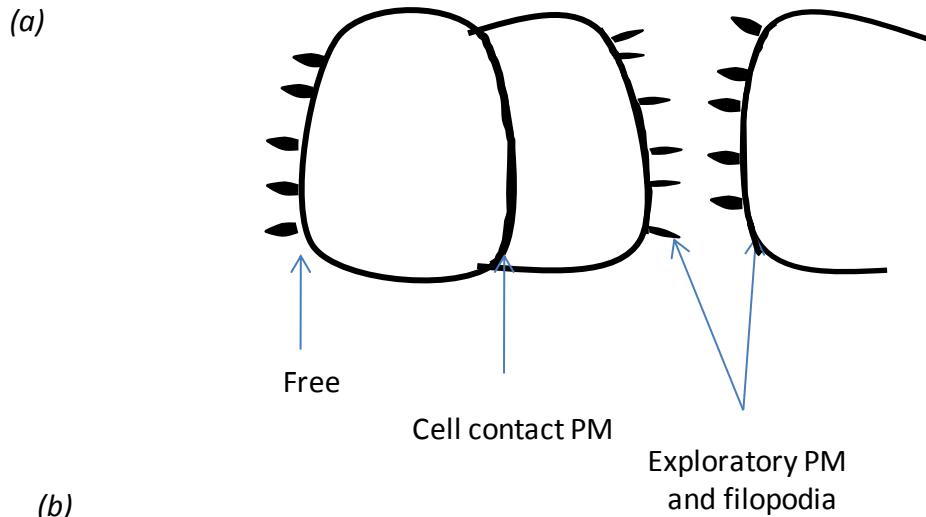
This study shows addition of ITX5061 to decrease the mobile fraction of SR-BI at areas of cell contact and exploratory regions, whereas effects on CD81 and CLDN-1 are restricted to the diffusion coefficient, increasing it at areas of 'free' PM and exploratory regions.

As addition of cholesterol to a membrane decreases its fluidity, a decrease in cholesterol transfer into the membrane relative to the control would have the effect of increasing the diffusion coefficient of proteins within the membrane, possibly across all structures. Although only those values at the exploratory region and free filopodia showed significant increases, all diffusion coefficients increased for CD81 and CLDN-1. This suggests a global change in membrane composition, possibly through the lipid metabolism function of SR-BI.

However, the diffusion coefficients of SR-BI did not vary so uniformly, with all apart from the PM and exploratory filopodia decreasing in diffusion coefficient. This may suggest that although there is a global effect on membrane composition, a specific effect on SR-BI activity

is mediated by ITX5061 binding which causes its diffusion coefficient to be altered. This may reflect the possibility that SR-BI can create distinct microdomains within the membrane.

The specific effects of ITX5061 on areas of cell contact or exploratory regions is interesting, as SR-BI is particularly important in cell-cell transmission (Brimacombe *et al.*, 2011). The changes in mobile fraction may represent a structural change in SR-BI following binding to ITX5061, causing a change in the way in which SR-BI interacts with other proteins in the membrane or the cytoskeleton.



(b)

SRB-1	Diffusion Coefficient				Mobile Fraction			
	Free PM vs. other structures	UT vs. E2	UTvs. E1E2	ITX7904vs. ITX5061	Free PM vs. other structures	UT vs. E2	UT vs. E1E2	ITX7904 vs ITX5061
PM	-	-	-	light red	-	-	-	grey
Filopodia	grey	-	-	dark blue	dark blue	-	-	light red
Exploratory filopodia	dark blue	-	-	light red	dark blue	-	-	dark blue
Exploratory PM	dark blue	-	-	dark blue	light red	-	-	dark blue
Cell contact PM	dark blue	-	-	grey	light red	-	-	dark blue
<b>CD81</b>								
PM	-		light red	dark red	-	dark blue	grey	grey
Filopodia	dark red	dark blue	light red	light red	dark blue	dark blue	light red	light red
Exploratory filopodia	dark blue	dark blue	dark blue	dark red	dark blue	dark blue	light red	dark blue
Exploratory PM	dark blue	light red	light red	dark red	grey	dark blue	light red	light red
Cell contact PM	light red	grey	light red	light red	light red	dark blue	dark blue	light red
<b>CLDN-1</b>								
PM	-	grey	grey	dark blue	-	dark blue	light red	light red
Filopodia	dark blue	dark red	light red	grey	dark blue	dark blue	dark blue	grey
Exploratory filopodia	grey	dark blue	light red	dark red	dark blue	dark blue	dark red	light red
Exploratory PM	grey	dark blue	dark blue	dark red	light red	dark blue	dark red	light red
Cell contact PM	light red	dark blue	dark blue	light red	grey	dark blue	dark blue	light red

**Figure 15: Trends observed from data presented in this report.** Structures examined in this report (a). Trends observed (b). Colour coding is as follows: light blue, Non significant decrease; dark blue, significant decrease; light red, non-significant increase; dark red, significant decrease; grey, no change.

Figure 15 shows the trends in receptor dynamics highlighted by this study. Although there are changes in receptor dynamics at between different cellular locations in all proteins studied, the majority of these are non-significant. Addition of the viral glycoproteins sE2 and sE1E2 affect CLDN-1 predominantly, and particularly at areas of exploratory contact, where the diffusion coefficient is decreased and mobile fraction increase. In contrast addition of these glycoproteins had little effect on CD81.

Addition of ITX5061 caused changes in the mobile fraction only of SR-BI, and in the diffusion coefficient only of CD81 and CLDN-1, although across a variety of structures.

In this report we describe the kinetics of the four receptors essential for HCV entry - SRB1, CD81, CLDN-1, and occludin. We show that these differ between cellular structures and are altered by the addition of the viral glycoproteins sE1E2 and the SRB1 inhibitor SRB1. The activity of viral receptors is essential to understanding the mechanism of HCV and will be useful in the development of therapies.

# STUDIES OF PLATELET ACTIN DYNAMICS USING LIFEACT-GFP: A POTENTIAL ROLE FOR ACTIN NODULES IN FILOPODIA FORMATION

By

Amy Barnes

*This project is submitted in partial fulfilment of the requirements for the award of the  
Master of Research in Biomedical Research*

College of Medical and Dental Sciences

University of Birmingham

Edgbaston

Birmingham

B292TT

August 2011

## ABSTRACT

Life act is a 17aa yeast-derived actin binding protein which has been shown to effectively label F-actin both *in vivo* and *in vitro* (Reidl *et al.*, 2008; 2010). The lifeact-GFP transgenic mouse has been shown to be phenotypically normal and to express the transgene in platelets, and thus offers a potentially viable model for the real-time observation of platelet actin dynamics. This has not previously been possible due to technical reasons.

This study aimed to verify the use of the lifeact-GFP transgenic mouse as a model for studying platelet actin dynamics in real time. In addition, transgenic platelets were used to further characterise actin nodules – punctate areas of dense actin staining (*Calaminus et al.*, 2008) with an as yet undefined function. It is possible that they have a role in actin remodelling, adhesion, or endocytosis.

The results of this study show that lifeact-GFP platelets are phenotypically similar to wild type platelets in terms of their aggregation and morphology during spreading. Therefore, they appear to constitute a valid model for further observations. In addition, using live imaging this study shows actin nodules to be relatively stationary structures with finite lifespans of 87 seconds. Their lifespan appears to be related to filopodia formation, and therefore they may mark the positions at which filopodia will form. Using immunofluorescence staining, this report shows actin nodules to colocalise with a number of focal adhesion proteins suggesting that actin nodules may have a role in adhesion. Finally, we show actin nodules do not colocalise with the endocytosis protein clathrin, and their frequency is not affected by addition of the dynamin-mediated endocytosis inhibitor Dynasore. Taken together, these data suggest that actin nodules provide a site for the initiation of

filopodia formation and may additionally play a role in adhesion of the developing filopodia to the extra cellular matrix.

## TABLE OF CONTENTS

### TABLE OF FIGURES

### ABBREVIATIONS

### ACKNOWLEDGEMENTS

## 1.0 INTRODUCTION

1.1 Platelets	54
1.2 Mechanisms of platelet activation	54
1.3 Actin	55
1.4 The platelet cytoskeleton	57
1.4.1 The resting platelet cytoskeleton	57
1.4.2 Cytoskeletal reorganisation during activation	57
1.5 Actin structures	58
1.5.1 Filopodia	58
1.5.2 Actin nodules	60
1.6 The Lifeact system	61
1.7 Aims	62

## 2. MATERIALS AND METHODS

2.1 Use of animals	63
2.2 Terminal bleeding of mice	63
2.3 Preparation of mouse platelets	63
2.4 Preparation of human platelets	64
2.5 Aggregation	64
2.6 Inhibitor testing	64
2.7 Phalloidin-FITC/Rhodamine staining	65
2.8 Immunofluorescence staining	65
2.9 Platelet imaging	66
2.9.1 Differential interference contrast (DIC) microscopy	66
2.9.2 Confocal microscopy	66
2.9.3 Total internal reflectance fluorescence (TIRF) microscopy	66
2.10 Image manipulation	67
2.11 Statistics	67

### 3.0 RESULTS

3.1 Lifeact-GFP transgenic platelets display similar aggregation curves to wild type platelets	68
--	----

3.2 Platelets undergo a series of distinct stages during platelet spreading, and these are replicated in lifeact-GFP transgenic mice	70
3.3 Actin nodule size	72
3.4 Actin nodules appear to have a limited lifespan	72
3.5 Dependence on actin nucleation and polymerisation	73
3.6 Actin nodules appear to be associated with filopodia	76
3.7 Dynamics of actin nodule movement	78
3.8 Colocalisation of focal adhesion proteins with actin nodules	78
3.9 Markers of endocytosis	82
4.0 DISCUSSION	85

## **TABLE OF FIGURES**

Figure 1: Actin nodules and filopodia	61
Figure 2: Aggregation of WT and lifeact-GFP platelets	69
Figure 3: Distinct stages of platelets spreading	71
Figure 4: Basic characteristics of actin nodules	73
Figure 5: Dependence of actin nodules and filopodia on Arp2/3-dependent nucleation and polymerisation in lifeact-GFP platelets	75

Figure 6 - Relationship between actin nodules and filopodia in lifeact-GFP mouse platelets	77
Figure 7: The association between actin nodules and filopodia.	80
Figure 8: Focal adhesion staining	81
Figure 9: Relationship between actin nodules and endocytosis	83

## **ABBREVIATIONS**

ACD: Acid citrate dextrose

ADP: Adenosine diphosphate

CLEC-1: C-type lectin-like receptor

CRP: C-reactive protein

DIC: Differential interference contrast

DMSO: Dimethyl sulfoxide

FAK: focal adhesion kinase

GFP: Green fluorescent protein

GFP: Green fluorescent protein

GTP: Guanosine triphosphate

I-BAR: inverse Bin/Amphiphysin/Rvs

IRSp53: Insulin receptor tyrosine kinase substrate p53

ITAM: Immunoreceptor tyrosine-based activation motif

LRP1: Low density lipoprotein-related protein 1

N-WASP: Wiskott-Aldrich syndrome protein

PAR1: Protease-activated receptor 1

PAR4: Protease-activated receptor 4

PKC: Protein kinase C

PLC $\beta$ : Phospholipase C  $\beta$

PLC $\gamma$ 2: Phospholipase C $\gamma$ 2

PRP: Platelet rich plasma

TIRF: Total internal reflectance fluorescence

TxA<sub>2</sub>: Thromboxane A<sub>2</sub>

vWF: von Willebrand Factor

WASP: Wiskott-Aldrich syndrome protein

## **ACKNOWLEDGMENTS**

I would like to thank Dr Steven Thomas for guidance in both the carrying out and writing of this study. I would also like to thank Professor Stephen Watson for guidance, and Mr. Craig Nash for experimental guidance. This work was carried out using funding from the Medical Research Council. The Nikon A1R confocal / TIRF microscope used in this research were obtained, through Birmingham Science City Translational Medicine Clinical Research and Infrastructure Trials Platform, with support from Advantage West Midlands (AWM).

## INTRODUCTION

### *1.1 Platelets*

Platelets are anucleate cell fragments which circulate in the bloodstream and become activated following contact with areas of damaged vessel wall. As a result of activation platelets spread, resulting in an increased surface which allows them to provide a physical barrier to blood loss from injured endothelial tissue. In addition, they form a surface area to which further platelets can adhere. A second result of activation is the secretion of prothrombotic factors, which allows activated platelets to initiate haemostasis by providing a surface on which thrombin is generated and fibrin can accumulate (Brass 2010). Additionally, platelets contribute to primary immunity by helping to trap bacteria in neutrophil-derived DNA nets, and stimulate angiogenesis and contribute inflammatory mediators (reviewed in (Leslie).

### *1.2 Mechanisms of platelet activation*

Following injury and endothelial denudation, the subendothelial extracellular matrix is exposed to blood flow. Exposed collagen accumulates circulating von Willebrand Factor (vWF), which makes contacts with the platelet GPIb-IX-V complex (Ruggeri *et al.*, 2007). These contacts are transient due to the fast on/off-rate of the interaction but are efficient at the high levels of shear present in blood vessels (Doggett *et al.* 2002).

The transient binding of vWF to GPIb-IX-V slows the speed of platelet movement sufficiently during rolling to allow binding of the low affinity immunoglobulin platelet surface receptor GPVI with exposed laminin and fibrillar collagen types I and III (Denis *et al.* 1998). This interaction clusters GPVI at the platelet surface (Inoue *et al.* 2006) and activates the platelets through inside-out signalling via integrins. The principal integrins involved in platelet activation are  $\alpha\text{IIb}\beta\text{3}$  and  $\alpha\text{2}\beta\text{1}$ , the former binds to VWF, fibronectin, and fibrinogen (Shattil *et al.*, 2004) and the latter to collagen (Sarratt *et al.* 2005).

Inside-out signalling leads to cytoskeletal remodelling, granule secretion, and thromboxane  $\text{A}_2$  formation ( $\text{TxA}_2$ ) (Nieswandt, *et al.* 2003). In addition, during this process the weak interactions formed between the platelet and the matrix are converted to stable adhesions. This increases the net affinity of collagen for GPVI, thus initiating a positive feedback loop of activation signals through this receptor (Shattil and Newman 2004).

Signalling through  $\alpha\text{IIb}\beta\text{3}$  is central to the cytoskeletal rearrangements which occur during platelet spreading. Downstream signalling from  $\alpha\text{IIb}\beta\text{3}$  through Src kinases and Syk activates second messenger proteins such as protein kinase c (PKC) and  $\text{Ca}^{2+}$  (Miranti *et al.* 1998; Thornber *et al.* 2006) and these lead to the assembly of actin structure such as lamellipodia, stress fibres, and filopodia (McCarty *et al.* 2005).

Following initial adhesion, platelets secrete dense granules and activate phospholipase  $\text{A}_2$ , leading to the release of adenosine diphosphate (ADP) and the formation of  $\text{TxA}_2$  (Nieswandt and Watson 2003). These two act synergistically to mediate additional platelet aggregation through further platelet tethering, activation and aggregation. Activation and haemostasis is further promoted by the generation of thrombin through the coagulation cascade which

activates platelets through platelet activated receptors 1 and 4 (PAR1 and PAR4) (Adam *et al.* 2003; Weeterings *et al.* 2006), and strengthens the clot by cleaving fibrinogen to fibrin. In addition, under high rates of shear, platelets shed part of their membrane, leaving trails of procoagulant microparticles (Reininger *et al.* 2006).

Therefore, there are two principal pathways through which platelets may become activated. The first is initiated by GPIV, and results in full platelet activation. The second is initiated by the stimulation of heterotrimeric G-protein coupled receptors by thrombin, ADP, and TxA<sub>2</sub>. The first and second pathways proceed through phospholipase C  $\gamma$ 2 (PLC $\gamma$ 2) and phospholipase C $\beta$  (PLC $\beta$ ) respectively (Stegner and Nieswandt 2011), both of which lead to calcium mobilisation and PK activation. Both PLC $\gamma$ 2 and PLC $\beta$  activate the Rho/Rho-kinase pathway, which goes on to phosphorylate myosin light chain and contributes to platelet shape change (Stegner and Nieswandt 2011).

### 1.3 Actin

Actin is a highly conserved 42 kDa protein, and is the most abundant protein in most eukaryotic cells. It exists in globular (G) and filamentous (F) forms, with G-actin being a double helical polymer of G actin subunits, and F-actin a polymer of these. F-actin filaments are polar in nature with a fast-growing (+) end to which monomers are added and a (-) end from which monomers disassociate.

The actin cytoskeleton is vast and extends throughout the cell, and can therefore alter cell morphology by assembling and disassembling polymers. In order to ensure a high level of

control of the actin cytoskeleton, actin dynamics are regulated by a large range of actin binding proteins (Siripala and Welch 2007a; 2007b), combinations of which produce cell type-specific organisation of the actin cytoskeleton.

The best characterised actin structures are the filopodia, stress fibres and lamellipodia, all of which are present at some point in the transition between resting and activated platelets (Hartwig *et al.*, 1992). Also, punctuate areas of intense actin staining have been identified during early spreading and are termed actin nodules (see section 1.4.2) (Calaminus *et al.* 2008).

## 1.4 The platelet cytoskeleton

### 1.4.1 The resting platelet cytoskeleton

The resting platelet is discoid in shape and contains a cytoskeleton robust enough to enable it to withstand the high rates of shear stress present during blood flow. The resting platelet cytoskeleton is formed of three main components: a spectrin based skeleton which adheres to the inner surface of the plasma membrane (1), a multiple microtubule coils which line the axis of the cell (Patel-Hett *et al.* 2008) (2), and an actin-based network which fills the cytoplasmic space (3). Platelet stimulation activates nucleation and branching of actin filaments, thus remodelling the platelet.

### 1.4.2 Cytoskeletal reorganisation during activation

During cell spreading, filopodia form the initial adhesion sites to the substratum and to which focal adhesion complex proteins are recruited (Mattila and Lappalainen 2008). Lamellipodia then extend between these as the platelet spreads. Additionally, under shear-stress filopodia have been observed to form tethers between platelets and VWF in a developing aggregate (Maxwell *et al.* 2006); (Nesbitt *et al.* 2009).

When fibrinogen and fibronectin engage with platelet surface receptors such as  $\alpha\text{IIb}\beta\text{3}$ , the tyrosine kinases Src, Syk and focal adhesion kinase (FAK) are recruited to the cytosolic cell surface and promote cytoskeletal reorganisation through activation of PKC and increases in intracellular  $\text{Ca}^{2+}$  (Mangin *et al.* 2003). These signals regulate actin polymerisation at the platelet membrane to allow the growth and extension of actin structures (McCarty *et al.* 2005; Watson *et al.*, 2009).

## 1.5 Actin structures

This study is concerned primarily with two actin structures present during platelet spreading – filopodia and actin nodules.

### 1.5.1 Filopodia

Filopodia are F-actin-rich fast growing projections (Figure 1a, 1b) orientated such the F-actin polymers have the '+' ends face towards the cell membrane (Small *et al.* 1978). Filopodia have roles in a wide range of cellular functions, including cell spreading wound healing,

adhesion, movement towards to chemoattractants, and embryonic development (Faix and Rottner 2006; Gupton and Gertler 2007).

There are two independent pathways which potentially lead to the formation of biologically distinct filopodia in platelets: the Cdc42 and RIF pathways. The difference in filopodia formed by each process may represent specific biological functions (Pellegrin and Mellor 2005).

In the first pathway, Cdc42 binds and activates either Wiskott Aldrich Syndrome protein (WASP) (Aspenstrom *et al.* 1996; Symons *et al.* 1996; Rohatgi *et al.* 1999; Prehoda *et al.* 2000) or insulin receptor tyrosine kinase substrate p53 (IRSp53) (Yamagishi *et al.* 2004) which activates neural (N-) WASP and Arp2/3, and Mena (Krugmann *et al.* 2001; Yamagishi *et al.* 2004; Scita *et al.* 2008). These promote actin nucleation and protect elongating filaments from capping respectively. IRSp53 is an inverse Bin/Amphiphysin/Rvs (I-BAR) domain protein that resides at the cell membrane and is thought to be involved in membrane deformation (Suetsugu *et al.* 2006; Mattila *et al.* 2007; Lim *et al.* 2008).

In contrast, RIF binds GTP and the formin mDia2, leading to the formation of unbranched actin filaments by directly nucleating actin assembly and preventing capping (Ellis and Mellor 2000; Pruyne *et al.* 2002; Sagot *et al.* 2002; Higashi *et al.* 2008).

Recent studies have shown that Rac1, Cdc42 and WASP are not essential for platelet filopodia formation and full platelet spreading (Snapper *et al.* 2001; Sukumvanich *et al.* 2004; McCarty *et al.* 2005; Pleines *et al.* 2010). Although the findings related to Cdc42 is controversial (Akbar 2011). Therefore, the second pathway or another may be the major effector of filopodia formation in platelets, although this remains to be tested. Another

potential effector is lipid-phosphatase related protein-1 (LRP1), although again this has not been verified (Sigal *et al.* 2007).

### 1.5.2 Actin nodules

A novel actin structure has been described (Calaminus *et al.* 2008) which is observed during early spreading. It consists of punctuate areas of intense F-actin staining (Figure 1a) which extend throughout the platelet and are termed actin nodules. These are distinct from other actin-rich structures such as podosomes, focal adhesions, focal complexes, invadopodia, ruffles, and endocytic vesicles (Calaminus *et al.* 2008) and are observed on a number of different substrates. Their appearance has been shown to be dependent on Src kinase activity and actin polymerisation, but is independent of PI3K activity, and inversely correlated with Rho-kinase and myosin-II activity. They were also shown to contain Arp2/3, Fyn, Rac, and  $\beta 1$  and  $\beta 3$ -integrins (Calaminus *et al.* 2008).

Whilst actin nodules have been shown not to be involved in exocytosis (Calaminus *et al.* 2008), it is possible that they are involved in endocytosis. Whilst platelets are adhered to the substratum, they endocytose fibrinogen from the plasma pool and traffic it to  $\alpha$ -granules, in a process which is thought occur by clathrin-dependent receptor-mediated endocytosis and the integrin  $\alpha IIb\beta 3$ . However, the mechanism is relatively undefined and needs further study (Handagama PJ 1987; Harrison *et al.* 1989).

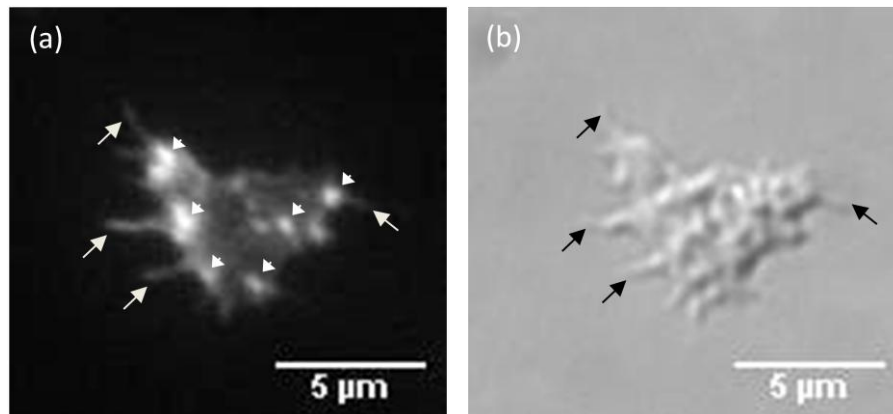


**Figure 1: Actin nodules and filopodia.** Representative images of filopodia (white arrows) and actin nodules (white arrowheads) in lifeact-GFP mouse platelets using confocal microscopy (a). Additionally, filopodia are displayed (black arrows) using differential interference contrast (DIC) microscopy (b). Confocal images were taken on a Leica DM IRE2 confocal microscope and DIC images were captured on a Zeiss Axiovert 200 M microscope.

## 1.6 Lifeact

Actin dynamics may be monitored by the expression of actin-green fluorescent protein (GFP) fusion proteins or by injection of fluorescently labelled actin. However, all reported actin fusion proteins are functionally impaired and rely on non-tagged actin to buffer the effects (Yamada *et al.* 2005). In addition, the technique is limited to cells which can be transfected and therefore it is unsuitable for use in platelets. Permeabilisation of fixed cells followed by staining with the fungal F-actin binding protein phalloidin has proved a viable method for investigating actin dynamics in platelets however the fixing processes removes the possibility of using phalloidin in live cell imaging, and results in the appearance of staining artefacts.

Lifect was first described in 2008 (Riedl *et al.* 2008). It is an actin binding protein encoded by a 17 amino acid peptide from *Saccharomyces cerevisiae* with the sequence MGVADKLIKKFESISKEE. A C-terminal fusion transgene of this peptide to fluorescent proteins has been shown to act as an efficient label of F-actin in vivo due to the small size of the peptide and its absence from higher organisms (Riedl *et al.* 2008).

Lifect offers a considerable improvement upon previous systems for monitoring actin dynamics as its low F-actin binding affinity does not cause any major adverse biological effects on actin dynamics (Riedl *et al.* 2008). Furthermore, transgenic mice carrying a lifect-fluorescent protein fusion have been shown to be phenotypically normal, viable, fertile, and to express the transgene in platelets (Riedl *et al.* 2010). This makes it a promising candidate for studying actin dynamics in live platelets.

### 1.7. Aims

In this study, I aim to validate the use of the Lifect-GFP transgenic mouse model as a system for studying platelet actin dynamics in real time, and to use this model to study the relationship between actin nodules and filopodia. I hypothesise that actin nodules play a key role in platelet spreading, possibly by acting as a precursor to the formation of other actin structures such as filopodia.

## 2. MATERIALS AND METHODS

### *2.1 Use of animals*

All animal studies were conducted in accordance with Home Office protocols in compliance with project license 30/2721. All animal handling was done by a licensed individual.

### *2.2 Terminal bleeding of mice*

Lifect-GFP and C57Blk6 (wild type, WT) mice were culled by inducing unconsciousness with isoflurane anesthesia followed by CO<sub>2</sub> asphyxiation. Whole blood was then collected into a 1 ml syringe containing 100µl acid citrate dextrose (ACD) with a 25 ml gauge needle from the thoracic aorta.

### *2.3 Preparation of mouse platelets*

Whole blood from terminally narcosed mice was centrifuged at 200g for 6 minutes and the platelet rich plasma (PRP) was collected. After addition of 200µl of Tyrodes buffer ( NaCl, 134 mM; KCl, 2.9 mM; Na<sub>2</sub>HPO<sub>4</sub>·12H<sub>2</sub>O, 0.34 mM; NaHCO<sub>3</sub>, 12.0 mM; HEPES, 20.0mM; MgCl<sub>2</sub>, 1.0mM) to the PRP, it was centrifuged 3 times at 200g for 6 minutes and each time the PRP removed until no more was visible. The final PRP was spun at 1000g for 5 minutes with 1mg/µl prostaglandin added. The resulting pellet was resuspended in 200µl of Tyrodes

solution at pH 7.7. This was diluted to a concentration of  $2 \times 10^7$ /ml in Tyrodes buffer at pH 7.3 for use in all experiments.

#### *2.4 Preparation of human platelets*

Human venous blood was drawn by venipuncture from healthy volunteers into sodium citrate and acid citrate dextrose. PRP was prepared by centrifugation of whole blood at 200g for 20 min. The platelets were then isolated from PRP by centrifugation at 1000g for 10 min in the presence of prostacyclin (0.1  $\mu$ g/ml). The pellet was resuspended in modified HEPES/Tyrodes buffer containing 0.1  $\mu$ g/ml prostacyclin. The platelets were washed once via centrifugation (1000g for 10 min) and resuspended at  $2 \times 10^7$  with HEPES/Tyrode buffer.

#### *2.5 Aggregation*

Platelet aggregation of wild type or lifeact-GFP platelets was monitored using 300  $\mu$ l of  $2 \times 10^8$  /ml PRP stimulated with ADP (AltaBiosciences, 3mM), rhodocytin (AltaBiosciences, 30nM), PAR4 peptide (AltaBiosciences, 250mM) or C-reactive protein (CRP) (AltaBiosciences, 3mg/ml). Stimulation of platelets was performed in a Chrono-Log aggregometer (Chrono-Log, PA, USA) with continuous stirring (1200 rpm) at 37 °C as previously described (McCarty *et al.* 2005).

#### *2.6 Inhibitor testing*

Platelets collected as above (section 2.3) were used at a concentration of  $2 \times 10^7$ /ml and incubated with inhibitors for 5 minutes before plating. Cytochalasin D (250255, Calbiochem) was used at 10  $\mu$ M, Dynasore (D7693, Sigma-Aldrich) at 50  $\mu$ M, and the Arp2/3 inhibitor

compound CK666 and relevant control CK689 (Merck Biosciences 182515 and 182517 respectively) were used at 20 $\mu$ M. DMSO (D8418, Sigma) at 0.1% and 0.3% was used as.

### *2.7 Phalloidin-FITC/Rhodamine staining*

Coverslips were incubated with 100 $\mu$ g/ml fibrinogen overnight at 4°C or for 1 hr at room temperature (RT) before being incubated with 5mg/ml bovine serum albumin at room temperature (RT) for 30 minutes. Platelets were then added at 2x10<sup>7</sup>/ml and fixed in 10% neutral buffered formalin solution (Sigma Aldrich, 7K189R5).

Platelets were permeabilised using 100 $\mu$ l of 50mM NH<sub>4</sub>Cl for 10 minutes at RT, before being washed in PBS incubated at RT for 5 minutes in 0.1% Triton at RT. Following a further wash, Phalloidin-FITC/Rhodamine (A12379, Invitrogen and R415, Invitrogen) and was added at a concentration of 4 $\mu$ g/ml and 2  $\mu$ g/ml respectively for 30 minutes at RT, washed in PBS, and mounted in hydromount (National Diagnostics, HS-106) and being stored at 4°C in PBS.

### *2.8 Immunofluorescence staining*

Platelets were collected (section 2.3 and 2.4) and fixed in 10% neutral buffered formalin solution (Sigma Aldrich, 7K189R5). These were then treated with NH<sub>4</sub>Cl for 10 minutes at room temperature and 0.1% Triton for 5 minutes at room temperature to prepare the platelets for staining. They were then incubated with primary antibodies to clathrin (BD Biosciences, 611784) at 0.125  $\mu$ g/ml, pFAK (611722 10/200BD Biosciences) at 1.25  $\mu$ g/ml, paxillin (610569, BD Transduction Lab, UK) at 1.25 $\mu$ g/ml, vinculin (abcam, ab11194) at 0.05  $\mu$ g/ml, p34 (7-227, Millipore) at 0.002 $\mu$ g/ml and talin (abcam, ab57758) at 0.002  $\mu$ g/ml. Control antibodies for mouse (Santa Cruz, SC-2025) were used at 0.8  $\mu$ g/ml, and for rabbit

(Santa Cruz, SC-2027) 0.8 µg/ml. Secondary antibodies to mouse (A10680, Invitrogen) and rabbit (A11008, Invitrogen) were both used at 4µg/ml and for 30 minutes at room temperature before washing and fixing with formalin before mounting. Both rabbit and mouse control IgGs were used at an appropriate concentration (1:500 for each).

## *2.9 Platelet imaging*

For imaging, platelets were used at a concentration of  $2 \times 10^7$ /ml. Where real time microscopy was used, platelets were suspended in pH 7.3 Tyrodes buffer.

### *2.9.1 Differential interference contrast (DIC) microscopy*

DIC images were captured with a Zeiss 63x oil immersion 1.40 NA plan-apochromat lens on a Zeiss Axiovert 200 M microscope. Digital images were captured by a Hamamatsu Orca 285 cooled digital camera (Cairn Research, Kent, UK) using Slidebook 5.0 (Intelligent Imaging Innovations, Inc.,).

### *2.9.2 Confocal microscopy*

Confocal images were taken on a Leica DM IRE2 confocal microscope illuminated using the 488 line of an argon laser and a 63x 1.4Na oil immersion objective.

### *2.9.3 Total internal reflectance fluorescence (TIRF) microscopy*

TIRF images were captured on a Nikon A1R confocal / TIRF microscope using with a 60x 1.49 NA objective and an Andor iXion EM-CCD.

### *2.10 Image manipulation*

Where necessary, images were cropped and overlaid using ImageJ image processing software. Also, the cell counter (Kurt de Vos, University of Sheffield) and manual particle tracking (Fabrice Cordelieres, Institut Curie) add-ins were used.

### *2.11 Statistics*

Statistical analyses and data representation were carried out using GraphPad Prism software (GraphPad software, San Diego), with significance calculated using the Student's T test with a Mann-Whitney post test:  $p < 0.05$  (\*),  $p < 0.01$  (\*\*), and  $p < 0.001$  (\*\*\*). All values quoted are means unless otherwise stated.

### 3.0 RESULTS

#### *3.1 Lifact-GFP transgenic platelets display similar aggregation curves to WT platelets*

Lifact-GFP mice were observed to have no obvious visual or behavioural defects in comparison to WT mice and were born at normal Mendelian ratio. In order to investigate whether Lifact-GFP platelets are defective, PRP was collected from a mouse expressing the Lifact-GFP transgene and from a control WT mouse. Platelet aggregation was performed following addition to PRP of ADP (3 $\mu$ M, Figure 2a), CRP (3 $\mu$ g/ml, Figure 2b), rhodocytin (30  $\mu$ M, Figure 2c), and PAR4 peptide (250 $\mu$ M, Figure 2d). These showed aggregation to be similar in both backgrounds, indicating that expression of lifact-GFP does not aberrantly affect the platelet function.

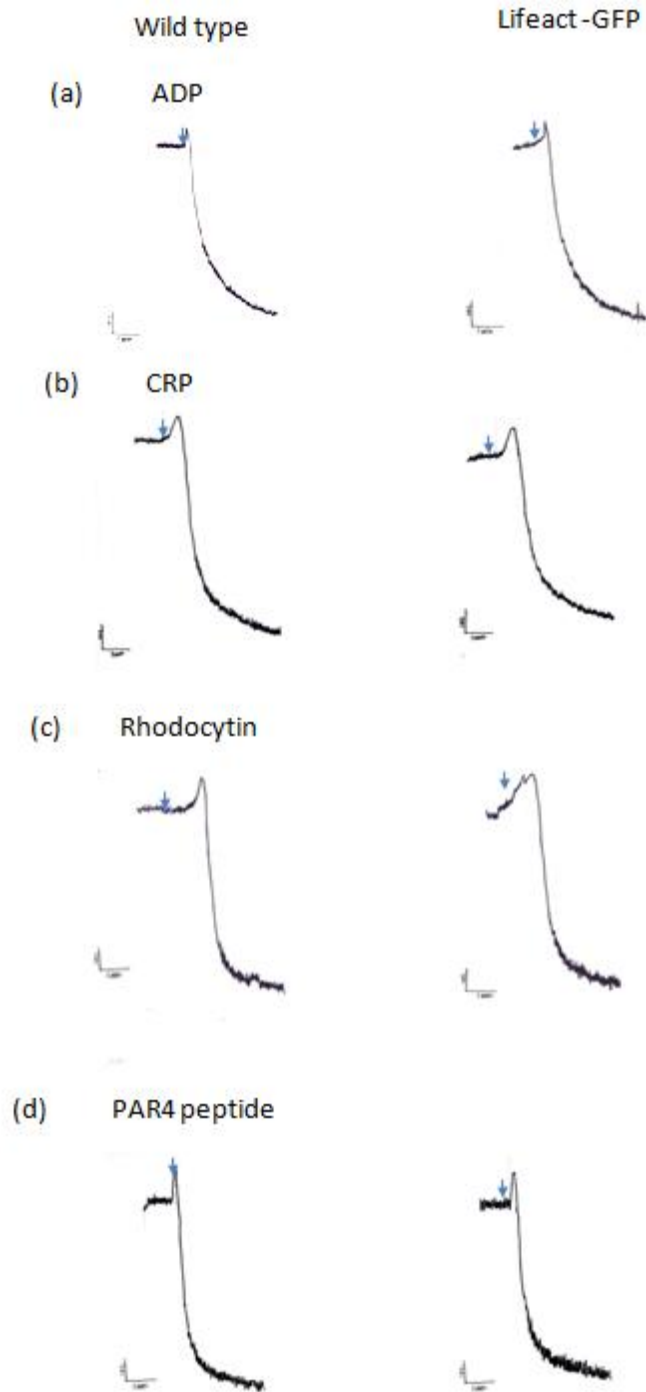


**Figure 2: Aggregation of wildtype and lifeact-GFP platelets.** Platelets from WT and lifeact-GFP mice were stimulated with ADP at  $3\mu\text{M}$  (a) CRP at  $3\mu\text{g/ml}$  (b) rhodocytin at  $30\mu\text{M}$  (c) PAR4 peptide at  $250\mu\text{M}$  (d). Aggregation traces were produced on Chrono-Log aggregometer. (Chrono-Log, PA).

### *3.2 Platelets undergo a series of distinct stages during platelet spreading, and these are replicated in lifeact-GFP transgenic mice*

That platelets undergo a series of distinct morphological changes upon a fibrinogen-coated surface has been well documented (Hartwig *et al.*, 1992) (Figure 3a-e). In the present study, I compared the morphological changes occurring in control platelets (Figure 3a-e) to those from lifeact-GFP platelets upon adhesion to fibrinogen.

On initial contact, platelets could be seen to have an occasional filopodia and usually no more than one actin nodule (Figure 3 a, f, k). With time, further filopodia and actin nodules appear (Figure 3 b, g, l, and c, h, m) followed by the generation of lamellipodia (Figure 3 d, i, n) and stress fibres (Figure 4 e, j, o).

Therefore, using epifluorescence microscopy platelets from WT and lifeact-GFP mice were observed to undergo a similar pattern of spreading on fibrinogen (Figure 4 f-j, k-o).

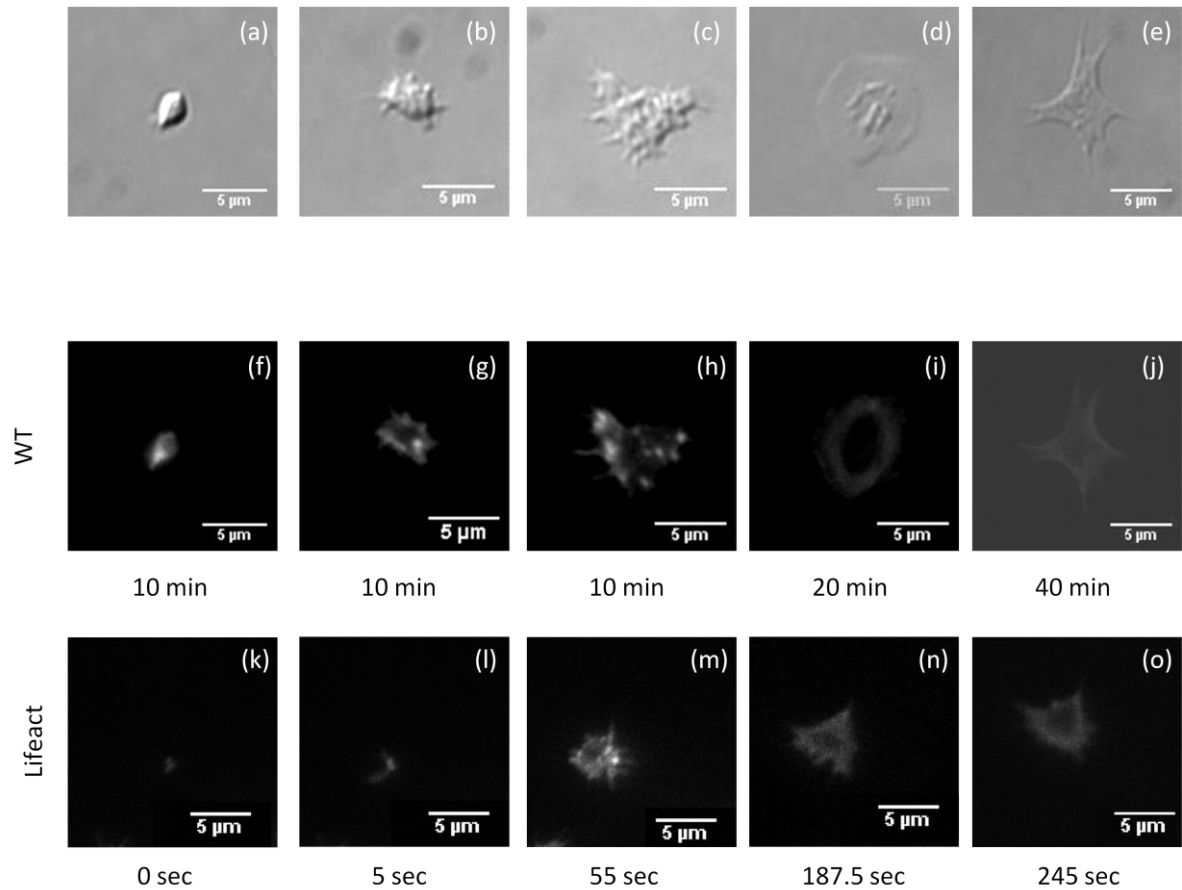


**Figure 3: Distinct stages of platelet spreading.** The distinct stages in platelet spreading (a-e) begin with initial contact on contact with a substrate (a) followed by development of initial actin nodules and filopodia (b), development of further nodules and filopodia (c) formation of lamella (d), and formation of stress fibres (e) (DIC images were captured on a Zeiss Axiovert 200 M microscope). These patterns are replicated by fixed phalloidin-stained WT platelets (f-g) (Images taken using a Zeiss Axiovert 200 M microscope) and in lifeact-GFP transgenic platelets (k-o) (TIRF images were imaged live on a Nikon A1R confocal / TIRF microscope).

### *3.3 Actin nodule size*

In order to establish the morphological similarities between actin nodules in WT and lifeact-GFP transgenic platelets, the diameter of actin nodules in each background was measured (Figure 4a). This revealed no significant difference in sizes between the two, although those in lifeact-GFP platelets were slightly larger (Figure 4a) than those of WT. Actin nodules in WT platelets had a median diameter of 0.46  $\mu\text{m}$  (SD 0.12  $\mu\text{m}$ ), whereas those from lifeact platelets had a diameter of 0.57  $\mu\text{m}$  (SD 0.16  $\mu\text{m}$ ).

### *3.4 Actin nodules appear to have a limited lifespan*

To examine the expression of actin nodules in more detail, the number of actin nodules per platelet was recorded each minute following initial contact with a fibrinogen substrate. The initial number of actin nodules is 2.5 per platelet at first contact, which increases to around 4 per platelet after 2 minutes. This number remains constant and does not increase with time (Figure 4b) suggesting that actin nodules may have a finite lifespan. Therefore, the average lifetime of actin nodules was measured and found to be 87 seconds (SD 4.23 seconds) (Figure 4c); although the majority of nodules had a lifetime of 30-60 seconds with a range of 17.5-180 seconds (Figure 4c). Therefore, actin nodules appear to have a finite lifespan.

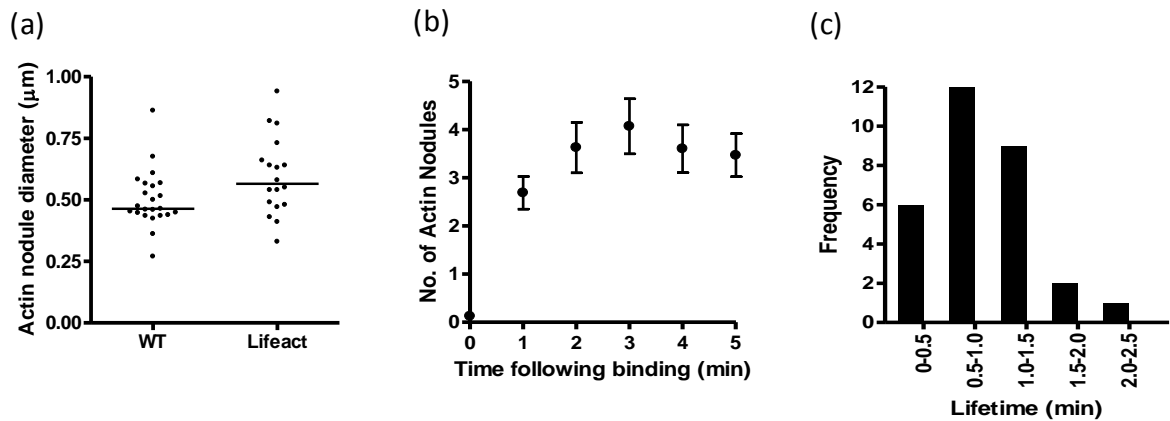


**Figure 4: Basic characteristics of actin nodules.** Median diameter of actin nodules in WT and lifeact-GFP platelets ( $n=39$ ) (a). Mean number of actin nodules present per platelet per minute in lifeact-GFP mouse platelets ( $n=16$ ) (b). The average lifespan of actin nodules in lifeact-GFP mouse platelets (mean = 87 seconds,  $SD = 4.64$ ,  $n=34$ ) at half-minute intervals following initial attachment of platelets to substrate (c). All observations made from images taken on a Nikon A1R confocal / TIRF microscope.

### 3.5 Dependence on actin nucleation and polymerisation

In order to establish the dependence of actin nodule formation on actin nucleation and polymerisation, the Arp2/3 inhibitor CK666 (20 $\mu$ M), control compound CK689 (20 $\mu$ M), and the actin polymerisation inhibitor cytochalasin D (10  $\mu$ M) were added to lifeact-GFP transgenic platelets prior to spreading (Figure 5). 0.1% DMSO was used as a control. Quantification of the number of actin nodules (Figure 5a) and filopodia (Figure 5b) per cell showed that addition of compound CK666 decreased the number of filopodia and nodules per cell in comparison to both CK689 and the DMSO control.

Addition of cytochalasin D inhibited entirely the formation of filopodia (Figure 5d), and also decreased the number of nodules to a similar level as those in platelets which had been treated with compound CK666 (Figure 5a).

Actin nodules in platelets treated with either CK666 or cytochalasin D appeared to be larger and more diffuse than those treated using control compounds (Figure 5 d and e compared to f and g). Therefore, the diameter of actin nodules was measured in all four populations (Figure 5c). This showed actin nodules in platelets treated with CK666 to be significantly larger than those treated with DMSO. Similarly, actin nodules in platelets treated with cytochalasin D also had a significantly larger diameter to those treated with DMSO (Figure 5c, d).

These data show that the formation of actin nodules and filopodia requires both actin polymerisation and Arp2/3-dependent nucleation.

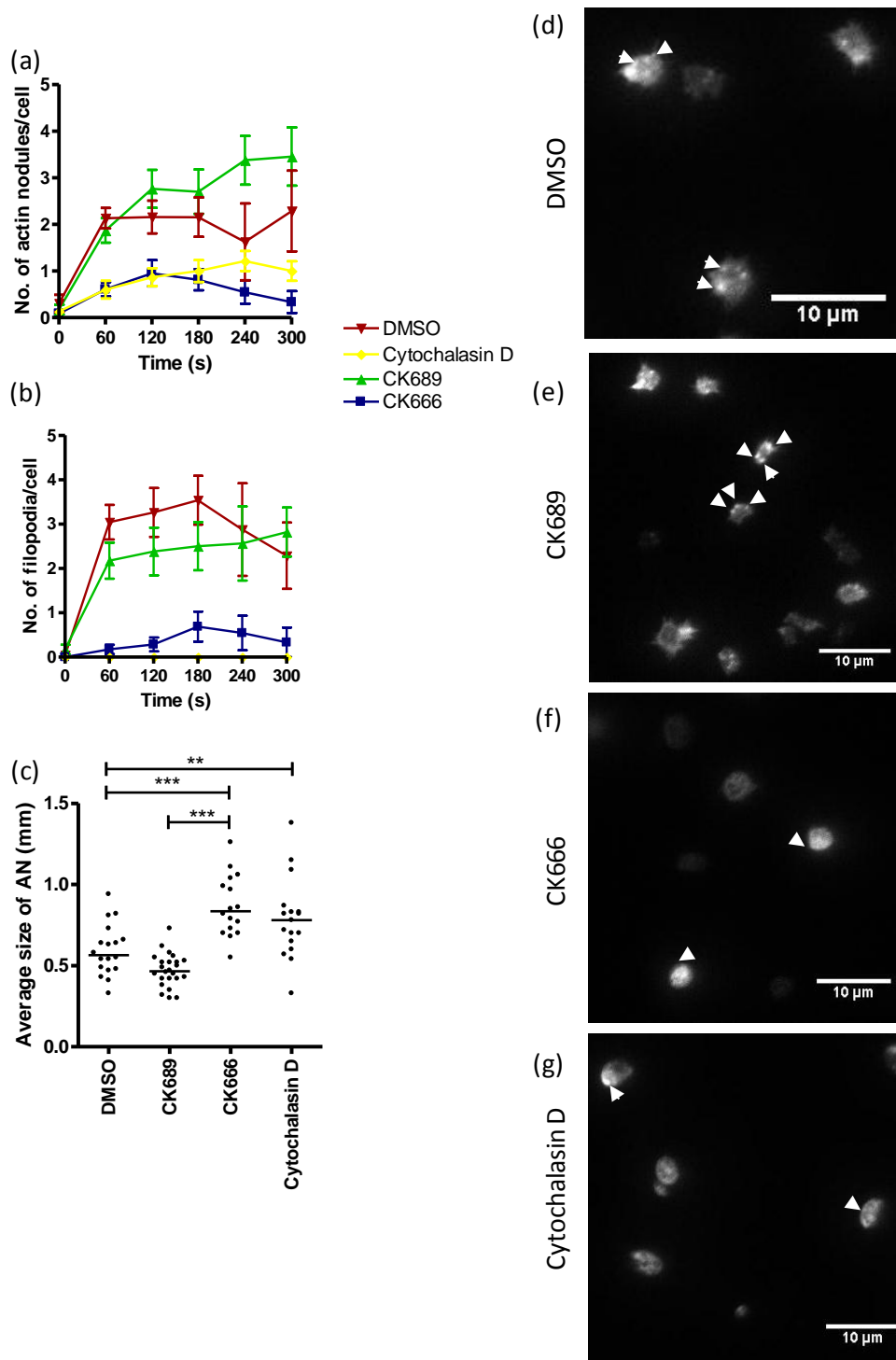


**Figure 5: Dependence of actin nodules and filopodia on Arp2/3-dependent nucleation and polymerisation in lifeact-GFP platelets.** Number of actin nodules (a) and filopodia (b) per cell after addition of DMSO (0.1%), the Arp2/3 inhibitor CK666 20 $\mu$ M, relevant control compound CK689  $\mu$ M, and cytochalasin D (10 $\mu$ M). Diameter of actin nodules following addition of these compounds (c). Appearance of platelets and actin nodules (white arrowheads) following addition of DMSO (d) the inhibitors CK689 (e) and CK666 (f) and cytochalasin D (g). N<15 for each compound.

### *3.6 Actin nodules appear to be associated with filopodia*

Following live imaging of Lifeact-GFP platelets it was noted that actin nodules appear to be localised to the base of filopodia (Figure 6a), therefore the relationship between actin nodules and filopodia was explored further. Initially, the region at the base of a filopodia was examined for 10 seconds before and after filopodia formation for the presence of an actin nodule (Figure 6b). This showed that in the majority of cases, an actin nodule was present prior to filopodia formation, and in around 50% of cases this nodule was present more than 10 seconds prior to filopodia formation (Figure 6b). This led us to further examine the development of the two structures by looking at the relationship between the two from the initial contact of the platelet with fibrinogen. In particular, the time at which an actin nodule appeared before filopodia formation was observed (Figure 6c), and the time after filopodia formation for which the nodule persists (Figure 6d). This revealed a peak in actin nodule formation 10 seconds before filopodia formation (Figure 6c), and that the majority of actin nodules disappeared within 75 seconds of filopodia formation (Figure 6d). Taken together, the data presented here allowed a schematic of the average lifespan of an actin nodule to be drawn (Figure 6e). This showed that actin nodules appear on average 18 seconds (SD 1.94 seconds) before a filopodia forms, and persist for an average of 69 seconds (SD 0.91 seconds) after filopodia formation, giving a mean lifespan of 87 seconds (SD 4.23 seconds).

These data show actin nodule lifespan to coordinate with filopodia formation.

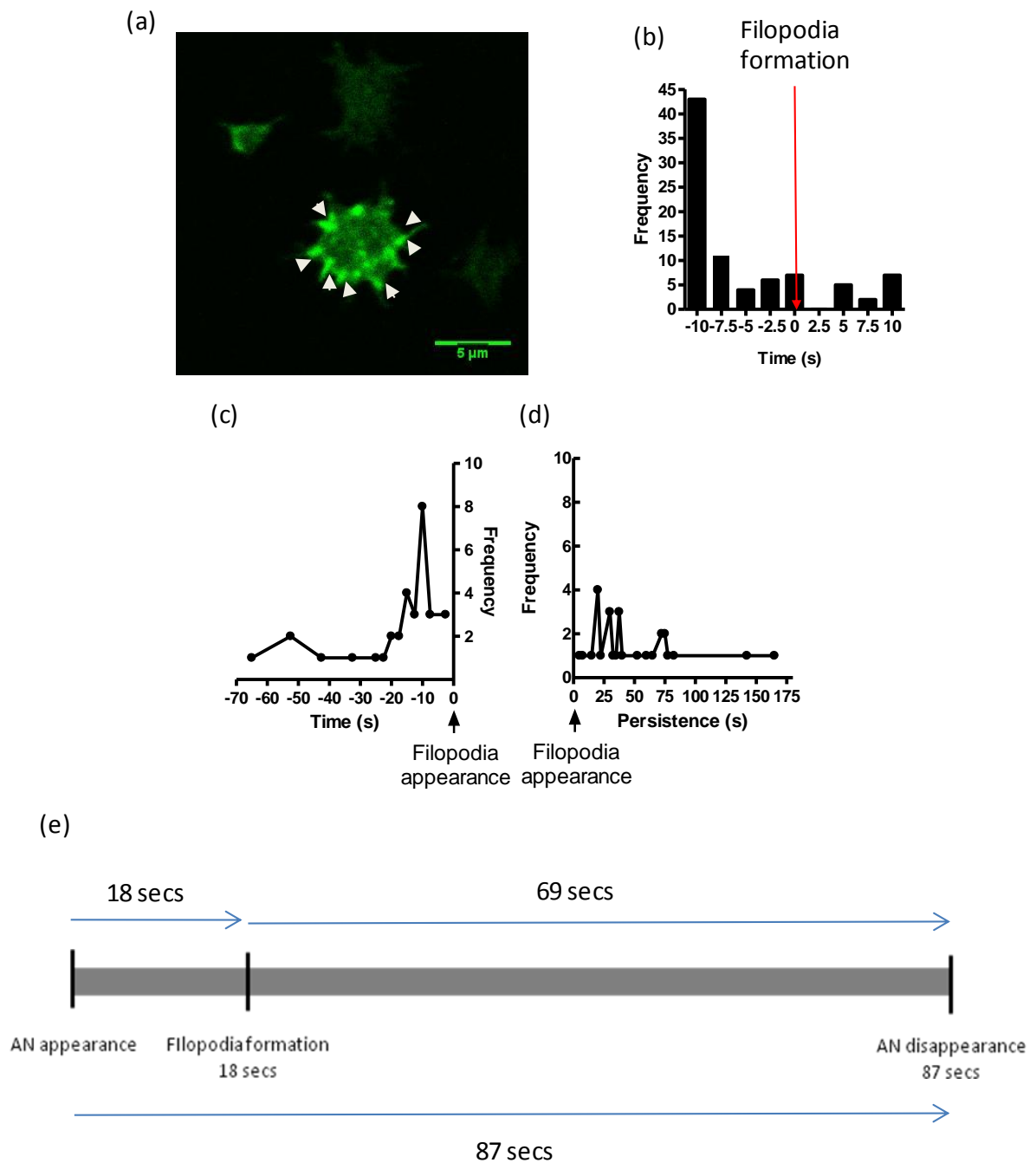


**Figure 6 - Relationship between actin nodules and filopodia in lifeact-GFP mouse platelets.** Actin nodules appear to be located at the base of filopodia (a) Time of actin nodule appearance in relation to filopodia appearance ( $n=85$ ) (b), frequency of actin nodules appearing per second before filopodia appearance ( $n=32$ ) (c), and frequency of actin nodule persistence following filopodia appearance ( $n=32$ ) (d). Schematic of actin nodule lifetime (e).

### 3.7 Dynamics of actin nodule movement

To determine if actin nodules move towards the filopod with which they are associated or whether they remain static, the particle tracking plugin for ImageJ (Fabrice Cordelieres, Institut Curie) was used to follow their movement (Figure 7a) over time (Figure 7 b-j). The resulting plots showed that actin nodules appear to remain relatively static with only small random movements being observed (Figure 7 b-j), which are usually around half of their own length ( $<0.2\mu\text{m}$ ). Therefore, it appears that actin nodules are relatively static and may represent adhesions or anchor points for filopodia.

### 3.8 Colocalisation of focal adhesion proteins with actin nodules

As actin nodules remain static at the base of filopodia, it is possible that they are equivalent to focal adhesions, albeit somewhat smaller in size. To investigate this, fixed human platelets were counterstained with FITC-phalloidin, and stained with antibodies to a number of focal adhesion proteins; the actin binding proteins vinculin, paxillin, p34, and talin, the integrin subunit  $\alpha\text{IIb}$ , and the focal adhesion protein pFAK (Figure 8 a-f). The subunit of the Arp2/3 complex was used as a positive control for actin nodules, as they have been shown to contain it (Calaminus *et al.* 2008). The results showed actin nodule colocalisation with vinculin (Figure 8a), paxillin (Figure 8b), p34 (Figure 8d), talin (Figure 8e), and  $\alpha\text{IIb}$  (Figure 8f), although they did not colocalise with pFAK (Figure 8c).

Therefore, actin nodules contain a number of proteins found at focal adhesions indicating that they may play a role in anchoring the platelet to the substrate and provide initiation points for filopodia formation.

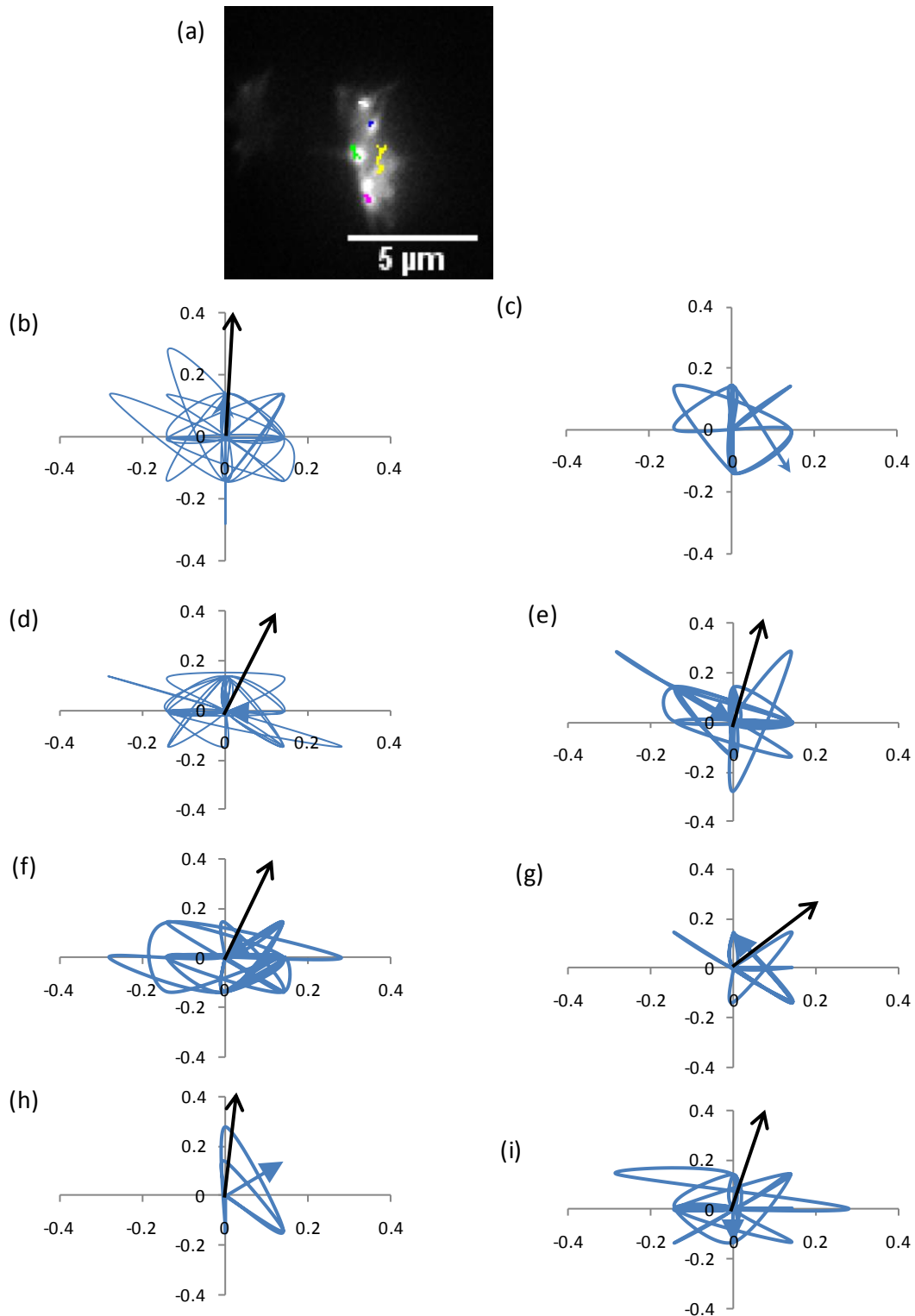


**Figure 7: The association between actin nodules and filopodia in lifeact-GFP platelets.** Particle tracking of an actin nodules using ImageJ. Each coloured line represents the trajectory of a single actin nodule (a). The directionality of actin nodule movements. Blue arrows represent the direction of movement of actin nodules at the last measured point and black arrows represent the angle of filopodia emergence from the associated actin nodule (b-i).

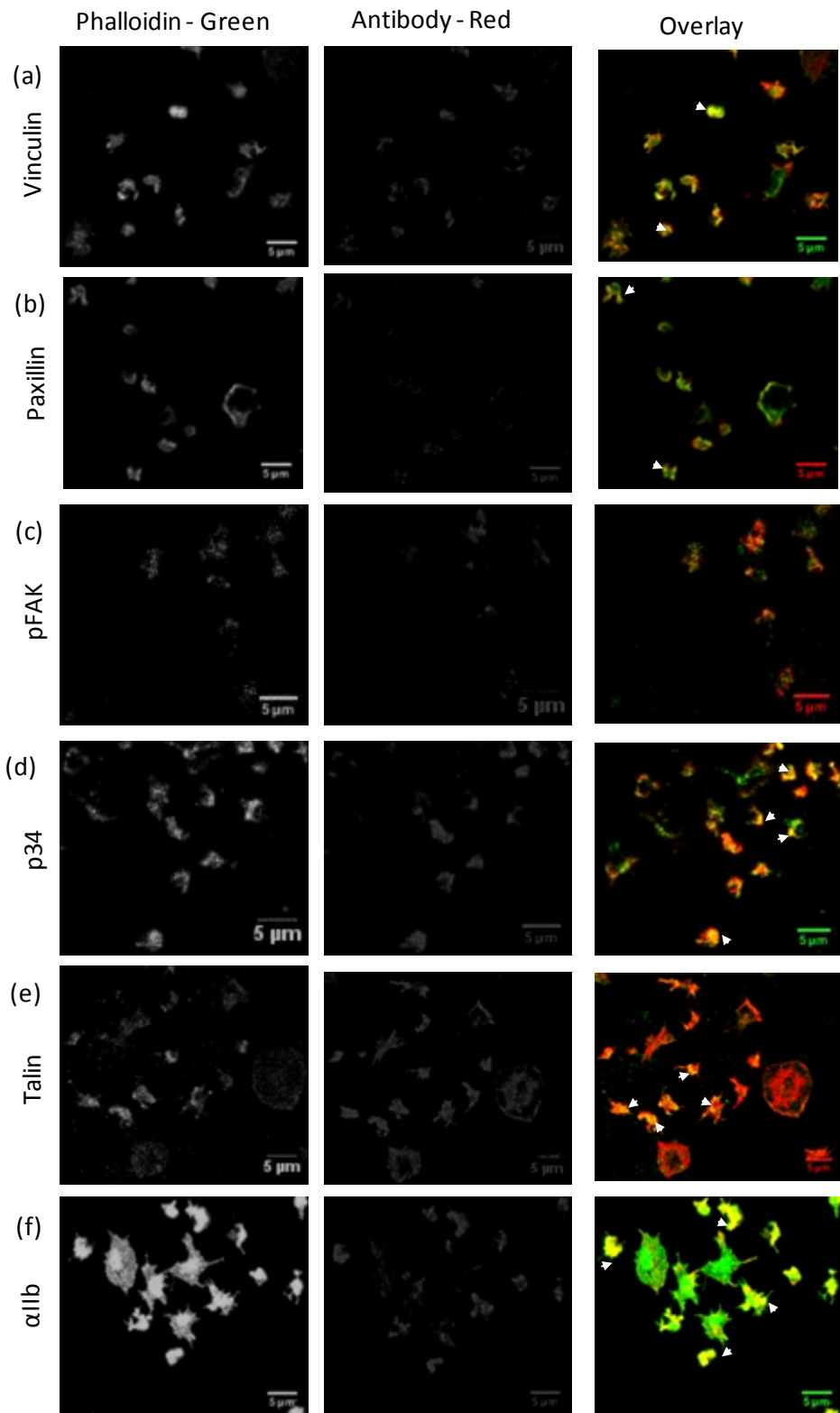


**Figure 8: Focal adhesion staining.** 488-linked staining of the focal adhesion proteins vinculin (a) paxillin (b), pFAK (c), p34 (d), talin (e), and  $\alpha$ IIb (f) in human platelets. Actin in platelets was costained with rhodamine and intensity normalised to relevant controls. Examples of cells expressing colocalisation are marked by white arrowheads. Images taken on a Leica DM IRE2 confocal microscope and a 63x 1.4Na oil immersion objective

### 3.9 Markers of endocytosis

It has been shown that actin nodules do not have a role in exocytosis (Calaminus *et al.* 2008), but it is possible that actin nodules are involved in endocytosis. Therefore, their relationship with dynamin- and clathrin-mediated endocytosis was examined. Using fixed human platelets in which the actin had been costained with rhodamine.

Human platelets containing actin costained with FITC were stained with an antibody to clathrin and the two did not appear to colocalise (Figure 9a). Furthermore, addition of the dynamin inhibitor Dynasore to lifeact-GFP appeared to have no effect on the number of actin nodules per cell (Figure 9b). In addition, quantification of the number of actin nodules per cell showed platelets treated with DMSO and Dynasore to have a similar frequency distribution of actin nodules per cell (Figure 9c). The peak number of actin nodules for both Dynasore and 0.3% DMSO treated platelets was 2 per cell, although the range of actin nodules per cell was greater in those treated with 0.3% DMSO (0-7 nodules/cell) than with Dynasore (0-12 nodules/cell).

Therefore, actin nodules do not appear to be involved in dynamin- or clathrin- mediated endocytosis.

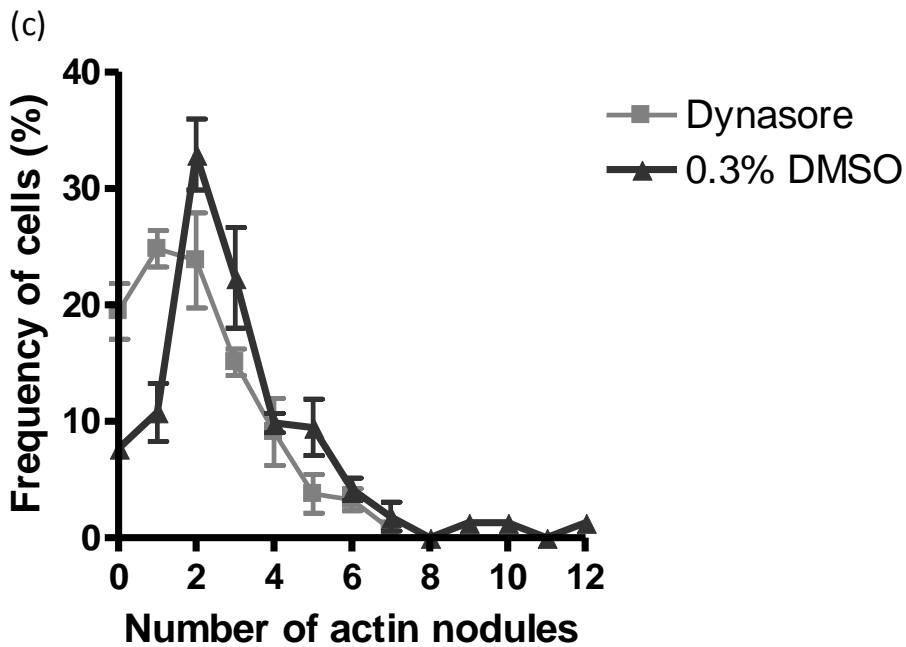
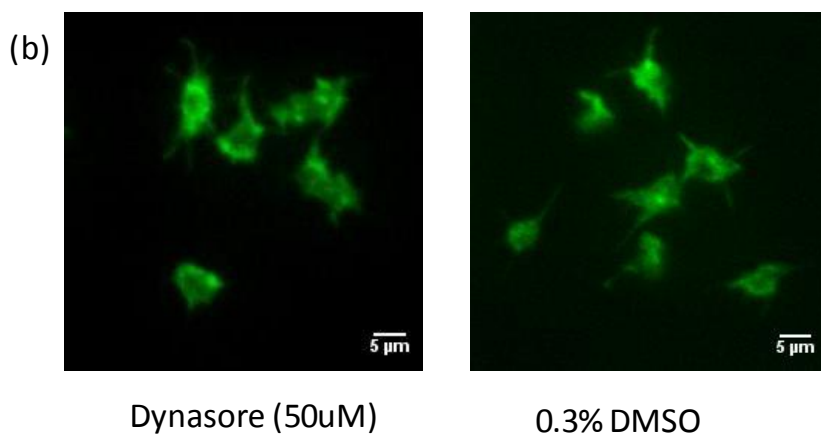
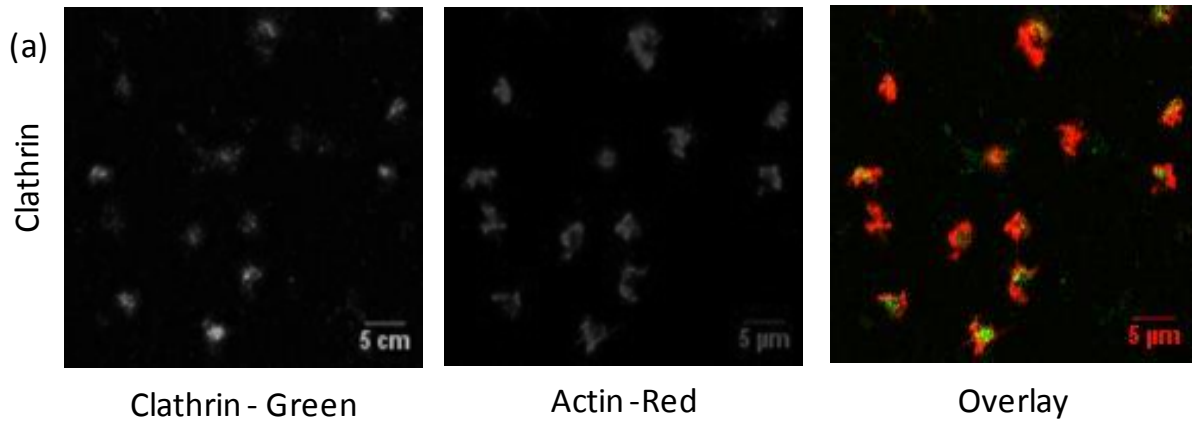


**Figure 9: Relationship between actin nodules and endocytosis.** Colocalisation of clathrin antibodies with FITC-stained actin in human fixed platelets (a). Appearance of lifeact-GFP platelets following addition of 50µM Dynasore and 0.3% DMSO (b). Percentage of cells expressing actin nodules addition of Dynasore to lifeact-GFP platelets.



#### 4. DISCUSSION

This study aimed to verify the Lifeact-GFP transgenic mouse as a model for studying platelet actin dynamics in real time, and to further describe the role of actin nodules in spreading platelets. The results of this study show that platelets obtained from mice expressing the lifeact-GFP transgene perform similarly to those obtained from wild type platelets in terms of platelet spreading and aggregation, and thus they appear to constitute a valid model for the visualisation of platelet actin dynamics. Therefore, these platelets were used to characterise actin nodules in real time in terms of their lifetime, dynamics, association with filopodia and their role in platelet spreading.

Lifeact platelets presented a considerable benefit to this study, as they allowed live imaging of platelet actin within minimal impact on actin dynamics and no artefacts of fixing or staining. In addition, live imaging allowed platelet spreading to be examined from the exact time of contact with substrate, and thus timing was more exact.

The functionality of lifeact-GFP platelets was investigated. Platelets were stimulated through P2Y<sub>1</sub> and P2Y<sub>12</sub>, GPVI, Clec2, and the thrombin receptor, and their aggregation compared to those of WT platelets. Lifeact-GFP transgenic platelets appeared to aggregate in a normally when compared to WT platelets. *In vivo* experiments were not carried out in the study, but mice appeared phenotypically and behaviourally normal with no evidence of clotting dysfunction. However, future experiments could determine if bleeding times are affected by using a tail bleed assay. Therefore, lifeact platelets appear to constitute a valid model for visualising actin dynamics in platelets.

Having established that the platelets function normally, their spreading was examined. Platelets have been shown to undergo a series of distinct morphological changes during platelet spreading (Hartwig *et al.*, 1992), beginning with the appearance of focal adhesions, followed by formation of filopodia and culminating in lamellipodia and stress fibre formation. The lifeact probe has been shown not to significantly perturb the actin cytoskeleton dynamics of a number of cell types including platelets *in vitro* or *in vivo* (Riedl *et al.* 2008; 2010). By comparing the spreading of lifeact platelets with those of fixed phalloidin-labelled wild-type platelets, the results presented here show that actin in lifeact-GFP platelets undergo the same series of changes.

Actin structures are well characterised; particularly filopodia, lamellipodia and stress fibres. In 2008, actin nodules were described as punctuate areas of actin staining present in platelets during early spreading (Calaminus *et al.* 2008). In order to gain further understanding of these structures, the lifetime of actin nodules was investigated and their characteristics studied in order to elucidate a possible function. In the original paper, actin nodules were shown to contain the actin nucleating complex Arp2/3, the small GTPases Rac, Rho, and the integrins  $\beta 1$  and  $\beta 3$  (Calaminus *et al.* 2008). Therefore, the authors suggested that they may play a role in adhesion or actin remodelling and suggested two of potential roles for the structures: (1) reservoir of actin for platelet spreading (2) initial adhesion sites or focal adhesion-type structures. However, it is also possible that they have a role in endocytosis.

The average width of an actin nodule does not vary significantly between WT and lifeact-GFP backgrounds, and in lifeact platelets the median diameter is  $0.57\mu\text{m}$ . This is smaller than

that quoted in the original paper (Calaminus *et al.* 2008) although this is likely due to the use of human platelets in that study, which are considerably larger than mouse platelets. In order to confirm that there is no change in size; platelets from both backgrounds could be fixed and stained in the same way.

By using real-time microscopy to synchronise platelet spreading, the results of this study show that the peak number of actin nodules form at 3 minutes following initiation of platelet spreading and then to remain fairly constant. This suggests that the structures have a finite lifetime, which was found to be 87 seconds, although the majority persisted for 30-60 seconds. This supports previous preliminary data attained using these mice (Amy Davies – unpublished) which suggests that the majority of actin nodules persist for 30-60 seconds.

During preliminary analysis, it was noted that actin nodules appeared to be associated with the base of developing filopodia, appearing around 18 seconds prior to the formation of filopodia and persisting for on average of 69 seconds following their appearance. The correlation of actin nodule lifespan with the formation of filopodia suggested a relationship between the two. Therefore, the spatial association of actin nodules and filopodia was investigated using particle tracking to determine if the nodules moved towards the extending filopodia or remained associated at the base. During the observation time, actin nodules appeared to remain relatively stable and moved less than half their own length with no apparent directionality. This finding suggests that while an actin nodule does appear to be associated with a filopod, it does not seem to actively move towards it. Instead, the small movements seen may represent movement of the actin nodule as the platelet spreads.

The possibility that actin nodules may be acting as a reservoir of actin for formation of actin structures during platelet spreading, specifically filopodia was further investigated. The actin polymerisation inhibitor cytochalasin D and the Arp2/3 inhibitor CK666 along with suitable DMSO controls were added to lifeact-GFP platelets. Addition of both inhibitors significantly decreased the number of actin nodules in platelets but did not ablate their presence entirely. This suggests either that a small number of actin nodules are present before spreading begins and that no more develop in the presence of these inhibitors, or that the effect of these inhibitors is not complete or a small number of nodules may still form in their presence. Interestingly, the actin nodules in the inhibited platelets appeared to be more diffuse than those in control samples, and they resembled morphologically actin nodule-like structures observed in 'resting' platelets i.e. those which have not yet been activated (Dr. Steven Thomas, personal correspondence). Measurement of the actin nodules in treated platelets showed these to be significantly larger than those treated with control compounds. If 'resting' platelets do contain actin nodules, it may be that these mature during spreading and that inhibition of actin nucleation and polymerisation prevent this.

These data confirm that both actin nucleation and polymerisation are necessary for the development of both structures, but does not confirm that actin nodules are necessary for the formation of filopodia. However, both processes appear to be important in the transition from 'resting-type' to 'spreading-type' structures, and suggests that they may be related to the function of these structures.

The stability of actin nodules observed using real-time microscopy suggests that they may be related to focal adhesion-like structures. Costaining with focal adhesion proteins showed

talin, vinculin and paxillin to be localised with the structures, but not pFAK. Repetition of this staining or staining with total FAK may clarify this result. However, the colocalisation of the majority of these proteins suggests that actin nodules may be related to focal adhesions. These structures generally contain integrins and costaining with antibodies to the major platelet integrin  $\alpha\text{IIb}\beta\text{3}$  showed the integrin to be present at these structures. This combined with the relatively static appearance of surface nodules indicates that at least some part of their role is in adhesion.

The final possible role of actin nodules is related to endocytosis. Staining of platelets with antibodies to clathrin showed that actin nodules and clathrin did not colocalise. Furthermore, treatment with the dynamin-mediated endocytosis inhibitor Dynasore did not significantly change the apparent distribution of platelets expressing certain numbers of actin nodules. These data suggest that actin nodules are not involved in clathrin or dynamin-mediated endocytosis, but repetition of clathrin staining using lifeact-GFP platelets is needed.

In conclusion, in this study, I show that lifeact-GFP mice are a suitable model for studying platelet actin dynamics, and that actin nodules may play a role in cytoskeletal remodelling or adhesion but are not likely to be involved in clathrin- or dynamin-mediated endocytosis. During cell spreading, filopodia form the initial attachments to the substrate, to which adhesion proteins are recruited (Mattila and Lappalainen, 2008). Therefore, adhesion in platelets may be initiated by structures which have the potential to form filopodia, and therefore the structures acquire adhesion proteins. Further work to verify this could follow the recruitment of these proteins to actin nodules.

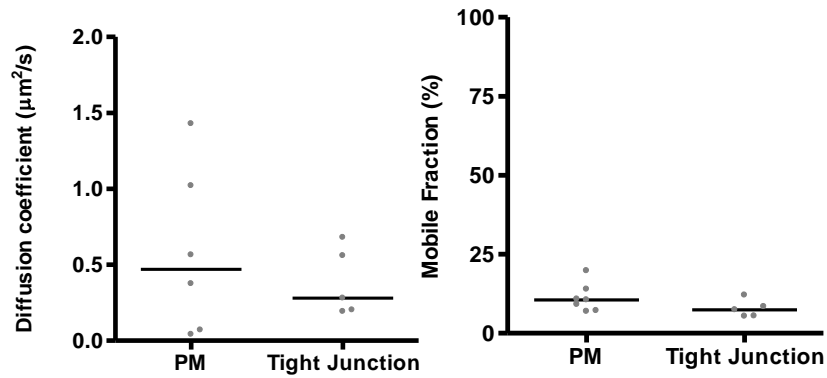
Additional further work could cover a variety of points. It would be interesting to monitor cytoskeletal rearrangements under conditions of shear stress to see if the structures observed during thrombus formation are dependent on actin nodule formation. In addition, observing the relationship between actin nodules and filopodia using epifluorescence microscopy may add considerable amounts of information as to the location and movements of actin nodules. In this study, total internal fluorescence reflectance (TIRF) microscopy was used; a technique in which only 100-200 nm of the platelet in contact with the glass slides is illuminated. Whilst this produces a clear image which is easy to interpret, it omits any information from further within the cell. Therefore it is possible that actin nodules may not disappear but simply move out of the plane of vision.

A working hypothesis of the role of filopodia based on the data presented here is as follows. If the actin nodule-like structures correspond to those observed in spreading platelets, they may represent an 'immature' actin nodule structure which matures during spreading. If this is correct, it may be that actin nodules are recruited to the cell membrane following contact of the platelet with a substrate. As the 'mature' structures colocalise with a number of proteins involved in focal adhesions including integrin  $\alpha$ IIb, it could be that contact of the platelet with the substrate causes clustering of integrin leading to recruitment of some focal adhesion-like proteins to these regions. The result of clustering of integrins is inside-out signalling, which has been shown to lead to cytoskeletal rearrangements. These rearrangements could lead to morphological changes in the actin nodules and subsequent filopodia formation.

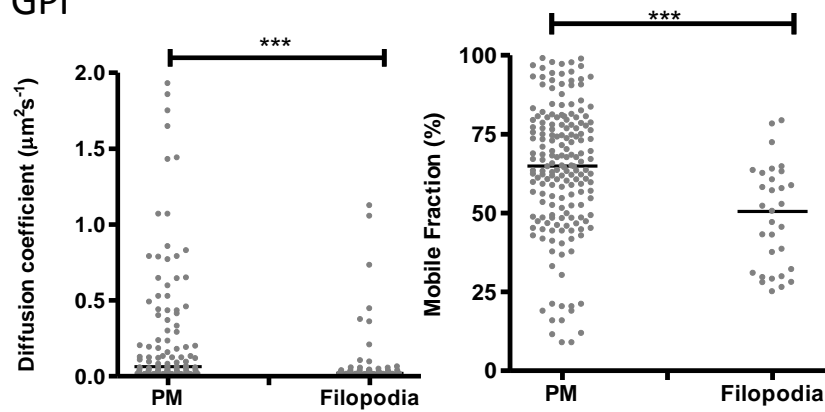
This hypothesis relies on the actin nodule-like structures within resting platelets being actin nodules., Therefore, further work to test this hypothesis would need to repeat the characterisations previously carried out in this report and previously (Calaminus *et al.*, 2008) in terms of the processes on which these structures are dependent and the proteins with which they colocalise.

## SUPPLEMENTARY DATA

## Occludin



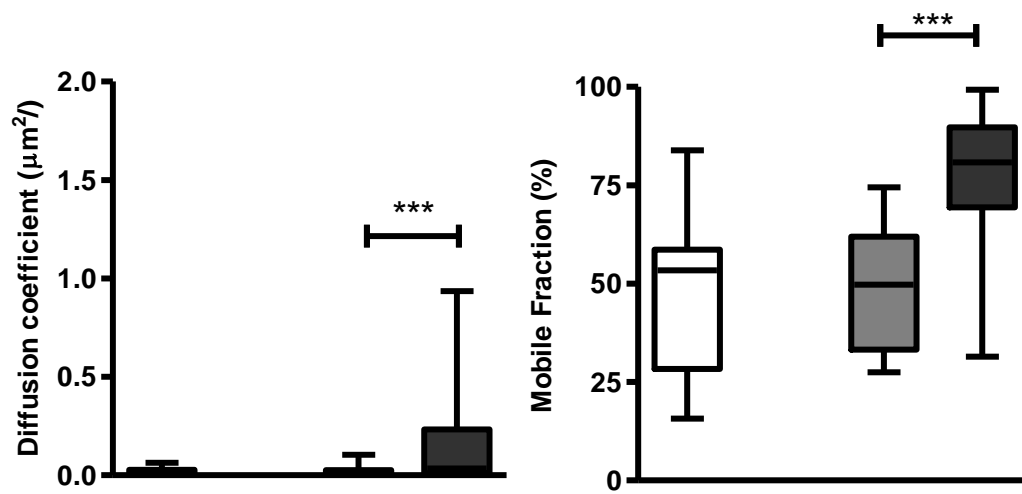
## GPI



**Supplementary Figure 1– Variance in diffusion coefficient and mobile fraction between PM and filopodia.** Variance in diffusion coefficient and mobile fraction between HepG2 cells transfected to express GFP-occludin ( $n>5$ ) and GFP-GPI ( $n>40$ ) at the PM and filopodia. Diffusion coefficient and mobile fraction were calculated as previously described using data from Zeiss software.  $N>15$ .

		<b>Median (IQ range)</b>	<b>Mean</b>	<b>S.D.</b>
Occludin diffusion coefficient ( $\mu\text{m}^2\text{s}^{-1}$ )	PM	<b>0.47</b> (1.2)	0.58	0.55
	Tight Junction	<b>0.28</b> (0.42)	0.38	0.22
Occludin mobile fraction (%)	PM	<b>10.54</b> (6.76)	11.17	4.49
	Tight Junction	<b>7.45</b> (4.84)	7.75	2.74
GPI diffusion coefficient ( $\mu\text{m}^2\text{s}^{-1}$ )	PM	<b>0.06</b> (0.33)	0.26	0.42
	Filopodia	<b>0.02</b> (0.03)	0.09	0.22
GPI mobile fraction (%)	PM	<b>64.94</b> (28.61)	63.96	20.38
	Filopodia	<b>50.47</b> (31.67)	48.62	16.23

**Supplementary Table 1: Median, interquartile range (IQ range), mean, and standard deviation (S.D) of data presented in Figure 10.** HepG2 cells were transfected to express GFP-occludin and GFP-GPI and bleached using a Zeiss Meta head laser scanning 780 confocal microscope. Statistics were calculated as previously described using data from Zeiss software.  $n > 21$ . Values calculated using GraphPad Prism Software.



**Supplementary Figure 2: Variance in diffusion coefficient and mobile fraction at specific cellular structures.** Variance in diffusion coefficient (a) and mobile fraction (b) between HepG2 cells transfected to express GFP-GPI at specific locations  $N > 15$ .

		<b>Median (IQ range)</b>	<b>Mean</b>	<b>S.D</b>
OCLDN Diffusion Coefficient ( $\mu\text{m}^2/\text{s}$ )	Cell contact PM	<b>0.07</b> (0)	0.23	0.29
	Tight junction	<b>0.28</b> (0.42)	0.38	0.22
OCLN Mobile Fraction (%)	Cell contact PM	<b>11.52</b> (8.72)	12.49	5.63
	Tight junction	<b>7.45</b> (4.84)	7.75	2.74
GPI Diffusion Coefficient ( $\mu\text{m}^2/\text{s}$ )	Cell contact PM	<b>0.04</b> (0.31)	0.24	0.41
	Exploratory filopodia	<b>0.01</b> (0.23)	0.19	0.36
	Exploratory PM	<b>0.003</b> (0.02)	0.07	0.19
GPI Mobile Fraction (%)	Cell contact PM	<b>79.33</b> (24.93)	73.84	21.25
	Exploratory filopodia	<b>53.39</b> (30.28)	46.57	18.74
	Exploratory PM	<b>50.4</b> (29.95)	51.17	19.03

**Supplementary Table 2: Median, interquartile range (IQ range), mean, and standard deviation (S.D) of occludin and GPI at specific cellular locations.** HepG2 cells were transfected to express GFP-occludin and GFP-GPI and bleached using a Zeiss Meta head laser scanning 780 confocal microscope. Diffusion coefficient and mobile fraction were calculated as previously described using data from Zeiss software. Values calculated using GraphPad Prism Software.



## BIBLIOGRAPHY

- Adam, F., M. C. Guillin, et al. (2003). "Glycoprotein Ib-mediated platelet activation. A signalling pathway triggered by thrombin." *Eur J Biochem* **270**(14): 2959-70.
- Akbar, H., Shang, X., Perveen, R., Berryman, M., Funk, K., Johnson, JF., Tandon, NN., Zheng, Y., (2011). "Gene Targeting Implicates Cdc42 GTPase in GPVI and Non-GPVI Mediated Platelet Filopodia Formation, Secretion and Aggregation." *PLoS ONE* **6**(7).
- Anzola, M. and J. J. Burgos (2003). "Hepatocellular carcinoma: molecular interactions between hepatitis C virus and p53 in hepatocarcinogenesis." *Expert Rev Mol Med* **5**(28): 1-16.
- Aspenstrom, P., U. Lindberg, et al. (1996). "Two GTPases, Cdc42 and Rac, bind directly to a protein implicated in the immunodeficiency disorder Wiskott-Aldrich syndrome." *Curr Biol* **6**(1): 70-5.
- Asselah, T. and P. Marcellin (2011). "New direct-acting antivirals' combination for the treatment of chronic hepatitis C." *Liver Int* **31** *Suppl 1*: 68-77.
- Barreiro, O., M. Zamai, et al. (2008). "Endothelial adhesion receptors are recruited to adherent leukocytes by inclusion in preformed tetraspanin nanoplatforms." *J Cell Biol* **183**(3): 527-42.
- Barth, H., R. Cerino, et al. (2005). "Scavenger receptor class B type I and hepatitis C virus infection of primary tupaia hepatocytes." *J Virol* **79**(9): 5774-85.
- Barth, H., E. K. Schnober, et al. (2006). "Viral and cellular determinants of the hepatitis C virus envelope-heparan sulfate interaction." *J Virol* **80**(21): 10579-90.
- Bartosch, B., J. Bukh, et al. (2003a). "In vitro assay for neutralizing antibody to hepatitis C virus: evidence for broadly conserved neutralization epitopes." *Proc Natl Acad Sci U S A* **100**(24): 14199-204.
- Bartosch, B., A. Vitelli, et al. (2003b). "Cell entry of hepatitis C virus requires a set of co-receptors that include the CD81 tetraspanin and the SR-B1 scavenger receptor." *J Biol Chem* **278**(43): 41624-30.
- Blanchard, E., S. Belouzard, et al. (2006). "Hepatitis C virus entry depends on clathrin-mediated endocytosis." *J Virol* **80**(14): 6964-72.
- Boucheix, C. and E. Rubinstein (2001). "Tetraspanins." *Cell Mol Life Sci* **58**(9): 1189-205.
- Brass, L. (2010). "Understanding and evaluating platelet function." *Hematology Am Soc Hematol Educ Program*: 387-96.
- Brazzoli, M., A. Bianchi, et al. (2008). "CD81 is a central regulator of cellular events required for hepatitis C virus infection of human hepatocytes." *J Virol* **82**(17): 8316-29.
- Brazzoli, M., A. Helenius, et al. (2005). "Folding and dimerization of hepatitis C virus E1 and E2 glycoproteins in stably transfected CHO cells." *Virology* **332**(1): 438-53.
- Brimacombe, C. L., J. Grove, et al. (2011). "Neutralizing antibody-resistant hepatitis C virus cell-to-cell transmission." *J Virol* **85**(1): 596-605.
- Calaminus, S. D., S. Thomas, et al. (2008). "Identification of a novel, actin-rich structure, the actin nodule, in the early stages of platelet spreading." *J Thromb Haemost* **6**(11): 1944-52.
- Callens, N., Y. Ciczora, et al. (2005). "Basic residues in hypervariable region 1 of hepatitis C virus envelope glycoprotein e2 contribute to virus entry." *J Virol* **79**(24): 15331-41.

- Claude, P. and D. A. Goodenough (1973). "Fracture faces of zonulae occludentes from "tight" and "leaky" epithelia." *J Cell Biol* **58**(2): 390-400.
- Cocquerel, L., C. Wychowski, et al. (2000). "Charged residues in the transmembrane domains of hepatitis C virus glycoproteins play a major role in the processing, subcellular localization, and assembly of these envelope proteins." *J Virol* **74**(8): 3623-33.
- Cohen, D., P. J. Brennwald, et al. (2004). "Mammalian PAR-1 determines epithelial lumen polarity by organizing the microtubule cytoskeleton." *J Cell Biol* **164**(5): 717-27.
- Coller, K. E., K. L. Berger, et al. (2009). "RNA interference and single particle tracking analysis of hepatitis C virus endocytosis." *PLoS Pathog* **5**(12): e1000702.
- Coyne, C., Shen, L, Turner, JR, Bergelson, JM (2007). "Coxsackievirus Entry across Epithelial Tight Junctions Requires Occludin and the Small GTPases Rab34 and Rab5." *Cell Host & Microbe* **2**: 181-192.
- Coyne, C. B. and J. M. Bergelson (2006). "Virus-induced Abl and Fyn kinase signals permit coxsackievirus entry through epithelial tight junctions." *Cell* **124**(1): 119-31.
- Cukierman, L., L. Meertens, et al. (2009). "Residues in a highly conserved claudin-1 motif are required for hepatitis C virus entry and mediate the formation of cell-cell contacts." *J Virol* **83**(11): 5477-84.
- Davis, C., Harris, H.J., McKeating, J.M. (In press). *The Involvement of Tight Junction protein Claudin-1 in Hepatitis C virus entry: 273-291.*
- Decaens, C., M. Durand, et al. (2008). "Which in vitro models could be best used to study hepatocyte polarity?" *Biol Cell* **100**(7): 387-98.
- Denis, C., N. Methia, et al. (1998). "A mouse model of severe von Willebrand disease: defects in hemostasis and thrombosis." *Proc Natl Acad Sci U S A* **95**(16): 9524-9.
- Doggett, T. A., G. Girdhar, et al. (2002). "Selectin-like kinetics and biomechanics promote rapid platelet adhesion in flow: the GPIb(alpha)-vWF tether bond." *Biophys J* **83**(1): 194-205.
- Dreux, M. and F. L. Cosset (2009). "Detection of neutralizing antibodies with HCV pseudoparticles (HCVpp)." *Methods Mol Biol* **510**: 427-38.
- Drummer, H. E., McKeating, J.M (2011). *Hepatitis C Virus Glycoprotein-dependent Entry. Hepatitis C Virus Glycoprotein-dependent Entry.* Y. H. SL Tan. Norfolk, UK, Caister Academic Press: 321-345.
- Dustin, L. B. and C. M. Rice (2007). "Flying under the radar: the immunobiology of hepatitis C." *Annu Rev Immunol* **25**: 71-99.
- Ellis, S. and H. Mellor (2000). "The novel Rho-family GTPase rif regulates coordinated actin-based membrane rearrangements." *Curr Biol* **10**(21): 1387-90.
- Espenel, C., E. Margeat, et al. (2008). "Single-molecule analysis of CD9 dynamics and partitioning reveals multiple modes of interaction in the tetraspanin web." *J Cell Biol* **182**(4): 765-76.
- Evans, M. J., T. von Hahn, et al. (2007). "Claudin-1 is a hepatitis C virus co-receptor required for a late step in entry." *Nature* **446**(7137): 801-5.
- Faix, J. and K. Rottner (2006). "The making of filopodia." *Curr Opin Cell Biol* **18**(1): 18-25.
- Farci, P., A. Shimoda, et al. (2000). "The outcome of acute hepatitis C predicted by the evolution of the viral quasispecies." *Science* **288**(5464): 339-44.
- Farquhar, M. G. and G. E. Palade (1963). "Junctional complexes in various epithelia." *J Cell Biol* **17**: 375-412.

- Fidge, N. H. (1999). "High density lipoprotein receptors, binding proteins, and ligands." *J Lipid Res* **40**(2): 187-201.
- Furuse, M., K. Fujita, et al. (1998). "Claudin-1 and -2: novel integral membrane proteins localizing at tight junctions with no sequence similarity to occludin." *J Cell Biol* **141**(7): 1539-50.
- Grove, J., T. Huby, et al. (2007). "Scavenger receptor BI and BII expression levels modulate hepatitis C virus infectivity." *J Virol* **81**(7): 3162-9.
- Gupton, S. L. and F. B. Gertler (2007). "Filopodia: the fingers that do the walking." *Sci STKE* **2007**(400): re5.
- Guttman, J. A. and B. B. Finlay (2009). "Tight junctions as targets of infectious agents." *Biochim Biophys Acta* **1788**(4): 832-41.
- Handagama PJ, G. J., Shuman MA, McEver RP, Bainton DF. (1987). "Incorporation of a circulating protein into megakaryocyte and platelet granules." *Proc Natl Acad Sci USA* **84**: 861-5.
- Harris, H. J., C. Davis, et al. (2010). "Claudin association with CD81 defines hepatitis C virus entry." *J Biol Chem* **285**(27): 21092-102.
- Harris, H. J., M. J. Farquhar, et al. (2008). "CD81 and claudin 1 coreceptor association: role in hepatitis C virus entry." *J Virol* **82**(10): 5007-20.
- Harrison, P., B. Wilbourn, et al. (1989). "Uptake of plasma fibrinogen into the alpha granules of human megakaryocytes and platelets." *J Clin Invest* **84**(4): 1320-4.
- Hartwig, J. H. (1992). "Mechanisms of actin rearrangements mediating platelet activation." *J Cell Biol* **118**(6): 1421-42.
- Higashi, T., T. Ikeda, et al. (2008). "Biochemical characterization of the Rho GTPase-regulated actin assembly by diaphanous-related formins, mDia1 and Daam1, in platelets." *J Biol Chem* **283**(13): 8746-55.
- Inoue, O., K. Suzuki-Inoue, et al. (2006). "Laminin stimulates spreading of platelets through integrin alpha6beta1-dependent activation of GPVI." *Blood* **107**(4): 1405-12.
- Koutsoudakis, G., A. Kaul, et al. (2006). "Characterization of the early steps of hepatitis C virus infection by using luciferase reporter viruses." *J Virol* **80**(11): 5308-20.
- Krieger, N., V. Lohmann, et al. (2001). "Enhancement of hepatitis C virus RNA replication by cell culture-adaptive mutations." *J Virol* **75**(10): 4614-24.
- Krieger, S. E., M. B. Zeisel, et al. (2010). "Inhibition of hepatitis C virus infection by anti-claudin-1 antibodies is mediated by neutralization of E2-CD81-claudin-1 associations." *Hepatology* **51**(4): 1144-57.
- Krugmann, S., I. Jordens, et al. (2001). "Cdc42 induces filopodia by promoting the formation of an IRSp53:Mena complex." *Curr Biol* **11**(21): 1645-55.
- Lavillette, D., E. I. Pecheur, et al. (2007). "Characterization of fusion determinants points to the involvement of three discrete regions of both E1 and E2 glycoproteins in the membrane fusion process of hepatitis C virus." *J Virol* **81**(16): 8752-65.
- Lavillette, D., A. W. Tarr, et al. (2005). "Characterization of host-range and cell entry properties of the major genotypes and subtypes of hepatitis C virus." *Hepatology* **41**(2): 265-74.
- Leslie, M. (2010). "Cell biology. Beyond clotting: the powers of platelets." *Science* **328**(5978): 562-4.

- Li, H. F., C. H. Huang, et al. (2009). "Mutagenesis of the fusion peptide-like domain of hepatitis C virus E1 glycoprotein: involvement in cell fusion and virus entry." *J Biomed Sci* **16**: 89.
- Lim, K. B., W. Bu, et al. (2008). "The Cdc42 effector IRSp53 generates filopodia by coupling membrane protrusion with actin dynamics." *J Biol Chem* **283**(29): 20454-72.
- Lindenbach, B. D., M. J. Evans, et al. (2005). "Complete replication of hepatitis C virus in cell culture." *Science* **309**(5734): 623-6.
- Liu, S., W. Yang, et al. (2009). "Tight junction proteins claudin-1 and occludin control hepatitis C virus entry and are downregulated during infection to prevent superinfection." *J Virol* **83**(4): 2011-4.
- Mangin, P., Y. Yuan, et al. (2003). "Signaling role for phospholipase C gamma 2 in platelet glycoprotein Ib alpha calcium flux and cytoskeletal reorganization. Involvement of a pathway distinct from FcR gamma chain and Fc gamma RIIA." *J Biol Chem* **278**(35): 32880-91.
- Masson, D., M. Koseki, et al. (2009). "Increased HDL cholesterol and apoA-I in humans and mice treated with a novel SR-BI inhibitor." *Arterioscler Thromb Vasc Biol* **29**(12): 2054-60.
- Matsuda, M., A. Kubo, et al. (2004). "A peculiar internalization of claudins, tight junction-specific adhesion molecules, during the intercellular movement of epithelial cells." *J Cell Sci* **117**(Pt 7): 1247-57.
- Mattila, P. K. and P. Lappalainen (2008). "Filopodia: molecular architecture and cellular functions." *Nat Rev Mol Cell Biol* **9**(6): 446-54.
- Mattila, P. K., A. Pykalainen, et al. (2007). "Missing-in-metastasis and IRSp53 deform PI(4,5)P2-rich membranes by an inverse BAR domain-like mechanism." *J Cell Biol* **176**(7): 953-64.
- Maxwell, M. J., S. M. Dopheide, et al. (2006). "Shear induces a unique series of morphological changes in translocating platelets: effects of morphology on translocation dynamics." *Arterioscler Thromb Vasc Biol* **26**(3): 663-9.
- McCarty, O. J., M. K. Larson, et al. (2005). "Rac1 is essential for platelet lamellipodia formation and aggregate stability under flow." *J Biol Chem* **280**(47): 39474-84.
- Mee, C. J., M. J. Farquhar, et al. (2010). "Hepatitis C virus infection reduces hepatocellular polarity in a vascular endothelial growth factor-dependent manner." *Gastroenterology* **138**(3): 1134-42.
- Mee, C. J., J. Grove, et al. (2008). "Effect of cell polarization on hepatitis C virus entry." *J Virol* **82**(1): 461-70.
- Mee, C. J., H. J. Harris, et al. (2009). "Polarization restricts hepatitis C virus entry into HepG2 hepatoma cells." *J Virol* **83**(12): 6211-21.
- Meunier, J. C., R. E. Engle, et al. (2005). "Evidence for cross-genotype neutralization of hepatitis C virus pseudo-particles and enhancement of infectivity by apolipoprotein C1." *Proc Natl Acad Sci U S A* **102**(12): 4560-5.
- Miranti, C. K., L. Leng, et al. (1998). "Identification of a novel integrin signaling pathway involving the kinase Syk and the guanine nucleotide exchange factor Vav1." *Curr Biol* **8**(24): 1289-99.
- Nesbitt, W. S., E. Westein, et al. (2009). "A shear gradient-dependent platelet aggregation mechanism drives thrombus formation." *Nat Med* **15**(6): 665-73.

- Nieswandt, B. and S. P. Watson (2003). "Platelet-collagen interaction: is GPVI the central receptor?" *Blood* **102**(2): 449-61.
- Patel-Hett, S., J. L. Richardson, et al. (2008). "Visualization of microtubule growth in living platelets reveals a dynamic marginal band with multiple microtubules." *Blood* **111**(9): 4605-16.
- Patel, A. H., J. Wood, et al. (2000). "Construction and characterization of chimeric hepatitis C virus E2 glycoproteins: analysis of regions critical for glycoprotein aggregation and CD81 binding." *J Gen Virol* **81**(Pt 12): 2873-83.
- Pellegrin, S. and H. Mellor (2005). "The Rho family GTPase Rif induces filopodia through mDia2." *Curr Biol* **15**(2): 129-33.
- Petracca, R., F. Falugi, et al. (2000). "Structure-function analysis of hepatitis C virus envelope-CD81 binding." *J Virol* **74**(10): 4824-30.
- Pileri, P., Y. Uematsu, et al. (1998). "Binding of hepatitis C virus to CD81." *Science* **282**(5390): 938-41.
- Piontek, J., L. Winkler, et al. (2008). "Formation of tight junction: determinants of homophilic interaction between classic claudins." *Faseb J* **22**(1): 146-58.
- Pleines, I., A. Eckly, et al. (2010). "Multiple alterations of platelet functions dominated by increased secretion in mice lacking Cdc42 in platelets." *Blood* **115**(16): 3364-73.
- Ploss, A., M. J. Evans, et al. (2009). "Human occludin is a hepatitis C virus entry factor required for infection of mouse cells." *Nature* **457**(7231): 882-6.
- Prehoda, K. E., J. A. Scott, et al. (2000). "Integration of multiple signals through cooperative regulation of the N-WASP-Arp2/3 complex." *Science* **290**(5492): 801-6.
- Pruyne, D., M. Evangelista, et al. (2002). "Role of formins in actin assembly: nucleation and barbed-end association." *Science* **297**(5581): 612-5.
- Rehermann, B. and M. Nascimbeni (2005). "Immunology of hepatitis B virus and hepatitis C virus infection." *Nat Rev Immunol* **5**(3): 215-29.
- Reininger, A. J., H. F. Heijnen, et al. (2006). "Mechanism of platelet adhesion to von Willebrand factor and microparticle formation under high shear stress." *Blood* **107**(9): 3537-45.
- Reynolds, G. M., H. J. Harris, et al. (2008). "Hepatitis C virus receptor expression in normal and diseased liver tissue." *Hepatology* **47**(2): 418-27.
- Ridley, A. J. (2011). "Life at the leading edge." *Cell* **145**(7): 1012-22.
- Riedl, J., A. H. Crevenna, et al. (2008). "Lifeact: a versatile marker to visualize F-actin." *Nat Methods* **5**(7): 605-7.
- Riedl, J., K. C. Flynn, et al. (2010). "Lifeact mice for studying F-actin dynamics." *Nat Methods* **7**(3): 168-9.
- Rohatgi, R., L. Ma, et al. (1999). "The interaction between N-WASP and the Arp2/3 complex links Cdc42-dependent signals to actin assembly." *Cell* **97**(2): 221-31.
- Ruggeri, Z. M. (2007). "The role of von Willebrand factor in thrombus formation." *Thromb Res* **120 Suppl 1**: S5-9.
- Sagot, I., A. A. Rodal, et al. (2002). "An actin nucleation mechanism mediated by Bni1 and profilin." *Nat Cell Biol* **4**(8): 626-31.
- Sarratt, K. L., H. Chen, et al. (2005). "GPVI and alpha2beta1 play independent critical roles during platelet adhesion and aggregate formation to collagen under flow." *Blood* **106**(4): 1268-77.

- Scarselli, E., H. Ansuini, et al. (2002). "The human scavenger receptor class B type I is a novel candidate receptor for the hepatitis C virus." *Embo J* **21**(19): 5017-25.
- Scita, G., S. Confalonieri, et al. (2008). "IRSp53: crossing the road of membrane and actin dynamics in the formation of membrane protrusions." *Trends Cell Biol* **18**(2): 52-60.
- Shattil, S. J. and P. J. Newman (2004). "Integrins: dynamic scaffolds for adhesion and signaling in platelets." *Blood* **104**(6): 1606-15.
- Shen, L. W., C R; Turner, J R (2008). "The tight junction protein complex undergoes rapid and continuous molecular remodeling at steady state." *J. Cell Biol.* **181**(4): 683-695.
- Sigal, Y. J., O. A. Quintero, et al. (2007). "Cdc42 and ARP2/3-independent regulation of filopodia by an integral membrane lipid-phosphatase-related protein." *J Cell Sci* **120**(Pt 2): 340-52.
- Siripala, A. D. and M. D. Welch (2007). "SnapShot: actin regulators I." *Cell* **128**(3): 626.
- Siripala, A. D. and M. D. Welch (2007). "SnapShot: actin regulators II." *Cell* **128**(5): 1014.
- Small, J. V., G. Isenberg, et al. (1978). "Polarity of actin at the leading edge of cultured cells." *Nature* **272**(5654): 638-9.
- Snapper, S. B., F. Takeshima, et al. (2001). "N-WASP deficiency reveals distinct pathways for cell surface projections and microbial actin-based motility." *Nat Cell Biol* **3**(10): 897-904.
- Sowinski, S., C. Jolly, et al. (2008). "Membrane nanotubes physically connect T cells over long distances presenting a novel route for HIV-1 transmission." *Nat Cell Biol* **10**(2): 211-9.
- Stamatovic, S. M., R. F. Keep, et al. (2009). "Caveolae-mediated internalization of occludin and claudin-5 during CCL2-induced tight junction remodeling in brain endothelial cells." *J Biol Chem* **284**(28): 19053-66.
- Stegner, D. and B. Nieswandt (2011). "Platelet receptor signaling in thrombus formation." *J Mol Med (Berl)* **89**(2): 109-21.
- Suetsugu, S., S. Kurisu, et al. (2006). "Optimization of WAVE2 complex-induced actin polymerization by membrane-bound IRSp53, PIP(3), and Rac." *J Cell Biol* **173**(4): 571-85.
- Sukumvanich, P., V. DesMarais, et al. (2004). "Cellular localization of activated N-WASP using a conformation-sensitive antibody." *Cell Motil Cytoskeleton* **59**(2): 141-52.
- Syder, A. J., H. Lee, et al. (2011). "Small molecule scavenger receptor BI antagonists are potent HCV entry inhibitors." *J Hepatol* **54**(1): 48-55.
- Symons, M., J. M. Derry, et al. (1996). "Wiskott-Aldrich syndrome protein, a novel effector for the GTPase CDC42Hs, is implicated in actin polymerization." *Cell* **84**(5): 723-34.
- Thornber, K., O. J. McCarty, et al. (2006). "Distinct but critical roles for integrin alphaIIb beta3 in platelet lamellipodia formation on fibrinogen, collagen-related peptide and thrombin." *Febs J* **273**(22): 5032-43.
- Vermehren, J. and C. Sarrazin (2011). "New HCV therapies on the horizon." *Clin Microbiol Infect* **17**(2): 122-34.
- Voisset, C., N. Callens, et al. (2005). "High density lipoproteins facilitate hepatitis C virus entry through the scavenger receptor class B type I." *J Biol Chem* **280**(9): 7793-9.
- von Hahn, T., B. D. Lindenbach, et al. (2006). "Oxidized low-density lipoprotein inhibits hepatitis C virus cell entry in human hepatoma cells." *Hepatology* **43**(5): 932-42.

- von Hahn, T., J. C. Yoon, et al. (2007). "Hepatitis C virus continuously escapes from neutralizing antibody and T-cell responses during chronic infection in vivo." *Gastroenterology* **132**(2): 667-78.
- Wagoner, J., A. Negash, et al. (2010). "Multiple effects of silymarin on the hepatitis C virus lifecycle." *Hepatology* **51**(6): 1912-21.
- Warren, A., D. G. Le Couteur, et al. (2006). "T lymphocytes interact with hepatocytes through fenestrations in murine liver sinusoidal endothelial cells." *Hepatology* **44**(5): 1182-90.
- Watson, S. P. (2009). "Platelet activation by extracellular matrix proteins in haemostasis and thrombosis." *Curr Pharm Des* **15**(12): 1358-72.
- Weeterings, C., J. Adelmeijer, et al. (2006). "Glycoprotein Ibalpha-mediated platelet adhesion and aggregation to immobilized thrombin under conditions of flow." *Arterioscler Thromb Vasc Biol* **26**(3): 670-5.
- Yamada, S., S. Pokutta, et al. (2005). "Deconstructing the cadherin-catenin-actin complex." *Cell* **123**(5): 889-901.
- Yamagishi, A., M. Masuda, et al. (2004). "A novel actin bundling/filopodium-forming domain conserved in insulin receptor tyrosine kinase substrate p53 and missing in metastasis protein." *J Biol Chem* **279**(15): 14929-36.
- Zeisel, M. B., H. Barth, et al. (2009). "Hepatitis C virus entry: molecular mechanisms and targets for antiviral therapy." *Front Biosci* **14**: 3274-85.
- Zhang, J., G. Randall, et al. (2004). "CD81 is required for hepatitis C virus glycoprotein-mediated viral infection." *J Virol* **78**(3): 1448-55.